DEC 8 1947

THE JOURNAL OF CHEMICAL PHYSICS

VOLUME 15 NUMBER 11

NOVEMBER, 1947

Published by the

AMERICAN INSTITUTE OF PHYSICS

Lancaster Press, Inc., New York, N. Y.

Two years [illegible]

K. J. [illegible]
A. L. [illegible]
[illegible]
George [illegible]
Bruno B. Zinn

[illegible] Wilson, Jr.

[illegible] exponents. The solidus (/) should be used wherever possible for fractions.

All illustrations should accompany manuscript and should always be referred to in the text. Line drawings should be made with India ink on plain white paper or on tracing cloth. Coordinate paper is not desirable, but if used it must be blue-lined with all coordinates to be reproduced drawn with India ink. Lettering should be of sufficient size to be legible after reduction.

Proofs and all correspondence concerning papers in the process of publication should be addressed to the Publications Manager, American Institute of Physics, 57 East 55 Street, New York 22, New York.

Subscription Price

The United States and Possessions, Canada and Mexico $10.00
Members 11.00

Back Numbers

Complete set: Vol. 1, 1931—Vol. 14, 1946 (except Vol. 1, No. 1) $140.00
Yearly rate: $11.00.
Single copies: $1.00 each.

Subscriptions and orders for single copies should be addressed to Prince and Lemon Streets, Lancaster, Pennsylvania, or to the American Institute of Physics, 57 East 55 Street, New York 22, New York.

Changes of address should be sent to the Business Manager, American Institute of Physics

[illegible] Prince and Lemon Streets, Lancaster, Pennsylvania

[illegible] Lancaster, Pa., under the Act of [illegible], 1918. Acceptance for [illegible], embodied in paragraph 4, Sec. [illegible], P. L. & R., authorized

THE JOURNAL
OF
CHEMICAL PHYSICS

VOLUME 15, NUMBER 11 NOVEMBER, 1947

Statistical Mechanics of Multimolecular Adsorption. III. Introductory Treatment of Horizontal Interactions. Capillary Condensation and Hysteresis[1a]

TERRELL L. HILL
Department of Chemistry, The University of Rochester, Rochester, New York

(Received January 23, 1947)

The elementary treatment of interactions and first order phase changes in localized and mobile monolayers is reviewed. Calculations on multimolecular adsorption and capillary condensation, which take into account horizontal interactions in an approximate manner, are presented. Several other topics are discussed briefly, including the quasi-chemical method and reversible hysteresis. It is suggested, on the basis of the capillary condensation calculations, that reversible hysteresis involves the use of metastable portions of the adsorption isotherm. The theory predicts, in agreement with experiment, that the adsorption curve should be below the desorption curve.

I. INTRODUCTION

IT is well known that the Brunauer-Emmett-Teller (BET) theory[1b] of multimolecular adsorption ignores horizontal interactions between adsorbed molecules. This is clear from the model which may be used in a statistical treatment to obtain the BET equation.[2,3] On the other hand, interactions between adsorbed molecules in the simpler case of monomolecular adsorption (these are, of course, necessarily horizontal interactions) have been taken into account in earlier work.[4–7]

In Section II we shall review briefly the elementary treatment of interactions and first order phase changes in monolayers. Then, in Sections III (adsorption on a free surface) and IV (adsorption between parallel walls), we shall discuss multimolecular adsorption, including horizontal interactions. However, these latter remarks will be based on calculations using equations which take the interactions into account in only a very approximate manner. So it will not be possible to come to definite conclusions here, and it would certainly be premature to try to compare the theory with experiment (except qualitatively) at this time.

In Section V we give somewhat more general equations, but calculations based on these equations have not yet been carried out. Several other points, including hysteresis, will also be discussed.

[1a] Presented at the symposium on gas adsorption of the Division of Colloid Chemistry, Chicago, September 11, 1946.
[1b] S. Brunauer, P. H. Emmett, and E. Teller, J. Am. Chem. Soc. **60**, 309 (1938).
[2] T. L. Hill, J. Chem. Phys. **14**, 263 (1946).
[3] A. B. D. Cassie, Trans. Faraday Soc. **41**, 450 (1945).
[4] H. M. Cassel, J. Phys. Chem. **48**, 195 (1944).
[5] In writing part II of this series, the paper[4] by Cassel had not come to the writer's attention. In this paper, Cassel obtained Eq. II (59), and essentially also Eq. II (38) by a thermodynamic use of a two-dimensional van der Waals' equation. This method is, however, less general since it does not allow an evaluation of the constant *C*. The statistical treatment gives *C*.
[6] R. H. Fowler, and E. A. Guggenheim, *Statistical Thermodynamics* (Cambridge University Press, London, 1939), Chapter X.
[7] T. L. Hill, J. Chem. Phys. **14**, 441 (1946).

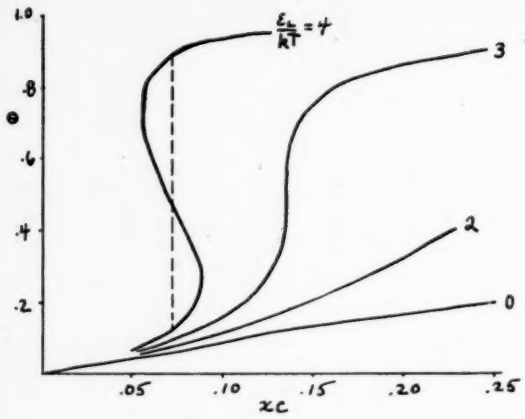

FIG. 1.

II. MONOMOLECULAR ADSORPTION

There are two special cases of particular interest: the adsorbed molecules may be localized at definite sites or they may be mobile, behaving as a two-dimensional gas. Intermediate cases are also possible and the transition may be studied theoretically,[7] but we shall not discuss this question here. Of the two special cases to be considered, mobile adsorption is probably the most important except at very low temperatures.[7]

Localized Adsorption

The calculations given here for both monomolecular and multimolecular adsorption are for a simple cubic lattice. The calculations for a monolayer are no more difficult for a close packed arrangement, but the equations for multimolecular adsorption do become more complicated (see Section V).

We have to evaluate the potential energy of interaction between the adsorbed molecules somehow. We do this by counting up the number of pairs of nearest neighbor sites occupied by adsorbed molecules. We make the very crude assumption that the available sites on the surface are occupied by adsorbed molecules in a completely random fashion. The next higher approximation would be to use the quasi-chemical equilibrium method.[6] However, this refinement does not here lead to any new qualitative features but only to quantitative improvements.

On these assumptions, one finds[6] for the adsorption isotherm (Eq. (1) is a special case of Eq. (9), to be derived below),

$$xc=\frac{\theta}{1-\theta}\exp\left(-\frac{4}{3}\frac{\epsilon_L}{kT}\theta\right), \tag{1}$$

where θ is the fraction of the available sites occupied, $x=p/p_0$ is the relative pressure, c is the familiar BET constant, and $-\epsilon_L$ is the average potential energy of the molecules in the liquid state (the meaning of ϵ_L is discussed more carefully in Section V). Isotherms calculated from Eq. (1) are shown in Fig. 1. For

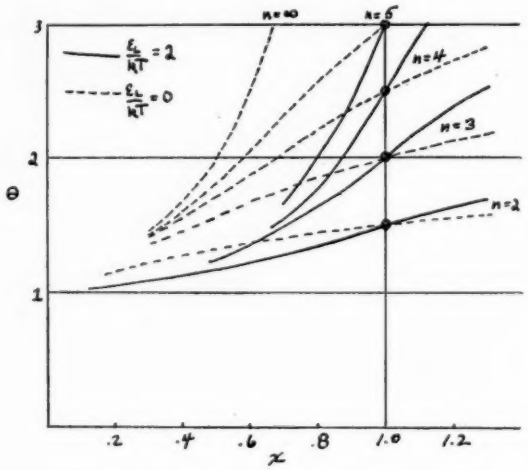

FIG. 2.

sufficiently large values of ϵ_L/kT, a first order phase change is predicted. The critical constants are $\theta_c=\frac{1}{2}$, $T_c=\epsilon_L/3k$ and $x_cc=e^{-2}=0.1353$. Since c is commonly of the order of 100, this critical behavior is to be expected at low pressures: x of the order of 10^{-3}. The curve for $\epsilon_L/kT=0$ is the Langmuir isotherm: $xc=\theta/(1-\theta)$.

Mobile Adsorption

We are faced here with the same difficult problem as in three dimensions: what is the equation-of-state of the gas? The reduction from three to two dimensions does not introduce any appreciable simplification. Also, the two-dimensional problem is complicated by the effects of the surface on the molecular interactions. For simplicity, and in the absence of any satisfactory alternative, we assume a two-dimensional van

der Waals' equation:

$$\left(\varphi+\frac{a'N^2}{\mathfrak{A}^2}\right)(\mathfrak{A}-Nb')=NkT. \qquad (2)$$

In Eq. (2), φ is the two-dimensional (spreading) pressure, $\mathfrak{A}$ is the area, N the number of molecules adsorbed in the area $\mathfrak{A}$, and a' and b' are two-dimensional van der Waals' constants. The adsorption isotherm which can be derived from this equation-of-state[4,7] is

$$xC=\frac{\theta}{1-\theta}\exp\left(\frac{\theta}{1-\theta}-\alpha\theta\right), \qquad (3)$$

$$\theta=Nb'/a, \quad \alpha=2a'/b'kT. \qquad (4)$$

The constant C is the analogue, for the mobile case, of the BET constant c. It is discussed further in Paper II of this series. The term $\theta/(1-\theta)$ in the exponential is due to repulsions

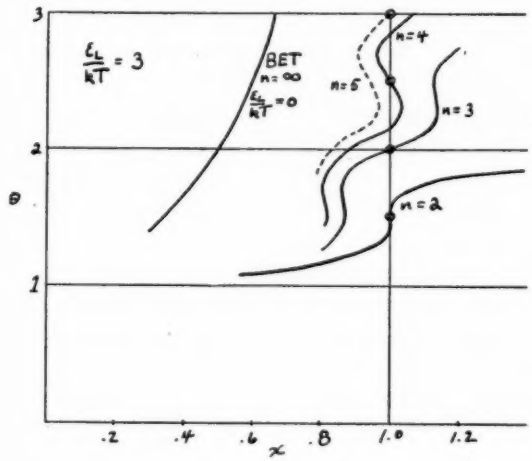

FIG. 3.

(finite volume of spheres) and has no counterpart in Eq. (1). The isotherms calculated from Eq. (3) (these isotherms are given in Fig. 2 of Paper II) exhibit the same general features as seen in Fig. 1 for the localized case. The critical constants are $\theta_c=\frac{1}{3}$, $T_c=8a'/27b'k$ and $x_cC=0.0869$. The comparisons between this critical temperature and the three-dimensional critical temperature and between these critical constants and experimental critical constants for n-heptane are discussed in some detail in Paper II and will not be repeated here.

III. MULTIMOLECULAR ADSORPTION ON A FREE SURFACE

The model on which the familiar BET equation,

$$\theta=\frac{v}{v_m}=\frac{cx}{(1-x)(1-x+cx)}, \qquad (5)$$

(where θ is the ratio of the number of molecules adsorbed per unit area to the number of available sites in the first layer per unit area) is based is the following: the first layer is localized; molecules build up higher layers by adding vertically to molecules already adsorbed; and horizontal interactions between molecules are neglected in all layers. Successive improvements in the BET model would follow from (1) taking into account horizontal interactions, (2) using a lattice more suitable than simple cubic and (3) allowing a more general type of filling in of the lattice.[2] In this paper we allow for (1) in a very crude way and, in Section V, we introduce other lattices approximately, as suggested by (2). However, all of the preliminary calculations given in this section and in Section IV are based on the simpler equations, to be derived below, for a simple cubic lattice.

The first layer is handled as described in Section II. There are again the two possibilities: the first layer is localized or it is mobile. We assume here that higher layers build up by vertical additions in the simple cubic lattice, each molecule being above a molecule in the layer below (so far, this is just the BET model). If there are X_i molecules per unit surface area in

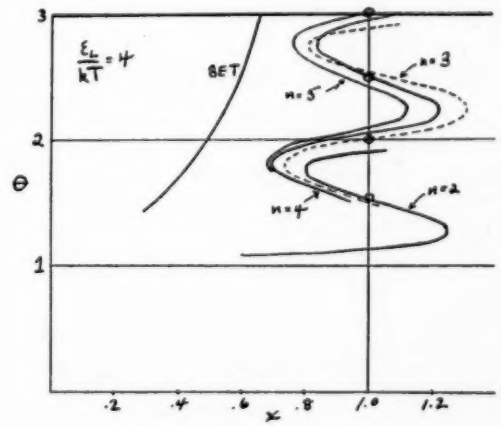

FIG. 4.

the i-th layer, then there are X_i sites available for molecules going into the $(i+1)$-th layer. Suppose that there are B sites per unit surface area available in the first layer ($B=1/b'$ in the mobile case). For the higher layers we make the same crude approximation, in order to count nearest neighbor pairs, that we made for the first layer in the localized case: we assume that the X_i molecules in the i-th layer are distributed completely at random over the B sites of the i-th layer (not all *available*) and the X_{i+1} molecules of the next higher layer are distributed at random over the X_i available sites and hence at random over all the B sites of the $(i+1)$-th layer. Consider a lattice site in the i-th layer, with z' nearest neighbor sites *in this layer* ($z'=4$ here). The probability that any site is occupied is X_i/B. Hence, any molecule in this layer has, on the average, $z'X_i/B$ nearest neighbors. So the total number of nearest neighbor pairs in this layer is $(\frac{1}{2})(X_i)(z'X_i/B)=(\frac{1}{2})(z'X_i^2/B)$. The factor $\frac{1}{2}$ prevents us from counting each pair twice.

One can proceed now to derive directly the equations for $n=\infty$ (n being the number of layers allowed—in imagination—on the free surface) and for either a localized or mobile first layer. However, it proves helpful in the calculations to use the equations for n finite (although the case of physical interest is $n=\infty$), so we shall derive these latter equations (first for the localized case) and let $n\to\infty$ later.

Suppose that N molecules have been adsorbed in n layers. Then,

$$N=X_1+X_2+\cdots+X_n. \tag{6}$$

From Eq. (32) of Paper I (see also Eqs. (19)–(21) in that paper), we have for the partition function (see the discussion of the quasi-chemical equilibrium method in Section V for a more careful treatment),

$$Q=\sum_{X_1}\cdots\sum_{X_{n-1}}\left\{\frac{[j_s\exp(\epsilon_1/kT)]^{X_1}j_L{}^{N-X_1}B!\exp(2\epsilon_L\mathfrak{N}/zkT)}{(B-X_1)!(X_1-X_2)!\cdots(X_{n-1}-X_n)!X_n!}\right\}, \tag{7}$$

where X_n is understood to be a function of N, $X_1, X_2, \cdots X_{n-1}$ as given by Eq. (6), $j_s\exp(\epsilon_1/kT)$ is the partition function[8] for an isolated molecule on the surface, $j_L\exp(\epsilon_L/kT)$ is the partition function[8] for a molecule in the liquid state, $\mathfrak{N}$ is the total (average) number of pairs of nearest neighbors (not just horizontal pairs) and is a function of $N, X_1, X_2, \cdots X_{n-1}$, and, finally, z is the *total* number of nearest neighbors in the lattice (and in the liquid since the lattice is supposed to be liquid-like). $z=6$ for a simple cubic lattice. The BET equation follows[2] from Eq. (7) if we put $n=\infty$, $\mathfrak{N}=N-X_1$, and $z=2$ (i.e. ignore the four nearest neighbors in the same layer ($z'=0$), and count only vertical nearest neighbors). In the model we are describing here, $z=6$ ($z'=4$) and

$$\mathfrak{N}=(2X_1^2/B)+(2X_2^2/B)+\cdots+(2X_n^2/B)+N-X_1. \tag{8}$$

$N-X_1$ is the contribution to $\mathfrak{N}$ of vertical pairs of nearest neighbors (as in the BET theory) while the other terms represent, approximately, the number of pairs of horizontal nearest neighbors.

The adsorption isotherm now follows from Eqs. (7) and (8) in a straightforward way already described.[2] One finds the set of n equations:

$$\begin{aligned}
x&=\frac{\theta_1-\theta_2}{1-\theta_1}\frac{1}{c}\exp[a(-4\theta_1)]\\
&=\frac{\theta_2-\theta_3}{\theta_1-\theta_2}\exp[a(-4\theta_2+2)]\\
&\ \ \vdots\\
&=\frac{\theta_n}{\theta_{n-1}-\theta_n}\exp[a(-4\theta_n+2)],\\
\theta&=v/v_m=\theta_1+\theta_2+\cdots+\theta_n,\\
\theta_i&=X_i/B,\\
a&=\epsilon_L/3kT.
\end{aligned} \tag{9}$$

It is easy to see that, for a mobile first layer, all of these n equations are the same as given here

[8] The liquid partition function is discussed further in Section V. $j_s=jj_nj_v$ where j is the internal partition function, j_n is the partition function for vibrations normal to the surface (one degree of freedom), and j_v is the partition function for vibrations parallel to the surface (two degrees of freedom). In the mobile case j_v goes over[7] into the partition function for a molecule in a two-dimensional gas.

except the first, which becomes

$$x=\frac{\theta_1-\theta_2}{1-\theta_1}\frac{1}{C}\exp\left(\frac{\theta_1}{1-\theta_1}-\alpha\theta_1\right), \qquad (10)$$

$$\alpha=2a'/b'kT.$$

We are interested in the solution, $\theta(x)$, of Eqs. (9) for $n=\infty$. There does not seem to be any hope of obtaining an explicit expression[9] for $\theta(x)$ so one must resort to numerical procedures. In principle, the case $n=\infty$ can be solved directly as follows, for given values of x, c and a: guess θ_1; using this θ_1, calculate θ_2 from the first equation; using θ_1 and θ_2, calculate θ_3 from the second equation; etc. The test of whether θ_1 has been guessed correctly is $\lim_{i\to\infty}\theta_i=0$. If the θ_i do not converge to zero, a new guess of θ_1 is made and the procedure is repeated. This method becomes complicated for larger values of a because in this case, for part of the range in x, θ can be a highly multiple valued function of x. In order to aid in isolating the different values of θ for a given x, it is helpful to solve the problem for, say, $n=2, 3, 4, \cdots$. Calculations have not actually been carried out as yet for $n=\infty$. The results to be presented here are for $n=2$, 3, 4, and 5.

It might be recalled at this point that these calculations are based on Eqs. (9), which equations were derived on the crude assumption of randomness in counting nearest neighbors. The next higher approximation would be to introduce the quasi-chemical equilibrium method. Although this method does not lead to new qualitative features when applied to monolayers, there is no assurance that the same will be true in multimolecular adsorption, though it is probably true.

In Fig. 2, we give the curves for $\epsilon_L/kT=0$ and 2 and $n=2$, 3, 4, and 5. For simplicity we have taken c as very large ($\theta_1=1$) and considered only the part of the curves above $\theta=1$. There is no difficulty in calculating the complete curves but the present simplification leads to curves which are independent of c (for large c—the case of most interest) and of whether or not the first layer is mobile or localized. For $\epsilon_L/kT=0$ we have essentially the BET case and we can write $\theta(x, n)$ explicitly. For $n=\infty$, $\theta=1/(1-x)$. The curves for $n=2$, 3, 4, and 5 converge toward the curve for $n=\infty$. Similarly, for $\epsilon_L/kT=2$, the curves for $n=2-5$ may be thought of as converging toward a curve which lies somewhat below the BET $n=\infty$ curve. It should be stated that the curves given here for $\epsilon_L/kT=2$, 3, and 4 (Figs. 2–4) are not extremely accurate. They are, however, sufficiently exact to illustrate the essential points.

There is a symmetry property of interest for all values of ϵ_L/kT (if we take $\theta_1=1$): $\ln x$ is an odd function of $\theta-(n+1)/2$. This being the case we give the curves up to $\theta=3$ only. It will be noted that the incomplete filling of capillaries at $x=1$ in the original BET treatment (also in the modified treatment[10] of Brunauer, Deming, Deming and Teller) is retained here for $\epsilon_L/kT=2$. This is obviously related to the symmetry property mentioned above. See also Figs. 3 and 4 in this connection. However, this is not the correct approach to capillary condensation and we defer further discussion of the subject to Section IV.

Figure 3 gives similar curves for $\epsilon_L/kT=3$. The curve for $n=2$ is a critical curve and loops appear in the curves for $n=3$ and $n=4$. The $n=5$ curve in this figure has not been calculated but just guessed (with some confidence). A BET curve is included for orientation; it is not the limiting curve. Figure 4 shows the somewhat more complicated behavior for $\epsilon_L/kT=4$. The $n=3$ curve is a calculated curve; it is dotted for convenience only. Below $\theta\cong 1.3$, the curves for $n=3-5$ virtually coincide with the $n=2$ curve. For $\theta<2$, it can be seen how these curves are converging toward an $n=\infty$ curve. In general, such convergence seems to be faster for larger values of ϵ_L/kT. Again a BET curve is included for orientation.

There seems to be some indication in Figs. 3 and 4 that, for sufficiently large values of ϵ_L/kT, Eqs. (9) ($n=\infty$) will predict step-like adsorption. This is not certain, however, and in any case this feature may or may not be a property of a more refined set of equations. But judging from the curves calculated so far, the general behavior of Eqs. (9) for $n=\infty$ would appear to be: (1) for small $\epsilon_L/kT>0$, $\theta(x)$ resembles the BET curve

[9] It might be remarked that Eqs. (9) can be written as a single non-linear second order difference equation with boundary conditions.

[10] S. Brunauer, L. S. Deming, W. E. Deming, and E. Teller, J. Am. Chem. Soc. **62**, 1723 (1940).

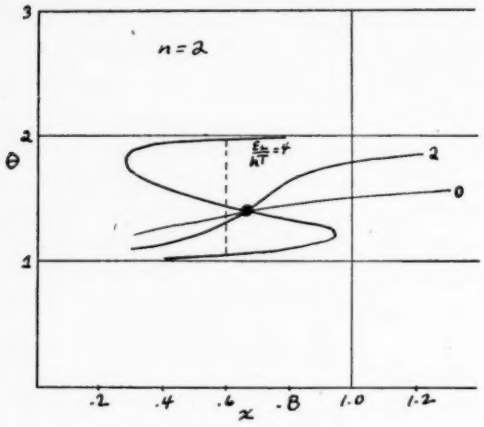

FIG. 5.

but lies below it; (2) for large ϵ_L/kT, loops appear which (a) decrease in amplitude and (b) move from $x<1$ toward $x=1$, as θ increases.

IV. MULTIMOLECULAR ADSORPTION BETWEEN PARALLEL WALLS

We take the same model as above, but consider that adsorption occurs between two parallel walls with room for $2n$ layers of adsorbed molecules. This model can be modified easily to apply to adsorption in cylinders or between parallel walls with $2n+1$ layers. However, we shall not discuss these systems here, since the same general arguments and results are obtained. The cylindrical equations will be of use in comparing theory with experiment since the model is more realistic.

We must now include in $\mathfrak{N}$ a term which gives the number of pairs of nearest neighbors between molecules in the n-th and $(n+1)$-th layers. In order to be consistent, we assume randomness; that is, we assume that the X_n molecules in each of these layers are distributed among the B sites at random and therefore without regard to the distribution in the other layer. So the probability that a molecule in the n-th layer will have a nearest neighbor in the $(n+1)$-th layer is X_n/B. There are then X_n^2/B such pairs of neighbors. We are going to consider only layers 1 to n (since, in an equilibrium distribution, layers $2n$ to $n+1$ behave identically), so we should assign only one-half of these pairs, $\frac{1}{2}(X_n^2/B)$, to $\mathfrak{N}$. Equation (7) still holds here but Eq. (8) becomes

$$\mathfrak{N}=\frac{2X_1^2}{B}+\cdots+\frac{2X_{n-1}^2}{B}+\frac{5}{2}\frac{X_n^2}{B}+N-X_1. \quad (11)$$

As a result of this modification, one finds that Eqs. (9) and (10) are unchanged except for the n-th equation which now reads

$$x=\frac{\theta_n}{\theta_{n-1}-\theta_n}\exp[a(-5\theta_n+2)]. \quad (12)$$

The change from $4\theta_n$ to $5\theta_n$ in the exponential corresponds physically to the extra energy Q introduced by Brunauer, Deming, Deming and Teller[10] in their modified BET treatment.

We give, in Figs. 5–7, a few examples based on the above model. We take c very large ($\theta_1=1$) in Figs. 5 and 6, but, for variety, in Fig. 7 we give the complete curve in a case with c small: $c=\frac{1}{10}$. Returning to Fig. 5 ($n=2$) we see that the predicted behavior is that the first layer fills in first and then the second layer fills in suddenly and practically completely, for $\epsilon_L/kT=4$, at about $x=0.6$. The behavior is different for $\epsilon_L/kT=0$ and 2. At saturation, the second layer is half full for $\epsilon_L/kT=0$, but 0.8 full for $\epsilon_L/kT=2$ and virtually full for $\epsilon_L/kT=4$. All three curves pass through the point $\theta=7/5$, $x=2/3$. This is not, however, the center of antisymmetry. Figure 6 shows similar curves for $n=3$. For $\epsilon_L/kT=4$, after the first layer is full, the second and third layers fill suddenly at about $x=0.7$ or 0.8. Comparing the $\epsilon_L/kT=4$ case for $n=2$ (Fig. 5) and for $n=3$ (Fig. 6), we note it is predicted here that smaller capillaries fill at smaller values of x, which is in qualitative agreement with the experimental facts. Figure 7 shows how, in some cases, the complete capillary can fill suddenly, including the first layer. There are, of course, many other possible cases, but these should serve as illustrations.

It should now be clear that it is possible in principle for a single theory to include (1) multimolecular adsorption on free surfaces and in capillaries and (2) capillary condensation either with or without the first layer being adsorbed first. The multimolecular adsorption and the capillary condensation points of view are therefore really not in conflict, as has been generally assumed.

The general feature of the curves for large ϵ_L/kT which leads to capillary condensation is the following: in adsorption on a free surface the loops give the appearance of wrapping them-

selves around the $x=1$ line (as θ increases from $\theta \cong 1$); in capillary adsorption the loops tend to do the same except for the loop associated with the last layer, this "top" loop being displaced (due to the extra nearest neighbor pairs) towards smaller values of x (Fig. 6 is an illustration of this). The above can be expressed more precisely in mathematical language but the essential feature is that just described. This displacement of the top loop requires, on thermodynamic grounds (see Section V), that the phase change include *all* loops and hence the capillary is filled (except for the first layer if it is already full) virtually completely in one jump.

A further remark might be in order here. Sudden jumps of the type described will be observed experimentally only if the adsorbent has a very uniform pore structure. Generally the effect will be smoothed out due to the pore size distribution.

V. MISCELLANEOUS TOPICS*

Lattices Other than Simple Cubic

Suppose we consider a general lattice in which each site has a total of z nearest neighbor sites, z' nearest neighbor sites in the same layer and $(\xi+1)$ nearest neighbor sites in the layer above and also in the layer below:

$$z=z'+2(\xi+1). \tag{13}$$

The number of pairs of nearest neighbors in the

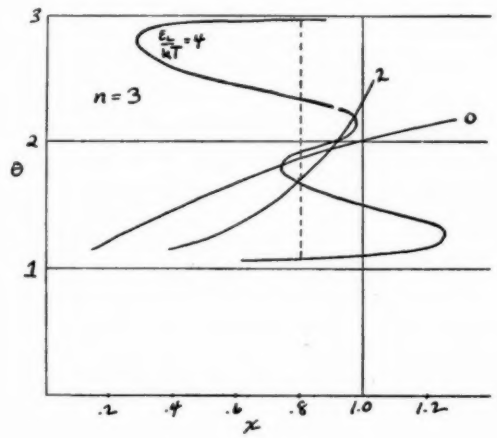

FIG. 6.

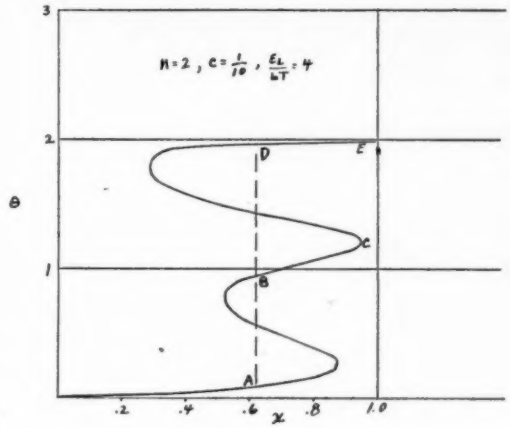

FIG. 7.

i-th layer is $(z'/2)(X_i^2/B)$. The number of pairs between the i-th and $(i+1)$-th layers is $X_{i+1}(1+\xi X_i/B)$. That is, each molecule in the $(i+1)$-th layer has *at least* one nearest neighbor in the i-th layer (or the molecule could not add to the lattice—on the assumption of vertical[11] building), and, on the average, has $\xi X_i/B$ additional ones on the randomness assumption. In the capillary (parallel wall) case, there are an additional $[(\xi+1)/2](X_n^2/B)$ pairs to be added to $\mathfrak{N}$ as before.

We assume that Eq. (7) still holds for all lattices. Actually, the factorial part of Eq. (7) is consistent with previous assumptions only for vertical[12] lattices (e.g., simple cubic). One can easily derive the strictly consistent factorial expression for non-vertical lattices. However, not only is it very complicated but a little reflection convinces one that, although it is consistent, it is actually probably less realistic than the original expression. At any rate, in the present discussion, we retain Eq. (7) but in place of Eq. (8) we have the more general expression,

$$\mathfrak{N}=\frac{z'}{2}\frac{X_1^2}{B}+\cdots+\frac{z'}{2}\frac{X_n^2}{B}+X_2\left(1+\frac{\xi X_1}{B}\right)+\cdots+X_n\left(1+\frac{\xi X_{n-1}}{B}\right). \tag{14}$$

* We include in this section a brief discussion of several additional points which may be of interest.

[11] By vertical building, we mean that a molecule can go into a site only if at least one nearest neighbor site in the next lower layer is already occupied. This is not the most general type of building but it is the only kind considered in this paper.

[12] By a vertical lattice we mean one in which each site is directly above a site in the next lower layer ($\xi=0$).

For the capillary case we add $[(\xi+1)/2](X_n^2/B)$ to the right hand member. One finds then, for a localized first layer,

$$x=\frac{\theta_1-\theta_2}{1-\theta_1}\frac{1}{c}\exp[a(-z'\theta_1-\xi\theta_2)]$$

$$=\frac{\theta_2-\theta_3}{\theta_1-\theta_2}\exp[a(-z'\theta_2-\xi\theta_1-\xi\theta_3+z/2-1)]$$

$$\vdots$$

$$=\frac{\theta_{n-1}-\theta_n}{\theta_{n-2}-\theta_{n-1}}\exp[a(-z'\theta_{n-1}-\xi\theta_{n-2}-\xi\theta_n+z/2-1)] \tag{15}$$

$$=\frac{\theta_n}{\theta_{n-1}-\theta_n}\exp[a(-z'\theta_n-\xi\theta_{n-1}+z/2-1)],$$

$$a=2\epsilon_L/zkT.$$

For a mobile first layer, it turns out that the first equation should be modified to read

$$x=\frac{\theta_1-\theta_2}{1-\theta_1}\frac{1}{C}\exp\left(\frac{\theta_1}{1-\theta_1}-\alpha\theta_1-a\xi\theta_2\right). \tag{16}$$

For adsorption between parallel walls, z' in the n-th equation should be changed according to

$$z'\rightarrow z'+\xi+1. \tag{17}$$

The cases of special interest are:

BET:

$$z=2,\quad z'=0,\quad \xi=0.$$

Simple cubic:

$$z=6,\quad z'=4,\quad \xi=0. \tag{18}$$

Close packed:

$$z=12,\quad z'=6,\quad \xi=2.$$

It is not correct to say that the BET theory is a special case such that $\epsilon_L/kT=0$, for this assumption is really not made (ϵ_L/kT occurs in c). Properly, the BET treatment should be characterized as a special case as is done in Eqs. 18 (i.e. $z=2$, $z'=0$; ξ is not an independent parameter). In Figs. 2–4, it is permissible to label the $\epsilon_L/kT=0$ curve as the BET curve for we are considering $\theta_1=1$ and $\theta>1$. The BET curve coincides for large c and $\theta>1$.

Limitations of a Lattice-type Model

We have confined ourselves in this series of papers to a model which emphasizes a lattice structure in the adsorbate. It is possible to assign, and we have assigned, certain necessary liquid-like properties to this adsorbate. However, the model is obviously not completely satisfactory (even if it did not lead to considerable algebraic complications), because it does not become isotropic for adsorbate molecules far from the surface. A lattice model is probably best for the first several layers, but a liquid-like model would seem to be more correct otherwise. One would like to include both features in a single general model but this would no doubt be rather difficult.

What Values of ϵ_L/kT Are of Physical Significance?

In order to try to answer this question we must say something about liquids. At the same time, this will be a good opportunity to be more specific about the meaning of j_L and ϵ_L. For a perfect gas of N molecules with a volume per molecule $v=V/N$, the partition function is

$$Q=\frac{1}{N!}\left[\left(\frac{2\pi mkT}{h^2}\right)^{\frac{3}{2}}Nvj\right]^N, \tag{19}$$

where j is the internal partition function. For an imperfect gas or liquid we can write Q formally as

$$Q=\frac{1}{N!}\left[\left(\frac{2\pi mkT}{h^2}\right)^{\frac{3}{2}}Nv_fj\exp(\chi/kT)\right]^N, \tag{20}$$

in which we have replaced v by an effective "free volume" per molecule v_f and introduced an average potential energy of interaction per molecule, $-\chi$, evaluated when each molecule is in the center of its "cell." In general, we should take both v_f and χ as functions of v and T, but the relatively slight dependence of χ on T is usually ignored.

It will be noticed that in the papers of this series we have implicitly adopted

$$Q=[j_L\exp(\epsilon_L/kT)]^N \tag{21}$$

as the partition function for the liquid. Hence

the correspondence is:

$$\epsilon_L(v) = \chi(v), \tag{22}$$

$$j_L(v, T) = \left(\frac{2\pi mkT}{h^2}\right)^{\frac{1}{3}} v_f(v, T) j(T) e. \tag{23}$$

If we use the harmonic oscillator model of a liquid,[2] Eq. (23) becomes

$$j_L(v, T) = \left(\frac{kT}{h\nu_L(v)}\right)^3 j(T) e. \tag{24}$$

We are especially interested here in $\epsilon_L(v)$. Unfortunately, there is no really satisfactory theory of liquids from which to obtain this function. However, in another paper[13] we have calculated $\epsilon_L(v)$, approximately, from experimental $P-V-T$ data on nitrogen and argon in their respective critical regions. If we assume that the temperature dependence of ϵ_L is negligible between the boiling point and critical point, we can then estimate ϵ_L/kT not only at the critical point but also at the boiling point. It is necessary to extrapolate $1/\epsilon_L(v)$ to zero at $v=0$ in order to extend somewhat the range in v (to include the smaller value of v at the boiling point) of the critical region data. One finds then, omitting further details: (1) at the critical point, $\epsilon_L/kT=2.1$ for nitrogen and 1.7 for argon; and (2) at the boiling point, $\epsilon_L/kT=6.2_5$ for nitrogen and 5.7_5 for argon. The average values are 1.9 (critical point) and 6.0 (boiling point).

The above approximate values of ϵ_L/kT should not be compared in magnitude with the values in Figs. 1–7, since these figures are based on certain crude assumptions and a simple cubic lattice. However, one can make the correspondence, approximately, as follows: we find the ratio of (1) ϵ_L/kT_c based on fairly accurate considerations for localized monomolecular adsorption to (2) ϵ_L/kT_c based on the assumptions of the present paper (this value is $\epsilon_L/kT_c=3$, from Eq. (1)), and assume that this ratio also holds for multimolecular adsorption (this assumption is consistent with a lattice-type model). We get the relatively exact value of ϵ_L/kT_c from the quasi-chemical equilibrium method, using $z=10.5$ for argon and 10.9 for nitrogen,[13] and taking $z'=z/2$ (i.e. we assume close packing with occasional random holes). Then,

$$\frac{\epsilon_L}{kT_c} = -\frac{z}{z'}\frac{w}{kT_c} = -2\frac{w}{kT_c} = 2z' \ln\frac{z'}{z'-2} \cong 5.0 \tag{25}$$

for both nitrogen and argon. Equation (25) shows the connection between our ϵ_L and Fowler and Guggenheim's[6] w, and gives ϵ_L/kT_c as a function of z' as found from the quasi-chemical equilibrim method.[6] So we should multiply 1.9 and 6.0 (above) by approximately $\frac{3}{5}$ to convert to the ϵ_L/kT scale of Figs. 1–7. We find $\epsilon_L/kT \cong 1.1$ (critical point) and 3.6 (boiling point). The present theory is obviously applicable only below the critical temperature, or, approximately, for $\epsilon_L/kT > 1.1$. Needless to say the above approximate numerical values should not be taken too seriously. However, they seem to be the best available at the present time.

The Criticism of the BET Equation by Cassel

Cassel has pointed out[4] that if we use the BET equation for $\Gamma(p)$ in the Gibbs equation,

$$\varphi(p) = \gamma_S - \gamma(p) = kT\int_0^p \Gamma(p)\, d\ln p, \tag{26}$$

where γ_S is the surface tension of the clean surface, $\gamma(p)$ is the sum of the surface tension of the adsorbate and the interfacial tension, and Γ is the surface concentration, then, for $p=p_0$, the integral becomes infinite whereas

$$\gamma_S - \gamma(p_0) = \gamma_S - \gamma_L - \gamma_{LS}$$

is certainly finite. Clearly, a correct theory should allow Γ to become infinite at $p=p_0$ but in such a way that the integral of Γ/p from $p=0$ to $p=p_0$ remains finite. Cassel attributed this failure in the BET theory to the neglect of lateral cohesion (horizontal interactions), and this certainly seems to be correct. It should be clear from Figs. 1–4 that the present treatment is in the direction of eliminating this difficulty, as expected.

Hysteresis and Capillary Condensation

As is well known, the thermodynamic theorem of equal areas is used to determine the point at which a phase change takes place when loops

[13] T. L. Hill, J. Phys. Chem. (in press).

are encountered. This theorem is general and applies to the complicated loops found here. However, in order to apply the theorem to the adsorption isotherm, θ must be plotted as a function of $\ln x$, not x. In the figures the dotted straight lines indicate phase changes. Those parts of the solid curves which are thus skipped by a phase change are metastable if $d\theta/dx$ is positive but unstable if $d\theta/dx$ is negative. The dotted lines represent the stable equilibrium behavior.

It would seem that reversible hysteresis can be interpreted on the above basis. For example, referring to Fig. 7, one might get adsorption along $ABCE$ and desorption along EDA. There are of course other conceivable paths in both adsorption and desorption making use of metastable parts of the curve, but in every case the adsorption path is *below* (or coincides with, in the reversible stable equilibrium case) the desorption path, as is found experimentally. This follows from the condition $d\theta/dx>0$ and because, in adsorption, the system can attain only those metastable sections of the complete curve which lie to the right of the dotted line, whereas in desorption, only metastable states to the left of the line are accessible. The same argument would apply to any other curve showing loops and capillary condensation. These effects will of course be smeared out in practice due to nonuniform pore structure.

If this argument is correct, it would not be necessary to have conical or bottle-necked capillaries to obtain hysteresis, though it may be particularly easy for capillaries of this type to get into the metastable states. From the statistical mechanical point of view, the problem of adsorption in such capillaries does not present any new features of a really fundamental nature (there are, however, new complications). There will be, as before, a single stable equilibrium curve predicted, and various metastable states possible.

Cassel[4] has discussed hysteresis from a point of view which resembles the present one in some respects.

Use of the Quasi-Chemical Equilibrium Method

We shall indicate briefly how the quasi-chemical method might be introduced in this problem as a refinement over the random assumption. We follow the argument given in Fowler and Guggenheim[6] for monolayers, and, for simplicity, we refer here to a simple cubic lattice with vertical building[11] in the lattice.

Using the same notation as above, the partition function is

$$Q=\sum_{X_1}\cdots\sum_{X_{n-1}}\sum_{\mathfrak{N}}\{g(\mathfrak{N},N,X_1,\cdots,X_{n-1},B)\times\exp(\epsilon_L\mathfrak{N}/3kT)\times[j_s\exp(\epsilon_1/kT)]^{X_1}j_L{}^{N-X_1}\},\quad(27)$$

where, for given values of $N, X_1, \cdots, X_{n-1}$ and B, $g(\mathfrak{N}, N, X_1, \cdots, X_{n-1}, B)$ is the number of distinguishable configurations having $\mathfrak{N}$ pairs of nearest neighbors. We define

$$\bar{\mathfrak{N}}(N,X_1,\cdots,X_{n-1},B,\epsilon_L/kT)$$

and

$$\mathfrak{N}'(N,X_1,\cdots,X_{n-1},B,\epsilon_L/kT)$$

by the following equations:

$$\bar{\mathfrak{N}}\sum_{\mathfrak{N}}g(\mathfrak{N},N,X_1,\cdots,X_{n-1},B)\times\exp(\epsilon_L\mathfrak{N}/3kT)=\sum_{\mathfrak{N}}\mathfrak{N}g(\mathfrak{N},N,X_1,\cdots,X_{n-1},B)\times\exp(\epsilon_L\mathfrak{N}/3kT),\quad(28)$$

$$\sum_{\mathfrak{N}}g(\mathfrak{N},N,X_1,\cdots,X_{n-1},B)\exp(\epsilon_L\mathfrak{N}/3kT)=\frac{\exp(\epsilon_L\mathfrak{N}'/3kT)B!}{(B-X_1)!(X_1-X_2)!\cdots(X_{n-1}-X_n)!X_n!},\quad(29)$$

where

$$X_n=N-(X_1+\cdots+X_{n-1})\quad(30)$$

$$\sum_{\mathfrak{N}}g(\mathfrak{N},N,X_1,\cdots,X_{n-1},B)=\frac{B!}{(B-X_1)!\cdots(X_{n-1}-X_n)!X_n!}.$$

We see from Eqs. (27) and (29) that

$$Q=\sum_{X_1}\cdots\sum_{X_{n-1}}\left\{\frac{[j_s\exp(\epsilon_L/kT)]^{X_1}j_L{}^{N-X_1}B!\exp(\epsilon_L\mathfrak{N}'/3kT)}{(B-X_1)!(X_1-X_2)!\cdots(X_{n-1}-X_n)!X_n!}\right\}.\quad(31)$$

One can also show, as usual, that

$$\bar{\mathfrak{N}} = -T^2 \frac{\partial(\mathfrak{N}'/T)}{\partial T}, \tag{32}$$

and that the contribution of the molecular interactions to the free energy is $-\epsilon_L \mathfrak{N}'/3$ and the contribution to the internal energy is $-\epsilon_L \bar{\mathfrak{N}}/3$. If $\bar{\mathfrak{N}}$ (and therefore $\mathfrak{N}'$) is independent of temperature, $\bar{\mathfrak{N}} = \mathfrak{N}'$. $\bar{\mathfrak{N}}$ is the ordinary statistical average value of $\mathfrak{N}$.

On the random assumption, $\bar{\mathfrak{N}}$ is independent of temperature, $\bar{\mathfrak{N}} = \mathfrak{N}'$, and hence Eq. (7) was used correctly. But the correct equation of more general validity is Eq. (31).

Equations (8) and (11) give the random approximation to $\bar{\mathfrak{N}}$ for the case we are discussing. The average number of horizontal interactions in the first layer is $2B\theta_1^2$, where $\theta_i = X_i/B$. The quasi-chemical method[6] gives, as a better approximation,

$$\bar{\mathfrak{N}}_1 = 2B\theta_1^2[1], \tag{33}$$

$$[i] = \frac{\beta_i - 1 + 2\theta_i}{\theta_i(\beta_i + 1)}, \tag{34}$$

$$\beta_i = \{1 - 4\theta_i(1-\theta_i)[1 - \exp(\epsilon_L/3kT)]\}^{\frac{1}{2}}. \tag{35}$$

The ratio R_1 of the refined to the crude value is $R_1 = [1]$. When $\epsilon_L/kT = 0$, $\beta_1 = [1] = R_1 = 1$. The X_2 molecules of the second layer are distributed on top of the X_1 molecules of the first layer. In the case of attraction ($\epsilon_L/kT > 0$) there is a tendency for the first layer molecules to cluster (horizontally), according to Eq. (33). Therefore, even if the second layer molecules were distributed completely at random on the available sites (the first layer molecules), the same clustering factor $[1]$ would persist in the second layer. But we do not expect a random distribution of X_2 on X_1; there should be an additional tendency to cluster due to the interactions between the X_2 molecules themselves. We assume that the correcting factor, in analogy with the situation in the first layer, is $R_2 = [2]$. Extending this type of argument (it applies for any value of ϵ_L/kT), we find, in place of Eq. (8),

$$\bar{\mathfrak{N}} = 2B\theta_1^2[1] + 2B\theta_2^2[1][2] + \cdots + 2B\theta_n^2[1][2]\cdots[n] + N - X_1. \tag{36}$$

In order to be consistent, in the case of adsorption between two parallel walls, we should assume a quasi-chemical equilibrium in counting the number of vertical pairs of nearest neighbors between the n-th and $(n+1)$-th layers. On applying the quasi-chemical argument to this system of sites and occupied sites, one finds that the number is $B\theta_n^2[n]$. So for capillary adsorption, we add $\frac{1}{2}B\theta_n^2[n]$ to $\bar{\mathfrak{N}}$ in Eq. (36).

The next step is to obtain $\mathfrak{N}'$ from $\bar{\mathfrak{N}}$ by integrating Eq. (32). One then substitutes $\mathfrak{N}'$ into Eq. (31) to obtain Q. Q is then used as before. Unfortunately, it appears that these steps can be carried out explicitly only for the very simplest cases.

THE JOURNAL OF CHEMICAL PHYSICS VOLUME 15, NUMBER 11 NOVEMBER, 1947

The Infra-Red Absorption Spectrum and Vibrational Frequency Assignment of Ketene

W. R. HARP, JR. AND R. S. RASMUSSEN
Shell Development Company, Emeryville, California

(Received June 2, 1947)

The infra-red absorption spectrum of ketene from 2μ to 15μ has been determined and a complete frequency assignment deduced. All the harmonic bands can be simply interpreted on this assignment. The fine structure of the 925-cm^{-1} band is discussed.

I. INTRODUCTION

KETENE is a simple and interesting molecule and one for which a complete frequency assignment should be possible. In spite of this, there is available very little spectroscopic information for ketene. The Raman spectrum of the liquid has been determined by Kopper[1] and the infra-red spectrum of the vapor under low resolution by Gershinowitz and Wilson.[2] The lack of more data is probably due to the difficulty of obtaining and maintaining a pure sample of ketene free from the dimer. The 2μ–15μ infra-red absorption spectrum of ketene (vapor), recorded under higher resolution than the earlier work, is reported here, along with a vibrational frequency assignment.

II. EXPERIMENTAL DETAILS

The sample of ketene used for this study was prepared in these laboratories. The method of preparation was essentially that of Rice, et al.[3] The preparation here differed from theirs in that the final purification in a vacuum-jacketed column was omitted. Instead, the product was rapidly vaporized through a long, water-cooled, spiral condenser (to remove unreacted acetone) into a dry-ice acetone-cooled receiver. The above procedure was repeated and about the middle third of the material was collected and used for these studies.

The sample container was kept at dry-ice acetone or liquid-nitrogen temperature except when sampling. Before the first vapor sample was taken into the absorption cell, the sample container was slowly warmed and the first material to vaporize was discarded until about three-fourths of the sample remained. This was done to eliminate any remaining ethylene dissolved in the ketene. No vapor sample was allowed to remain in the absorption cell for more than about an hour, so that several samples were taken to obtain the complete absorption spectrum.

The spectrograph used was an automatic-recording rocksalt-prism instrument,[4] evacuated to eliminate CO_2 and H_2O vapor absorption. The length of the absorption cell was 15 cm. The wave-lengths are reproducible to within $\pm 0.01\mu$ for λ greater than 5μ. For wave-lengths shorter than 5μ, the reproducibility is somewhat less, becoming about $\pm 0.02\mu$ at 3μ. These reproducibilities are indicated by calibration check runs on ammonia, ethylene, and carbon dioxide. The absolute accuracy of the wave-lengths depends on the proper correlation of absorption maxima in spectra of these same vapors with published grating values, allowing for the differences in resolution between instruments. Since some effort was made to do this well, it is probable that the absolute error is very nearly the same as the reproducibility error. The spectral intervals subtended by the slits (twice the "spectral-slit widths") are indicated on the spectrum (Fig. 1). The accuracies of the intensities shown may be no better than ± 10 percent in transmission units, but the relative intensities are probably much better. Transmission values shown in Fig. 1 are taken from a single recording at each pressure.

III. EXPERIMENTAL RESULTS

The observed wave-lengths, frequencies, and intensities of infra-red absorption maxima are given in Table I.

[1] H. Kopper, Zeits f. physik. Chemie **B34**, 396 (1936).
[2] H. Gershinowitz and E. B. Wilson, Jr., J. Chem. Phys. **5**, 500 (1937).
[3] F. O. Rice, J. Greenberg, C. E. Waters, and R. E. Vollrath, J. Am. Chem. Soc. **56**, 1760 (1934).
[4] R. R. Brattain, Phys. Rev. **60**, 164 (1941).

The initial spectrum (300 mm) showed bands at 5.74μ and 8.25μ which by their positions and shapes suggested an impurity of acetone, the two strongest bands in the acetone spectrum being at these wave-lengths. A recheck of these regions with a new sample showed the two bands to be much reduced in intensity, but still present. Hence, it is highly probable that the bands arise from adventitious acetone, and the dotted portions of Fig. 1 in the 5.5μ–6.0μ and 8.1μ–8.4μ regions indicate the probable absorption curve with the acetone eliminated. The source of this impurity is uncertain, since if acetone were present in the ketene sample it should have remained behind when the ketene was taken off.

Two of the fine-structure peaks, at 9.94μ and 11.22μ, are anomalous in that they are relatively stronger in the 300 mm spectrum than in the 100 mm one. Since the two strongest bands of liquid diketene[5] are near 9.93μ and 11.43μ, it is probable that these anomalous intensities arise from a trace of this compound which was formed during the high-pressure run and which distorted the ketene spectrum in these regions. The amount of dimer formed in the lower-pressure runs would be expected to be negligible, assuming second-order kinetics. The probable true absorption curve in the 10μ and 11μ regions due to ketene alone is indicated by the dotted lines in Fig. 1.

The remainder of the spectrum is presumably due to ketene only. In particular, no indications of ethylene or methane are present. Ethylene would show bands near 5.3μ and 6.9μ, and methane near 7.6μ. The strongest band of ethylene has a strong, sharp Q branch at 10.52μ, which in principle could account for the peak at this position in the ketene spectrum. However, this peak fits in well with the other maxima in the region and is not anomalously intense, so there is no need to adduce ethylene impurity to explain it.

Although acetylene has never been noted as an impurity of ketene, the moderate band at the unusual position, 3.07μ, was suggestive of this compound. However, lack of absorption at 7.67μ,

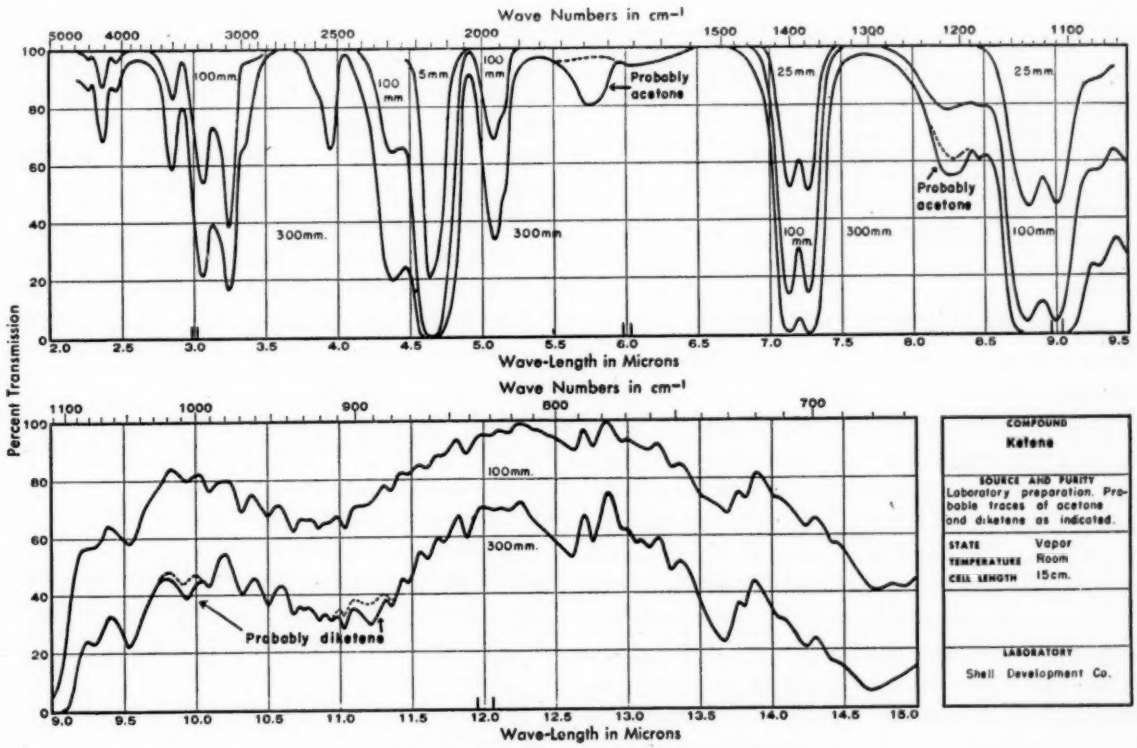

FIG. 1. Absorption spectrum of ketene vapor.

[5] Unpublished work of this laboratory; also, very recently, D. H. Whiffen and H. W. Thompson, J. Chem. Soc. (Lond.) 1005 (1946).

TABLE I. Wave-lengths, frequencies, and intensities of infra-red absorption maxima of ketene vapor.

λ(μ)	ω(cm⁻¹)	Intensity cell:150 mm press.:100 mm	λ(μ)	ω(cm⁻¹)	Intensity cell: 150 mm press.: 100 mm
2.27	4405	0	9.94***	1006	
2.365	4230	1	10.10	990	
2.455	4075	0	10.33	968	
2.85	3510	1	10.505	952	
3.065	3265	4	10.685	936	
3.245	3080	6	10.75	930	
~3.36	~2975	0	10.86	921	
~3.84	~2605	0s	10.95	913	
3.94	2540	1	11.04	906	3
4.37	2290	3s	11.22***	891	
4.64	2155	10	11.36	880	
5.085	1967	3	11.48	871	
~5.15	~1940	1s	11.62	861	
~5.74*	~1740	0	11.73	853	
~6.05	~1655	0	11.89	843	
7.135	1402	8	12.06	829	
7.265	1376		12.18	821	
~8.24**	~1215	2	~12.4	~805	0s
8.46	1182	0	12.62	792	1
8.80	1136	9	12.765	783	1
9.00	1111		12.97	771	
~9.30	~1075	3	13.07	765	
9.54	1048		13.15	760	
~9.72	~1030	0s	13.31	751	
			~13.52	~740	
			13.68	731	2
			13.81	724	
			~14.04	~710	
			~14.43	~695	
			14.72	679	
			14.94	669	

* Probably due to acetone.
** Probably due in part to acetone.
*** Probably due in part to diketene.
s shoulder on adjacent stronger band.

and lack of the very sharp Q branch at 13.69μ, precludes explaining the 3.07μ band as due to acetylene.

IV. FREQUENCIES OF KETENE

In accordance with well-understood structural principles, the ketene molecule may be assigned to the symmetry group C_{2v}. That is, there are one two-fold rotation axis and two vertical reflection planes, mutually perpendicular and passing through the axis. The molecular vibrations of ketene then fall into four representations with the symmetry characteristics shown in Table II. Selection rules permit the appearance of all four classes in the Raman and of all but the A_2 class in the infra-red. However, since there are no fundamental vibrations of the ketene molecule of representation A_2, all the fundamental vibrations should appear in both the infra-red and Raman spectra.

Since the molecule is very nearly a symmetrical rotator, all vibrations of the A_1 representation correspond to parallel bands, and vibrations of the B_1 and B_2 representations to perpendicular bands. The least moment of inertia is so low[6] that the parallel-type bands should have nearly the appearance of linear-molecule parallel bands, i.e., show marked P and R branches, but only a very weak Q branch.[7] The $P-R$ separation should be about 23 cm^{-1}. The perpendicular bands should appear as structureless rounded bands (if unresolved) or as equally spaced P_Q and R_Q branches ($\Delta J=0$, $\Delta K=\pm 1$) with the $\Delta J=\pm 1$, $\Delta K=\pm 1$ transitions furnishing an effectively continuous background (if partially resolved).

For bands short of 6μ, the spectrograph used did not have sufficient resolution to distinguish the true envelopes of the bands. However, of the longer wave-length bands, it is clear that the pairs of peaks at 7.13μ–7.27μ, 8.80μ–9.00μ, and probably also 9.31μ–9.55μ, represent A_1 (parallel) bands. The $P-R$ separations of these are 26, 25, and 27 cm^{-1}, respectively, which are in satisfactory agreement with the value calculated above on the simple theory. The series of peaks between 9.8μ and 12.0μ undoubtedly are attributable to a B_1 or B_2 (perpendicular) band. The region from 12.0μ to 15μ presents a confused aspect, consisting of very irregularly spaced and almost randomly intense maxima. Since there is reason to believe that one of the fundamentals of the perpendicular type lies at 16.7μ (see below), the most reasonable interpretation of this region is that it is a superposition of a weak perpendicular band (of type B_2 and hence with a weak Q branch appearing as the peak at 13.68μ) on the short-wave side of a strong band with center near 16.7μ. The lack of a rudimentary Q branch in the 10.8μ perpendicular band is some indication that this band is of the B_1 type, the dipole change being along the intermediate axis of inertia.

In Table III are shown the infra-red band centers and symmetry types, as discussed above. The centers of the unresolved bands are taken as the absorption maxima, of the parallel bands as the midpoint between the P and R branches,

[6] The moments calculated from the C=C and C=O distances given by J. Y. Beach and D. P. Stevenson, J. Chem. Phys. **6**, 75 (1938) and the assumption of 120° hydrogen angles and a 1.06A C—H distance, are 1.71, 124.0, and 125.7 at.wt. units × A².

[7] S. L. Gerhard and D. M. Dennison, Phys. Rev. **43**, 197 (1933).

and of the 11μ perpendicular band as 10.8μ. The Raman spectrum given by Kopper is also shown. The line at 998 cm^{-1} was questioned by Kopper, since it appeared only on one plate. The 801 cm^{-1} shift was thought by Kopper to be due to impurity of acetone. The present authors further question the line at 1344 cm^{-1}. As will be seen below, this cannot be attributed to a ketene fundamental nor to any overtone or combination. Since one of the expected impurities is ethylene, and since the strongest Raman line of ethylene vapor is at 1342 cm^{-1},[8] it is reasonable to attribute the line to this impurity.

V. VIBRATIONAL ASSIGNMENT

In Table IV are given the types and symmetries of the various fundamental vibrations. It is clear that the very strong infra-red band at 2155 cm^{-1} represents one of the double-bond stretching vibrations, since mechanical interaction between the adjacent double bonds should result in a large shift out of the customary double-bond region ($\sim$6μ). The analogous band in allene is found at 1980 cm^{-1}.[9] The lack of a corresponding strong Raman line is somewhat curious. The only Raman line in the vicinity is a weak one at 2049 cm^{-1}, and if this is to be correlated with the 2155 cm^{-1} infra-red band the shift must be attributed to a large liquid-vapor effect. Since the vibration is essentially an antisymmetrical combination of the two stretching vibrations, the weakness of the Raman line must arise from the near equality of the polarizability *vs.* bond-length function for the two bonds, since for a molecule symmetrical in the stretching coordinates the line would be forbidden.

The other double-bond stretching vibration, essentially the symmetrical combination of the individual bond stretchings, may be assigned as the 1124 cm^{-1} frequency. This corresponds to the strongest Raman line (1130 cm^{-1}), and the infra-red band is of the correct symmetry. The analogous frequency of allene is at 1069 cm^{-1}.[9]

The HCH-bending frequency, expected to be in the 1400 cm^{-1} region by analogy with other organic molecules, is clearly assignable to the 1391 cm^{-1} infra-red band and 1386 cm^{-1} Raman line. The two CH-stretching frequencies are assignable to the 3080 cm^{-1} infra-red band (B_1) and the infra-red and Raman frequency near 2950 cm^{-1} (A_1). The only Raman line corresponding to the infra-red 3080 cm^{-1} band is that at 3015 cm^{-1}, the large shift being ascribable to an anomalously large liquid-vapor effect. The symmetry characters appended are assumed from the usual observation that the symmetric CH stretching frequencies are lower than the antisymmetric.

The assignment of the remaining vibrations—the two CH_2-wagging and two CCO-bending motions—is not so clearcut. These are all perpendicular motions, and are expected to be of considerably lower frequency than those discussed

TABLE II. Symmetry designations for ketene.

Representation	Rotation about 2-fold axis	Reflection through plane of hydrogen atoms	Reflection through plane perpendicular to plane of hydrogen atoms
A_1	+	+	+
A_2	+	−	−
B_1	−	+	−
B_2	−	−	+

TABLE III. Infra-red and Raman frequencies (in cm^{-1}) of ketene.

Infra-red (vapor) ω	symmetry	Raman (liquid) ω	Assignment
		510(1b)*	Fundamental} C=C=O bending
		599(1/2b)	Fundamental}
731(2)	B_2	715(1/2b)	Fundamental; CH_2 out-of-plane wagging
		801(1/2b)	Probably acetone impurity
925(3)	Prob. B_1		Fundamental; CH_2 in-plane wagging
		998(1)	Probably spurious
1062(3)	A_1		2×510=1020
1124(9)	A_1	1130(6b)	Fundamental; C=C=O stretching
1182(0)	?		P branch of 1198
		1198(1)	2×599=1198
1215(2)	?		R branch of 1198
		1344(2)	Probably ethylene impurity
1391(8)	A_1	1386(1b)	Fundamental; HCH bending
~1655(0)	?		1124+510=1634
		1895(1/2)	1124+731=1855
~1940(1s)	?		1391+510=1901
1967(3)	?		1391+599=1990**
2155(10)	NR	2049(1/2b)	Fundamental; C=C=O stretching
2290(3s)	NR		1391+925=2326; 2×1124=2248
2540(1)	NR		1391+1124=2515
~2605(0s)	NR		1391+2×599=2589
~2975(0)	NR	2952(5)	Fundamental; A_1 CH stretching**
3080(6)	NR	3015(4b)	Fundamental; B_1 CH stretching**
3265(4)	NR		2155+1124=3279
3510(1)	NR		2155+1391=3546
4075(0)	NR		2965+1124=4089
4230(1)	NR		3080+1124=4204; 2×2155=4310
4405(0)	NR		2965+1391=4356; 3080+1391=4471

NR=not resolved.
s=shoulder on adjacent stronger band.
* A value of 530 cm^{-1} for the vapor-phase value gives a better fit for the overtones.
** Assignments incorrect; see note added in proof at end of paper.

[8] See G. Herzberg, *Infra-red and Raman Spectra of Polyatomic Molecules* (D. Van Nostrand Company, Inc., New York, 1945), p. 326.
[9] J. W. Linnett and W. H. Avery, J. Chem. Phys. 6, 686 (1938).

above. It is on this basis that the 1344 cm^{-1} Raman line was attributed to an impurity, since it cannot be explained as a fundamental or as an overtone (see discussion of overtones below). There are four observed frequencies capable of being assigned to these fundamentals: the Raman shifts at 510 and 599 cm^{-1}, and the infra-red bands at 731 (Raman: 715 cm^{-1}) and 925 cm^{-1}. The lack of lower frequencies is significant, since if no fundamentals are less than 510 cm^{-1} then none of these four can be interpreted as a harmonic, nor with any probability as a difference band. Hence, the four may be taken as the most reasonable values for the remaining four fundamentals. The frequency at 599 cm^{-1} is the probable source of the infra-red band giving rise to the increasing absorption toward the long-wave end of the spectrum.

Assignment of these four frequencies as the remaining fundamentals receives some confirmation from a consideration of the overtone and combination bands. The 1062 cm^{-1} infra-red band (symmetry A_1) can be assigned as 2×510. Assuming the symmetries of the 731 and 925 cm^{-1} bands to be B_2 and B_1, respectively, as discussed earlier, the symmetries of the two lowest frequencies must be B_1 and B_2, and hence their combination should be inactive (representation A_2). The first overtone of the 599 cm^{-1} frequency fits very well as the 1198 cm^{-1} Raman line and the pair of infra-red maxima at 1182 and 1215 cm^{-1}, assuming these to be the P and R branches of an A_1 band at 1198 cm^{-1}.

On the basis of the set of fundamentals deduced above it is possible to explain satisfactorily all the other overtone bands, as shown in Table III. Only one of these, the very weak shoulder at 3.84μ (2605 cm^{-1}), needs to be assigned as a third harmonic. Since there are relatively few fundamentals, the fact that such an assignment can be made is good support for the assignment. All the stronger overtones contain at least one component fundamental of high intensity.

TABLE IV. Symmetry classes of vibrations for ketene (C_{2v} symmetry).

Type of vibration	A_1	A_2	B_1	B_2	Expected region (cm^{-1})
1 C=C stretching	1	0	0	0	1000–2000
1 C=O stretching	1	0	0	0	
2 C—H stretching	1	0	1	0	3000
2 C=C=O bending	0	0	1	1	<800
1 HCH bending	1	0	0	0	1400
2 CH_2 wagging	0	0	1	1	700–1000

One further slight modification in the assignment will be made. As noted above, the 1062 cm^{-1} infra-red band is best accounted for as 2×510. Since the difference here is much too large to be ascribable to anharmonicity only, it is probable that the fundamental frequency for the vapor molecule is near 530 cm^{-1}, and the difference between this and the observed Raman line at 510 cm^{-1} is a liquid-vapor shift. In this connection, the large liquid-vapor shift on the 2155 cm^{-1} and 3080 cm^{-1} bands may be pointed out (see above). Use of 530 cm^{-1} as the true value of the fundamental gives a much better fit on all the other overtones involving this frequency. Hence, the finally deduced set of fundamental frequencies is: 530(B_1 or B_2), 599(B_2 or B_1), 731(B_2), 925(B_1), 1124(A_1), 1391(A_1), 2155(A_1), 2960(A_1), 3080(B_1). Using these, all sixteen second harmonic bands assigned in Table III fit the calculated sums to 1 percent on the average, and in the worst case (1895 cm^{-1} assigned as 1124+731 =1855) to 2.7 percent.

There remains the question as to which pair of the four lowest frequencies (530, 599, 731, 925 cm^{-1}) corresponds essentially to the CCO bending vibrations and which pair to the CH_2 wagging vibrations. As analogous cases for the skeletal bending frequencies of an X=C=Y system, we may consider carbon dioxide and allene. For the former this frequency is at 667 cm^{-1},[10] and for the latter 353 cm^{-1}.[9] The large difference may be due either to differences in the inherent deformability of the C=C and the C=O systems or to the resonance in CO_2 (resonance structures of the type $^{(-)}O—C\equiv O^{(+)}$). In either case ketene should be intermediate, since from the electron-diffraction determination of the double-bond distances in ketene, considerable resonance with structure $^{(+)}O\equiv C—C^{(-)}H_2$ is indicated (Stevenson and Beach, ref. 6). Hence, the pair of frequencies in ketene at 530 and 599 cm^{-1} may be assigned to the skeletal bending vibrations, the splitting being due to the loss of symmetry occasioned by the CH_2 group. The 731 and 925 cm^{-1} bands are then to be assigned to the CH_2 vibrations, and may be compared with the analogous frequencies

[10] D. M. Dennison, Rev. Mod. Phys. **12**, 175 (1940).

in allene[9,11] (845 and 1030 cm^{-1}) and in formaldehyde[12] (1165 and 1278 cm^{-1}).

VI. FINE STRUCTURE OF THE 925 cm^{-1} BAND

The only band whose fine structure is free enough of interference to be discussed is that near 925 cm^{-1}; the 731 cm^{-1} band is too badly overlaid by the lower-frequency band (599 cm^{-1}) to be interpretable.

Although the resolution is not sufficient for any definitive study of the band, it is clear that the sub-band Q branch spacings exhibit the convergence phenomenon first discussed by Nielsen in connection with formaldehyde,[13] and later beautifully illustrated by Thompson and Harris in the spectrum of allene.[11] The spacing at the high-frequency end of the band is about 16 cm^{-1}, and at the low frequency end 9 cm^{-1}, the convergence to low frequencies being due presumably to Coriolis interaction with the nearby 731 cm^{-1} band. The situation is not so simple as with the allene case, however, where the intermediate spacing near the band center was very nearly that indicated by the simple symmetric-rotator theory, $(I_c^{-1}+I_A^{-1})h/4\pi^2$. For ketene the simple theory predicts a spacing of $\sim$19 cm^{-1} (i.e., about twice that of allene, from the twofold reduction in off-axis hydrogen nuclei). The observed spacing is less than this over the whole band, indicating some further vibration-rotation interaction, which is apparently absent in the allene[11] and formaldehyde[13] spectra. The band is anomalous also in that the intermediate spacing (i.e., that midway between the limiting spacings at the band ends), which is about 13 cm^{-1}, does not occur at the band center as judged by the intensity maximum (925 cm^{-1}), but is displaced to about 890 cm^{-1}.

VII. THE C=C AND C=O BOND-STRETCHING FORCE CONSTANTS

In view of recent interest in the polarities and other bond characteristics of the double bonds in ketene,[14,15] some consideration has been given to the bond-stretching force constants. However, it seems clear from the discussion given below that the infra-red spectrum is incapable of furnishing reliable information on the bond orders.

TABLE V. Double-bond-stretching force constants, in dynes/cm.

Molecule	C=C constant	C=O constant	Interaction constant
$H_2C=CH_2$	$10.87\cdot10^5$	...	...
$H_2C=C=CH_2$	9.59	...	$-0.12\cdot10^5$
$H_2C=C=O$	9.70	$13.43\cdot10^5$	(−0.12)
$H_2C=C=O$	8.30	15.75	(0.61)
$H_2C=C=O$	7.65	17.26	(1.33)
$O=C=O$	...	15.52	1.33
$H_2C=O$	...	13.48	...

Calculations were made on ethylene and allene (as examples of pure CC double bonds), formaldehyde (as an example of a typical ketonic or aldehydic CO double bond), carbon dioxide, and ketene. The CH_2 group was treated as a point mass of weight 14. Observed fundamental frequencies were used throughout rather than true harmonic frequencies, since sufficient data for determining the latter are not available for all molecules considered. The double-bond stretching frequencies of ethylene (1623 cm^{-1})[8] and formaldehyde (1750 cm^{-1})[12] lead immediately to the force constants shown in Table V. The other three molecules (allene, ketene, and carbon dioxide) are linear and triatomic under the assumptions used. The complete quadratic potential function for the parallel vibrations is then,

$$2V=K_1\Delta r_1^2+K_2\Delta r_2^2+2k\Delta r_1\Delta r_2.$$

For allene and carbon dioxide the molecular symmetry requires $K_1=K_2$, so that the two constants shown in Table V were determinable from the two observed frequencies (allene: 1071, 1980 cm^{-1};[16] carbon dioxide: 1337, 2349 cm^{-1} [17]). It is seen that the allene C=C constant is less than that of ethylene; whether this represents an actual difference in bond character, or whether it is spurious and the result of ignoring the hydrogen motions, is not known. The interaction constant between the two bonds is satisfactorily small. The C=O constant of CO_2 is appreciably greater than that of formaldehyde, which fact has been often pointed out as evidence for the partial triple-bond character of the bond in CO_2. The

[11] H. W. Thompson and G. P. Harris, Trans. Faraday Soc. **40**, 295 (1941).
[12] E. S. Ebers and H. H. Nielsen, J. Chem. Phys. **6**, 311 (1938).
[13] H. H. Nielsen, J. Chem. Phys. **5**, 818, 822 (1937).
[14] N. B. Hannay and C. P. Smyth, J. Am. Chem. Soc. **68**, 1357 (1946).
[15] A. D. Walsh, J. Am. Chem. Soc. **68**, 2408 (1946).
[16] See reference 8, p. 339.
[17] See reference 8, p. 173, Table 41.

CO_2 interaction constant is rather large, which is perhaps not unexpected since the participation of the various resonance structures will be altered on changing one of the CO distances, and this in turn will affect the potential energy function of the other bond.

In applying the above potential function to ketene, it is clear that some assumption must be made about the magnitude of the interaction constant k, since the two observed frequencies (1124 cm^{-1}, 2155 cm^{-1}) must be used to determine the principal constants. Furthermore, the principal constants obtained depend strongly on the choice of k. Table V shows this dependence, with k assumed to have the same value as in allene, as in carbon dioxide, and as an average of these. The C=O stretching constant can be made to vary from a value essentially the same as that of formaldehyde to a value greater than that of CO_2. In the absence of any *a priori* choice for k, about all that can be said is that it is probably stronger than the bond of formaldehyde. The C=C bond turns out to be equal to or more probably weaker than the bond in allene.

ACKNOWLEDGMENTS

The authors wish to thank Dr. D. S. Melstrom and Mr. R. T. Holm for preparation of the ketene, and Mr. H. F. Gray, Jr. for assistance in the force-constant calculations. They also acknowledge the assistance of Mrs. Z. Alcorn and Miss R. Hatch in operating the spectrograph and drawing the absorption curve.

Note Added in Proof: A paper on this same subject by Halverson and Williams[18] appeared after submission of this manuscript. Because of the increased resolution afforded by a lithium fluoride prism, these authors obtained results which necessitate modification of two of the assignments proposed above. However, the assignment of one of the fundamentals by Halverson and Williams in a different manner from that proposed above is felt by the present authors to be questionable, and is discussed below.

The two assignments of our Table III which must clearly be modified are: (1) the B_1 CH stretching frequency must be placed at 3162 cm^{-1} and the A_1 at 3066 cm^{-1}, as assigned by Halverson and Williams (our resolution was insufficient to disclose the weak perpendicular band at 3162 cm^{-1}); (2) the band at 1967 cm^{-1} cannot be attributed to the combination 1391 (A_1)+599 (B_1 or B_2), since Halverson and Williams show this band to be parallel (A_1).

The assignment which remains in question is that of one of the CH_2 wagging vibrations. In the region where the two CH_2 wagging frequencies are to be expected, there occur two noticeable bands (731 and ~925 cm^{-1}), the spectrum obtained by ourselves agreeing with that of Halverson and Williams throughout this region. There is agreement that one of these fundamentals is at ~925 cm^{-1} Halverson and Williams explained the 731 cm^{-1} band as due to an impurity, on the basis of the persistence of a band at this position when the ketene was allowed to polymerize on long standing; and placed the other fundamental at 1011 cm^{-1}, principally on the consideration that a band near 1000 cm^{-1} is necessary to account for 1967 cm^{-1} as an overtone of A_1 symmetry. There are, however, three objections to be raised to this assignment. Firstly, the spectrum itself shows no indications of a distinct band near 1011 cm^{-1}, the peaks in the region being ascribable to the fine structure of the ~925 cm^{-1} band. This in itself is not a strong point, since one of the allowed ethylene bands is extremely weak and difficult to observe. Secondly, there exists a Raman line at 715 cm^{-1} which can be correlated with the infra-red 731 cm^{-1} band as a fundamental, but is not explained at all on Halverson and Williams' assignment. Thirdly, the present authors are of the opinion that the 731 cm^{-1} infra-red band is not due to impurity, since particular efforts, which were adequately but not wholly successful, were made to avoid polymers or other impurities. The most likely polymeric impurity, diketene, was either absent or present in only very small amounts as attested by the weakness of bands at positions where diketene has extremely strong bands. Further, the intensity of the 731 cm^{-1} band relative to other ketene bands was constant within our limits of error in the various spectra we obtained, although we never allowed a sample to remain more than about an hour under observation. The finding by Halverson and Williams of a

[18] F. Halverson and V. Z. Williams, J. Chem. Phys. **15**, 552 (1947).

band at this position in a sample of polymerized ketene may easily be a case of coincidence of bands. In view of these considerations, the authors are inclined to assign ~925 and 731 cm^{-1} as the two CH_2 wagging fundamentals, as was done in the present paper, and to seek some other explanation of the 1967 cm^{-1} band.

As Halverson and Williams have implied, it is not possible to explain the 1967 cm^{-1} band as an overtone, combination, or difference band (other than in the manner criticized above). Also it does not seem possible to explain it as the C=C=O stretching vibration (fundamental: 2155 cm^{-1}) shifted by interaction with an excited low frequency, i.e. a band of the type $(\nu_{C=C=O}+\nu_{low})-\nu_{low}$. Judging from CO_2 and N_2O, the shift to be expected for this reason is only a few cm^{-1}. The most plausible, but not wholly satisfactory, explanation of the 1967 cm^{-1} band is that it is the isotopic analog for the $C^{12}=C^{13}=O^{16}$ molecule of the 2155 cm^{-1} band. The intensity ratio is close to 100:1, exactly as is necessary. However, force-constant calculations based on either the simplified linear-triatomic molecule approximation used in this paper, or on the more extended treatment given by Halverson and Williams, predict an isotopic shift in the neighborhood of 50–100 cm^{-1} instead of the required 200 cm^{-1} shift.

It is clear that further work toward resolving the bands from 700 to 1050 cm^{-1} is needed before an unequivocal assignment can be made.

THE JOURNAL OF CHEMICAL PHYSICS VOLUME 15, NUMBER 11 NOVEMBER, 1947

Hydrodynamic Properties of Sea Water at the Front of a Shock Wave*

J. M. RICHARDSON**
Baker Laboratory, Cornell University, Ithaca, N. Y.

AND

A. B. ARONS*** AND R. R. HALVERSON****
Underwater Explosives Research Laboratory, Woods Hole Oceanographic Institution, Woods Hole, Massachusetts

(Received June 2, 1947)

The Rankine-Hugoniot relations have been applied to appropriate equation-of-state data in order to calculate the propagation velocity, particle velocity, enthalpy increment, Riemann function, etc. at shock fronts of various amplitudes in sea water. One set of tables provides values over a wide pressure range (up to about 80 kilobars) and is principally intended for use in conjunction with theories of propagation of shock waves originated by underwater explosions. A second set of tables contains values which are closely spaced up to pressures of 14 kilobars. These are calculated with somewhat greater precision and are intended for use in connection with experimental measurements of particle and propagation velocities, etc.

I. INTRODUCTION

IT has long been recognized that the velocity of propagation of sound waves of finite amplitude in a fluid medium is a function of the pressure in the wave. Lamb[1] ascribes the early development of the theory to independent investigations of Earnshaw and Riemann. Qualitatively this work indicated that, since the higher pressure portions of a wave travel with greater velocity, an arbitrarily-shaped pressure pulse of finite amplitude must, during propagation, alter its shape in such a manner as to build up into a shock front. By applying the laws of conservation of mass, energy, and momentum to the transfer of matter across the shock front, Rankine and Hugoniot obtained a set of three relations among the five variables: pressure, density, particle velocity (u), shock front

* The work described in this report was performed under National Defense Research Committee Contracts OEMsr-121 with Cornell University and OEMsr-569 with the Woods Hole Oceanographic Institution.

** Present address: Bell Telephone Laboratories, Inc., Murray Hill, N. J.

*** Present address: Department of Physics, Stevens Institute of Technology, Hoboken, N. J.

**** Deceased.

[1] H. Lamb, *Hydrodynamics* (Cambridge University Press, London, 1932) 6th Ed., p. 481.

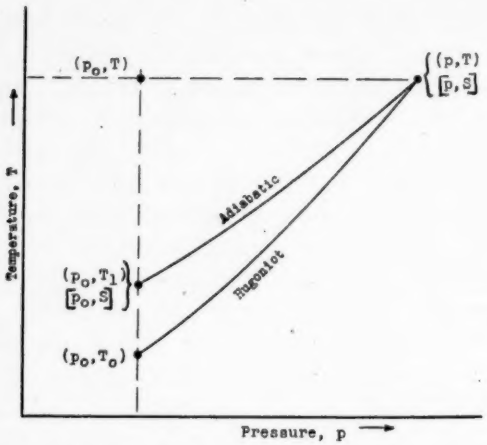

FIG. 1. Adiabatic and Hugoniot contours in $p-T$ plane.

velocity (U), and enthalpy increment (ΔH). These relations, when applied to data on the equation-of-state and specific heat, make it possible to calculate u, U, and ΔH and to evaluate certain other functions applicable to the theory of the formation and propagation of shock waves originated by explosions.[2]

Precise knowledge of u and U also makes it possible to calculate shock wave pressures in cases where the particle velocity or propagation velocity can be measured. The purpose of the calculations described below was to apply the Hugoniot relations to appropriate equation-of-state data for sea water in order to provide (a) tables of the desired functions up to very high pressures (*ca.* 80 kilobars) for use in the theory of propagation of underwater explosion waves,[2] and (b) tables of particle and propagation velocity at fairly close pressure intervals in a lower pressure region (up to *ca.* 14 kilobars).

II. OUTLINE OF THE THEORY AND COMPUTATIONAL PROCEDURES

In this section we give an account of the hydrodynamical and thermodynamical relations, and the computational procedures leading to the numerical results tabulated in Sections III and IV. For the convenience of the reader a glossary of symbols is presented in Appendix III.

When a shock wave advances with velocity U into a stationary fluid of unperturbed pressure p_0 and specific volume v_0, the pressure p, specific volume v, and particle velocity u of the fluid behind the shock front are determined by the Rankine[3]-Hugoniot[4] conditions, which express the conservation of mass, momentum, and energy of an element of fluid passing through the front. For the purposes of this paper, these conditions may conveniently be written

$$u=[(p-p_0)(v_0-v)]^{\frac{1}{2}}, \tag{2.1}$$

$$U=v_0[(p-p_0)/(v_0-v)]^{\frac{1}{2}}, \tag{2.2}$$

$$\Delta H=(1/2)(p-p_0)(v+v_0). \tag{2.3}$$

In the last equation, ΔH is the specific enthalpy increment of an element of fluid when it passes through the front. The specific enthalpy is defined as the sum of the internal energy per gram and the pressure-volume product, pv.

Given equation of state and specific heat data for the fluid, any three of the variables p, v, U and u may be determined as functions of the fourth. Here we shall regard p as the independent variable. For certain hydrodynamic applications we must have, in addition to v, U, and u as functions of p, the sound velocity

$$c=(\partial p/\partial \rho)_S^{\frac{1}{2}}; \quad \rho=1/v, \tag{2.4}$$

the Riemann σ-function†

$$\sigma=\int_{p_0}^{p}[v[p', S]/c[p', S]]dp', \tag{2.5}$$

and the undissipated enthalpy

$$\omega=\int_{p_0}^{p}v[p', S]dp', \tag{2.6}$$

where S is the entropy.

In practice, one must resort to successive approximations to effect a reduction of the Hugoniot conditions, combined with equation-of-state and specific heat data, to a set of relations expressing u, U, and v as functions of p. To this

[2] J. G. Kirkwood and H. Bethe, *The Pressure Wave Produced by an Underwater Explosion* (Dept. of Commerce Bibliography No. PB 32182), OSRD Report No. 588, Part I.

[3] W. J. M. Rankine, Trans. Roy. Soc. London, **A160**, 277 (1870).

[4] H. Hugoniot, J. de l'ecole polyt. **51**, 3 (1887); **58**, 1 (1888).

† The Riemann σ-function occurs in Riemann's form of the hydrodynamical equations, which, for the case of spherical symmetry, may be written (see reference 1):

$$[(\partial/\partial t)+(c+u)(\partial/\partial r)](\sigma+u)=-2cu/r,$$
$$[(\partial/\partial t)-(c-u)(\partial/\partial r)](\sigma-u)=0,$$

where t is the time and r is the radial coordinate. The other quantities have already been defined.

end, it is expedient first to consider certain quantities as functions of pressure and temperature, p and T, or pressure and entropy, p and S. Before proceeding to a more detailed discussion of the calculations it may perhaps help to orient the reader if we consider, qualitatively, contours of some pertinent quantities in the p–T plane. In Fig. 1, the possible states of a given fluid just behind the shock front lie along a single curve, which we have labeled "Hugoniot." An element of fluid initially in the state (p_0, T_0) which has attained a state (p, T) just behind the shock front finally returns to a state (p_0, T_1) along the adiabatic, so labeled in the figure. Also included are the designations of a few points on a p–S basis using square brackets according to the convention introduced in Part b of this section. In general, T_1 is larger than T_0 because of the dissipation occuring at the front. The central part of our problem is the determination of the Hugoniot curve.

We shall consider in Part a the calculations due to Arons and Halverson[5] which are intended to be accurate in the range of relatively low pressure (*ca.* 0 to 20 kilobars). These results as stated in the introduction are intended for the determination of the peak pressure of a shock wave from measured values of the shock front velocity U or particle velocity u. In Part b, we shall consider the calculations of Kirkwood and Richardson,[6] the results of which were originally intended for the applications of the shock wave propagation theory of Kirkwood and Bethe[2] which required data over a higher range of pressures (*ca.* 20 to 50 kilobars).

a. Calculations of Arons and Halverson

Here we outline the calculations[7] suitable for the relatively low pressure range (*ca.* 0 to 20 kilobars) based upon the equation-of-state and specific heat data discussed in detail in Appendix I. For the range 0 to 1.5 kilobars, the Ekman equation-of-state was used; in the range 0 to 25 kilobars, the Tait equation-of-state,

$$v(0, T)-v(p, T)/v(0, T)=(1/n)\log[1+p/B(t)], \qquad t=(T-273.16)°\text{C}. \quad (2.7)$$

In the first case, the initial temperature was $t_0=15°$C; in the second, $t_0=25°$C. In both cases, the initial pressure $p_0=0$. Neither of the two equations-of-state are complete in the sense that $v_0=v(0, T)$ must be determined by auxiliary thermal expansion data (also discussed in Appendix I).

We express the enthalpy and volume increments

$$\begin{aligned}\Delta H&=H(p, T)-H(0, T_0),\\ \Delta v&=v(p, T)-v(0, T_0),\end{aligned} \quad (2.8)$$

in terms of line integrals, first along an isobar from $(0, T_0)$ to $(0, T)$ and, secondly, along an isotherm from $(0, T)$ to (p, T) (see Fig. 1). For the enthalpy increment we obtain

$$\begin{aligned}&\Delta H=\Delta_p H+\Delta_T H,\\ &\Delta_p H=\int_{T_0}^{T} C_p(0, T')dT'=\bar{c}_p\Delta T,\\ &\Delta_T H=\int_0^p\left[v(p', T)-T\frac{\partial v(p', T)}{\partial T}\right]dp',\\ &\Delta T=T-T_0,\end{aligned} \quad (2.9)$$

where $c_p(0, T)$ is the specific heat extrapolated to zero pressure and $\bar{c}_p$ is the mean of c_p over the temperature range ΔT.

For the volume increment we obtain

$$\begin{aligned}&\Delta v=\Delta_p v+\Delta_T v,\\ &\Delta_p v=v(0, T)-v(0, T_0)=\bar{\beta}_0\Delta T,\\ &\Delta_T v=v(p, T)-v(0, T),\end{aligned} \quad (2.10)$$

where $\bar{\beta}_0$ is the mean thermal expansion at zero pressure over the temperature range ΔT.

From the last Hugoniot condition, Eq. (2.3), and Eq. (2.9) we obtain

$$\Delta T=\frac{[v(0, T_0)+(1/2)(\Delta_T v)]p-\Delta_T H}{\bar{c}_p-(1/2)(\bar{\beta}_0 p)}, \quad (2.11)$$

where $\Delta_T H$ is to be calculated by means of the third of Eq. (2.9) and the appropriate equation-of-state, and where $\Delta_T v$ is to be obtained from compressibility data. The right-hand side of Eq. (2.11) depends, of course, on the temperature T. The determination of ΔT is accomplished by the method of successive approximations. A trial

[5] A. B. Arons and R. R. Halverson, *Hugoniot Calculations for Sea Water at the Shock Front*, OSRD Report No. 6577, NDRC No. A-469.

[6] J. G. Kirkwood and J. M. Richardson, *The Pressure Wave Produced by an Underwater Explosion, Part III*, OSRD Report No. 813 (Dept. of Commerce Bibliography No. PB 32184).

[7] J. G. Kirkwood and E. Montroll, *Pressure Wave Produced by an Underwater Explosion, II*, OSRD Report No. 676 (Dept. of Commerce Bibliography PB-32183).

TABLE I. $U-c_0/c_0$, u, and ΔH in low pressure region (based on Ekman equation-of-state). Sea water: Initial temperature 15°C; salinity 32 parts per thousand (3.79 wt. percent NaCl); $c_0=4922.8$ ft/sec $=1500.5$ m/sec.

A				B			
$p-p_0$ (kbar)	$\frac{U-c_0}{c_0}$ (%)	u (m/sec)	ΔH (cal/gm)	$p-p_0$ (lb/in²)	$\frac{U-c_0}{c_0}$ (%)	u (ft/sec)	ΔH (cal/gm)
0.00	0.00	0.0	0.0	0	0.00	0.0	0.0
.25	2.07	15.1	5.8	2,000	1.14	29.1	3.2
.50	4.03	31.2	11.5	4,000	2.27	57.6	6.4
.75	5.93	46.2	17.2	6,000	3.35	85.5	9.6
1.00	7.81	60.5	23.0	8,000	4.43	112.9	12.7
1.25	9.65	74.4	28.5	10,000	5.48	139.7	15.9
1.50	11.44	87.7	34.1	12,000	6.53	166.0	19.0
				14,000	7.56	191.8	22.1
				16,000	8.58	217.1	25.2
				18,000	9.59	242.0	28.3
				20,000	10.57	266.5	31.4
				22,000	11.55	290.6	34.5

TABLE II. $U-c_0/c_0$, u, and ΔH in intermediate pressure region (1.5 to 25 kilobars) (based on Tait equation-of-state; $n=7.800$, $B=3.012$). Sea water: Initial temperature 25°C; salinity 32 parts per thousand (3.79 wt. percent NaCl): $c_0=5014.7$ ft/sec $=1528.5$ m/sec.

A				B			
$p-p_0$ (kbar)	$\frac{U-c_0}{c_0}$ (%)	u (m/sec)	ΔH (cal/gm)	$p-p_0$ (lb/in²)	$\frac{U-c_0}{c_0}$ (%)	u (ft/sec)	ΔH (cal/gm)
0.0	0.00	0.0	0.0	0	0.0	0	0.0
1.0	8.18	59.2	23.0	20,000	11.0	258	31.3
1.5	11.88	85.5	34.2	30,000	15.8	375	46.6
2.0	15.39	110.1	45.3	40,000	20.5	483	62.0
2.5	18.71	135.0	56.3	50,000	24.7	584	77.0
3.0	21.88	157.8	67.2	60,000	28.7	676	92.0
4.0	27.84	200.5	88.8	70,000	32.5	767	107.0
5.0	33.39	240.2	110.1	80,000	36.0	853	121.0
6.0	38.59	277.5	131.2	90,000	39.4	937	135.0
8.0	48.13	346.1	172.9	100,000	42.8	1014	150.0
10.0	56.73	408.9	214.0	120,000	49.2	1168	178.0
12.0	64.70	466.9	254.8	140,000	55.2	1312	207.0
14.0	72.25	510.9	295.2	160,000	60.8	1445	235.0
25.0	108.40	769.1	514.4	180,000	66.3	1564	263.0
				200,000	71.5	1662	291.0

value of ΔT is used in evaluating the right-hand side giving a more accurate value of ΔT on the left-hand side, and the process is repeated until the results of two successive steps differ by a sufficiently small amount. One or two steps generally suffice.

We have thus obtained T as a function of p along the Hugoniot curve (see Fig. 1). It is now possible to calculate immediately the particle velocity u, the propagation velocity U, and the specific volume v as functions of p behind the shock front. The results using the Ekman equation-of-state and the Tait equation-of-state are tabulated in Tables I and II, respectively, of Section III.

b. The Calculations of Richardson and Kirkwood

Here we outline the calculations[6] intended for the applications of the shock wave propagation theory of Kirkwood and Bethe.[2] These are based upon the equation-of-state and specific heat data discussed in detail in Appendix II. We use a modified Tait equation-of-state connecting $v(p, T)$ and $v(0, T)$ to be discussed below. In most respects, the data is made to fit the properties of an aqueous 0.7 molal NaCl solution assumed to be roughly equivalent to sea water of salinity $s=32$ parts per thousand (see Section 1 of Appendix I).

In these calculations the initial pressure p_0 is taken to be zero, and several different initial temperatures T_0 are used: 0°C, 20°C, and 40°C.

Before indicating the precise nature of the modification of the Tait equation, it is desirable to mention that in this part two different pairs of independent variables will be used: pressure and temperature (p, T), and pressure and entropy $[p, S]$. Consequently, in order to indicate which pair are used in a function, we will use parenthesis to indicate the first pair and square brackets to indicate the second, i.e. $v(p, T)$ and $v[p, S]$.

The modified form of Tait equation introduced by Kirkwood[2, 6] is

$$\log(v_1/v)=(1/n)\log(1+p/A[S]), \quad (2.12)$$

where

$$v=v[p, S]=v(p, T[p, S]), \quad v_1=v[0, S],$$

(see Fig. 1) n is an empirical constant, and the function $A[S]$ is related to the function $B(t)$ in the original isothermal form of the Tait equation, Eq. (2.7), as follows,

$$A[S]=B(t[0, S]), \quad t=(T-273.16)°\text{C}. \quad (2.13)$$

The reasons for introducing this modification of the Tait equation are at least twofold: (1) the anomaly of a vanishing specific volume $v(p, T)$ at a finite pressure along a given adiabatic (which does not differ markedly from the Hugoniot curve in the case of water) is removed to a higher pressure by replacing $[v(0, T)-v(p, T)]/[v(0, T)]$

TABLE III. Values of $U-c_0/c_0$ for different temperatures and salinities at a shock wave peak pressure of 1.00 kilobar.

Salinity (parts per 1000)	Temperature (°C)	$U-c_0/c_0$ (%)
32	15	7.81
32	25	7.81
35	15	7.76

by $\log(v[0, S]/v[p, S])$, and (2) the calculation of quantities defined by line integrals along adiabatics is greatly simplified by taking S instead of T as one of the independent variables.

The function $A[S]$ is related simply to c_1, the sound velocity at zero pressure and entropy S according to Eq. (2.4) as follows

$$A[S]=c_1^2/nv_1; \quad c_1=c[0, S]. \tag{2.14}$$

On the basis of Bridgman's p–v–T data for pure water, an average value of n equal to 7.15 has been selected for the present calculations. In Section 2 of Appendix II, it is shown that n deviates from this value by less than 4 percent in a large pressure-temperature field bounded by adiabatics starting at zero pressure and temperatures of 20°C and 60°C, respectively, and extending to pressures of 25,000 kg/cm². We assume that n has the same value for an aqueous 0.7 molal NaCl solution as for pure water, and we obtain by interpolation the required values of $B(t)$ from R. E. Gibson's values of $B(t)$ for dilute aqueous NaCl solutions (see Appendix II, Section 1). The appropriate heat capacity and thermal expansion data are discussed in Section 1 of Appendix II.

We now proceed to the calculation of the quantities u, U, c, σ, and ω. We first express these quantities with use of Eq. (2.12) in terms of p,

$$v=v(p, T)=v[p, S], \quad v_0=v(0, T_0),$$

$v_1=v(0, T_1)=v[0, S]$, and $c_1=c(0, T_1)=c[0, S]$ (see Eqs. (2.1)–(2.6), also Fig. 1) as follows:

$$u=[p(v_0-v)]^{\frac{1}{2}}, \tag{2.15}$$

$$U=pv_0/u, \tag{2.16}$$

$$c=c_1(v_1/v)^{(n-1)/2}, \tag{2.17}$$

$$\sigma=\frac{2c_1}{n-1}[(v_1/v)^{(n-1)/2}-1], \tag{2.18}$$

$$\omega=\frac{c_1^2}{n-1}[(v_1/v)^{n-1}-1], \tag{2.19}$$

Once the temperature T_1, to which an element of fluid returns along the adiabatic intersecting the Hugoniot curve at (p, T), is determined, all of the above quantities may be determined as functions of p. To accomplish this, the enthalpy increment, ΔH, occurring in the third Hugoniot condition, Eq. (2.3), is written as the sum of two line integrals, the first along an isobar from $(0, T_0)=[0, S_0]$ to $(0, T_1)=[0, S]$ and the second along an adiabatic from $(0, T_1)=[0, S]$ to $(p, T)=[p, S]$ (see Fig. 1), giving:

$$\Delta H=\omega+h,$$

$$\omega=\int_0^p v[p', S]dp', \tag{2.20}$$

$$h=\int_{S_0}^{S} T[0, S']dS'=\int_{T_0}^{T_1} c_p(0, T')dT',$$

where ω is the undissipated enthalpy already defined by Eq. (2.6) with $p_0=0$ and given explicitly in terms of c_1, v_1, and v in Eq. (2.19). The dissipated enthalpy h can be determined as an explicit function of T_0 and T_1 from specific heat data (Appendix II, Section 1). Combining the third Hugoniot condition, Eq. (2.3), with Eqs. (2.19) and (2.20) we obtain the relation

$$\frac{h}{c_1^2}=\frac{1}{2n}\left[y-\frac{n+1}{n-1}(y^{(1-1/n)}-1)-y^{-1/n}\right]-\frac{v_1-v_0}{2nv_1}(y-1), \tag{2.21}$$

TABLE IV. Properties of sea water at a shock front. (Initial temperature 0°C; salinity 0.7 m NaCl; $C_0=1443$ m/sec.)

p (kilobar)	u (m/sec)	U (m/sec)	c (m/sec)	σ (m/sec)	$\omega\times10^{-6}$ (m/sec)²	h (joule/gm)	v (cm³/gm)
0	0	—	—	0	0	0	0.9915
5	257.0	1930	2190	253.5	0.4565	6.740	.8593
10	433.0	2290	2720	420.5	0.8720	25.80	.8040
15	575.0	2585	3145	552.0	1.270	54.40	.7710
20	697.5	2845	3510	664.0	1.655	86.55	.7483
25	805.5	3075	3835	763.5	2.030	122.5	.7319
30	905.0	3285	4125	855.5	2.405	160.5	.7186
35	997.0	3480	4395	940.5	2.770	201.5	.7075
40	1080	3665	4640	1020	3.140	244.0	.6989
50	1240	4000	5095	1175	3.860	331.0	.6842
60	1385	4300	5495	1315	4.575	419.0	.6728
70	1515	4585	5870	1455	5.285	509.0	.6641
80	1635	4855	6225	1585	6.000	595.5	.6579
90	1740	5120	6570	1705	6.730	676.0	.6542

TABLE V. Properties of sea water at a shock front. (Initial temperature 20°C; salinity 0.7 m NaCl; $C_0=1517$ m/sec.)

p (kilobar)	u (m/sec)	U (m/sec)	c (m/sec)	σ (m/sec)	$\omega\times10^{-6}$ (m/sec)²	h (joule/gm)	v (cm³/gm)
0	0	—	—	0	0	0	0.9929
5	251.0	1975	2230	248.5	0.4595	5.570	.8668
10	425.5	2335	2755	415.5	0.8790	23.45	.8120
15	567.0	2630	3175	549.0	1.280	49.35	.7787
20	689.0	2880	3535	663.0	1.670	80.05	.7555
25	798.0	3110	3855	765.0	2.050	115.0	.7381
30	897.5	3320	4140	859.0	2.425	152.5	.7243
35	990.0	3510	4405	946.5	2.795	192.0	.7130
40	1075	3690	4650	1030	3.160	233.0	.7034
50	1235	4020	5100	1185	3.885	317.5	.6880
60	1380	4325	5505	1330	4.605	404.5	.6765
70	1510	4610	5880	1465	5.320	489.5	.6679
80	1625	4885	6240	1600	6.050	573.5	.6626

TABLE VI. Properties of sea water at a shock front. (Initial temperature 40°C; salinity 0.7 m NaCl.)

p (kilobar)	u (m/sec)	U (m/sec)	c (m/sec)	σ (m/sec)	$\omega \times 10^{-6}$ (m/sec)^2	h (joule/gm)	v (cm^3/gm)
0	0	—	—	0	0	0	0.9993
5	249.5	2005	2255	247.0	0.4630	5.59	.8749
10	423.5	2360	2775	415.0	0.8870	22.75	.8198
51	566.5	2645	3195	550.0	1.290	48.30	.7859
20	689.0	2900	3550	666.5	1.685	78.70	.7621
25	798.5	3130	3865	770.5	2.065	113.5	.7441
30	899.0	3335	4150	866.0	2.445	151.0	.7298
35	992.0	3525	4415	955.5	2.815	189.5	.7179
40	1080	3705	4660	1040	3.185	230.5	.7080
50	1240	4035	5110	1200	3.915	315.0	.6926
60	1380	4340	5515	1345	4.640	400.5	.6813
70	1510	4635	5900	1485	5.370	483.0	.6737

where $y=(v_1/v)^n$. With the aid of tables of n/c_1^2 and v_1 as functions of T_1 and T_0, Eq. (2.21) may be solved by successive approximations giving T_1 as a function of the parameter y. Since the equation of state, Eq. (2.12), may be expressed simply as $p=B(T_1-273.16)[y-1]$, the temperature T_1 may be determined as a function of the pressure p by a tabular elimination of y. By graphical interpolation, T_1 is finally determined for the desired integral values of p (in kilobars), and the functions u, U, c, σ, and ω are then computed as functions of p by means of Eqs. (2.15)–(2.19).

III. NUMERICAL RESULTS OF ARONS AND HALVERSON

In fundamental shock wave studies, it is frequently necessary to know values of $U-c_0/c_0$ and u at given pressure levels to the highest possible degree of accuracy. With this object in view, the calculation methods described in Section 2A were applied to the best available equation-to-state data. The numerical results are given in Tables I and II. A critical discussion of the equation-of-state data will be found in Appendix I together with references to the sources from which they were obtained.

Table I gives results for the "low pressure" region, covering shock wave peak pressures of from 0 to 1.50 kilobars (*ca.* 22,000 p.s.i.). The calculations in this table were based upon the Ekman equation-of-state for sea water (see Appendix I) which is used in the calculation of sound velocity for echo-ranging tables.

Since the Ekman equation deviates appreciably from experimental compressibility data at pressures exceeding 2 kilobars, this equation was abandoned in the "intermediate pressure" region. The results in Table II are applicable principally to the region between 1.5 and 14 kilobars (*ca.* 200,000 p.s.i.) and are based on a careful fit of the Tait equation to Adams's experimental compressibility data (see Appendix I).

Tables I and II were computed for certain specific values of temperature and sea water salinity (equivalent to 0.675 molal NaCl), and it is shown in Table III that the value of $U-c_0/c_0$ is not very sensitive to changes in these variables.

IV. NUMERICAL RESULTS OF KIRKWOOD AND RICHARDSON

In Tables IV to VI, the particle velocity u, the shock front velocity U, the sound velocity c, the Riemann σ-function, the undissipated enthalpy ω, the dissipated enthalpy h, and the specific volume v of sea water (0.7 molal NaCl solution) are presented as functions of pressure p along three Hugoniot curves, starting at zero pressure and the temperatures 0°C, 20°C and 40°C, respectively. These results have been calculated by the procedures of Part b of Section 2 and the data of Appendix II. The results above 30 kilobars represent extrapolations beyond the range of experimental data; consequently the validity of the results above, say, 50 kilobars, is questionable.

In closing this discussion of the calculations, the authors wish to acknowledge their gratitude and appreciation to Professor J. G. Kirkwood of Cornell University for his contributions in initiating the work and in supplying valuable guidance and advice.

APPENDIX I††

1. Salinity and Temperature Conditions

All calculations were made for sea water having a salinity of 32 parts per thousand (the average salinity of sea water at Woods Hole, Massachusetts). Salinity is defined in terms of directly measured chlorinity as:

$$s=0.030+1.8050\ \mathrm{Cl}$$

where s and Cl are expressed in parts per thousand.

It was calculated from the average composition

†† Equation-of-state data used in computation of Tables I and II.

of sea water that (on the basis of *ionic strength*) a salinity of 32 parts per thousand is equivalent to an NaCl solution having a molality of 0.675 or a weight percentage of 3.79 percent NaCl.

Table I was computed for an initial temperature of 15°C because this temperature is a rough average of conditions normally encountered in experimental work. Table II was computed for an initial temperature of 25°C because this was the temperature quoted for the available compressibility data.[8] Table III shows that the results are not sensitive to small variations in temperature and salinity.

2. Specific Volume and Coefficient and Thermal Expansion

The best sources of data seem to be the oceanographical tables of Knudsen.[9] Second power equations in t(°C) were fitted to the data tabulated for $s=32$:

For Table I:

$$v(t)=0.97709+2.05\times10^{-4}(t-15)+4\times10^{-6}(t-15)^2.$$

For Table II:

$$v(t)=0.97956+2.85\times10^{-4}(t-25)+4\times10^{-6}(t-25)^2.$$

3. Heat Capacity

The heat capacity data used in computing Tables I and II are those quoted by S. Kuwahara:[10]

$$C_p=C_{p'}-0.0004226t+0.000006321t^2 \text{ cal./gm°C},$$

TABLE VII. Comparison of experimentally measured sound velocity with calculations based on the Ekman Compressibility Equation. (Salinity = 31.7 parts per thousand.)

Temperature (°C)	Velocity of sound (ft/sec) Measured	Calculated	Deviation (%)
10.9	4887.7	4875.6	0.26
11.6	4885.8	4883.8	0.04
11.6	4893.1	4883.8	0.19
11.5	4902.4	4882.5	0.41
11.1	4888.3	4878.5	0.20

[8] Adams, J. Am. Chem. Soc. **53**, 3769 (1931).

[9] *Oceanographical Tables*, Comissariat of Agriculture, USSR, Moscow, 1931. (A general compilation of oceanographic data by N. N. Zubov.)

[10] S. Kuwahara, *Velocity of Sound in Sea Water and Calculation of the Velocity for Use in Sonic Sounding* (Hydrographic Dept. I.J.N. Tokyo, 1938).

TABLE VIII. Comparison of Adams's experimental compressibilities and the empirical fit given by the Ekman and Tait equations.

	$(v_0-v)/v_0$				
	Adams (experimental)		Ekman equation	Tait* equation	
P (kbar)	Pure H_2O	3.79% NaCl	$S=32$ (Table I)	$n=7.800$ $B=3.012$ (Table II)	$n=7.445$ $B=3.156$
0.0	0.0000	0.0000	0.0000	0.0000	0.0000
0.5	.0212	.0196	.0198	.0197	.0198
1.0	.0393	.0368	.0370	.0368	.0370
1.5	.0555	.0522	.0522	.0518	.0522
2.0	.0699	.0658	.0655	.0653	.0659
3.0	.0945	.0894	.0871	.0887	.0897
4.0	.1152	.1091	—	.1083	.1095
5.0	.1330	.1265	—	.1254	.1275
6.0	.1485	.1417	—	.1405	.1431
7.0	.1622	.1552	—	.1540	.1569
8.0	.1746	.1670	—	.1662	.1695
9.0	.1858	.1781	—	.1775	.1812
10.0	.1964	.1886	—	.1876	.1917
11.0	.2059	.1980	—	.1972	.2017

* $(v_0-v)/v_0=(1/n)\log(1+p/B)$.

where

$$C_{p'}=1.005-0.004136s+0.0001098s^2-0.000001324s^3.$$

In the above equations, t is temperature in °C and s is salinity in parts per 1000. These data are in good agreement with those used by Kirkwood and Richardson, quote in Appendix II.

4. Compressibility Data for Low Pressure Region (Table I)

The following equation was used in computing Table I:

$$10^5\mu=\frac{4886}{1+0.183p}-[227+28.33t-0.551t^2+0.004t^3]+p[105.5+9.50t-0.158t^2]-1.5p^2t-\left(\frac{\gamma-28}{10}\right)[147.3-2.72t+0.04t^2-p(32.4-0.87t+0.02t^2)]+\left(\frac{\gamma-28}{10}\right)^2[4.5-0.1t-p(1.8-0.06t)],$$

where p is pressure in kilobars, t is temperature in degrees centigrade, and μ is defined by:

$$v=v_0(1-\mu p),$$

γ is defined by:

$$\gamma=-0.069+1.4708\ \text{Cl}-0.001570\ \text{Cl}^2+0.0000398\ \text{Cl}^3.$$

The above empirical equation for sea water compressibility is due to Ekman[11] and has been widely used for computation of sound velocity in sea water.[10,12] The validity of the Ekman equation for sound velocity calculations was verified experimentally as indicated in Table VII.

Experimental sound velocity measurements were made by recording with a rotating drum camera the signals applied to a cathode ray oscilloscope by two very small piezoelectric gauges placed a known distance apart. The sound source was a No. 8 detonator cap placed far enough away from the gauges so that the effect of finite pressure amplitude was less than 0.03 percent. An error of about 0.2 percent was inherent in the experimental work owing to slight errors in the alignment of the two recording gauges with the sound source. This accounts for the magnitude and systematic nature of the discrepancy apparent in Table VII.

Further verification of the applicability of Ekman's equation in the region up to 1.50 kilobars is given in Table VIII where values obtained from the equation are compared with the experimental values of Adams for NaCl solutions.

5. Compressibility Data for Intermediate Pressure Region (Table II)

As indicated in Part 1 of this appendix, a sea water salinity of 32 parts per thousand corresponds to a 3.79 weight percent solution of NaCl. The compressibility of NaCl solution of this concentration was obtained by graphical interpolation of Adams's data.[8]

The Tait equation in the form:

$$v(0, T)-v(p, T)/v(0, T)=(1/n)\log[1+p/B(t)],$$
$$t=(T-273.16)°\text{C}$$

was then fitted to Adams's data. In an effort to check the Tait equation against the Ekman equation used for computation of Table I, a fit was first made to the lower pressure region. Values of n and $B(25°\text{C})$ were so selected that the equation not only fitted the data of Adams with adequate precision but also yielded the correct velocity of sound in the limit of zero pressure. This additional restriction (that the equation give $c_0=1528$ m/sec. at 25°C and $s=32$) required that $nB(25°\text{C})=23.497$, the latter relation being obtained from the thermodynamic equations:

$$\left(\frac{\partial v}{\partial p}\right)_T=-\frac{v_0^2}{c_0^2}-\frac{T}{c_p}\left(\frac{\partial v}{\partial T}\right)_p^2,$$

$$\left(\frac{\partial v}{\partial p}\right)_T=-\frac{v_0}{nB(t)}\text{ at } p=0.$$

In this case n was taken as 7.445 and $B(25°\text{C})$ as 3.156 kilobars, and the resulting equation fits the data of Adams quite closely up to pressures of about 4 kilobars as shown in Table VIII. For purposes of further calculation, the temperature *variation* of B was assumed to be the same as that used by Kirkwood and Richardson on the basis of a private communication from Gibson (see Appendix II). Calculation of $U-c_0/c_0$ at 1.00 kilobar yielded a value of 7.85 percent, in good agreement with the value of 7.81 percent obtained from the Ekman equation.

Having verified the accuracy of results obtained from the Tait equation when fitted as described above, the same technique was used to fit the equation to the intermediate pressure range (up to values for 11 kilobars quoted by Adams; it was assumed safe to extrapolate the resulting equation to pressures of 14 or 15 kilobars). It was found that the best fit of the data as well as a correct value for the velocity of sound were obtained by taking $n=7.800$ and $B(25°\text{C})=3.012$, the temperature variation of B again being assumed to be that mentioned above. The Tait equation containing these parameters was then used for the computation of Table II. The fit of the equation to Adams's data is shown in Table VIII.

TABLE IX. Values of n computed from $p-v-T$ data (using $n=7.15$ in computation of ΔT).

t_0* (°C)	p (kg/cm²) 5000	15,000	25,000
20	7.211	7.183	7.130
40	7.360	7.126	6.969
60	7.411	7.054	6.868

* t_0=centigrade temperature through which the adiabatic for S passes at zero pressure.

[11] V. W. Ekman, *Publications de Circonstance No. 43* (Conceil Permanent Internationale Pour L'Exploration de la Mer. November 1908).

[12] Matthews, *Tables of the Velocity of Sound in Pure Water and Sea Water for Use in Echo Sounding and Sound Ranging* (Hydrographic Dept., Admiralty, H.D. No. 282).

APPENDIX II

1. Data Employed in the Computations of Part B of Section II

In the modified Tait equation, Eq. (2.12), the function $A[S]=B(t)$, where $t=T[0, S]-273.16$,

is determined from the empirical values of $B(t)$, fitting the original isothermal Tait equation, Eq. (2.7), to experimental data. R. E. Gibson[13] gives third-degree t-expansions of $B(t)$ for various molalities of NaCl. By interpolating the coefficients (the constant term numerically and the other graphically) for a molality of 0.7, one obtains $B(t)=3.134-1.65\times10^{-3}(t-55)-1.181\times10^{-4}(t-55)^2+5.32\times10^{-7}(t-55)^3$ kilobars.

The specific heat $c_p(0, T)$ for a 0.7 molal NaCl solution was obtained by interpolation from the values quoted in the *International Critical Tables* and *Physikalischchemische Tabellen*. The resulting set of values is fitted adequately by the expression

$$c_p(0, t+273.16)=3.9644+6.24\times10^{-4}t \text{ joule/gm. deg.}$$

From Gibson and Loeffler[14] a set of values of $v(0, T)$ covering the range from 25°C to 95°C inclusive was obtained for a 0.7 molal NaCl solution by means of empirical equations giving $v(0, T)$ as a function of concentration for each temperature. In extrapolating to higher temperatures, the relation,

$$v(0, t+273.16)=0.994150+2.929\times10^{-4}(t-25)+3.241\times10^{-6}(t-25)^2 \text{ cm}^3/\text{gm}.$$

was used; for lower temperatures ($t<10$°C),

$$v(0, t+273.16)=0.991442+6.025\times10^{-6}(t-3.8)^2 \text{ cm}^3/\text{gm}.$$

2. Test of the Modified Tait Equation with Bridgman's Data for Pure Water. Determination of the Characteristic Constant n.

The modified Tait equation-of-state, Eq. (2.12), may for our present purposes be written in the form

$$\log(v[0, S]/v[p, S])=(1/n)\log(1+p/A[S]) \quad \text{(II-1)}$$

where $A[S]$ is related to the $B(t)$ in the original isothermal equation of state as follows,

$$A[S]=B(t_0),\quad t_0=T_0-273.16,\quad T_0=T[0, S]. \quad \text{(II-2)}$$

According to the convention introduced in Part B of Section II, parentheses ( ) after a function denotes that the independent variables are p and T, whereas square brackets [ ] denote that they are p and S.

Now we wish to test Eq. (II-1) with Bridgman's[15] p–v–T data for pure water with the ultimate object of finding the best value for n. We assume implicitly that n does not vary rapidly with NaCl concentration. To make the comparison, we first must know the values of the temperature T corresponding to the various points $[p, S]$, the calculation of which we consider below.

Letting $T(0, S]=T_0$, $T[p, S]=T$, and $T-T_0=\Delta T$, we have

$$\Delta T=\int_0^p \frac{\partial T[p, S]}{\partial p}dp=\int_0^p \frac{\partial v[p, S]}{\partial S}dp. \quad \text{(II-3)}$$

Using Eq. (II-1), a simple calculation yields

$$\Delta T=\frac{G}{(1+p/A)^{1/n}}[(1+D)(1+p/A)-(n+D)(1+p/A)^{1/n}+n-1], \quad \text{(II-4)}$$

where

$$A=A[S]=B(t_0),$$

$$G=\frac{A'[S]v[0, S]}{n-1}=\frac{T_0B'(t_0)\cdot v(0, T_0)}{(n-1)\cdot c_p(0, T_0)},$$

$$D=\frac{nA[S]\dfrac{\partial v[0, S]}{\partial S}}{A'[S]v[0, S]}=\frac{nB(t_0)\beta_0}{B'(t_0)v(0, T_0)},$$

$$\beta_0=\left(\frac{\partial v(0, T)}{\partial T}\right)_{T=T_0}.$$

To calculate T, given a specified p and $T_0=T[0, S]$, a tentative value of $n=7.15$ was chosen for use in Eq. (II-4). The corresponding value of $v[p, S]=v(p, T)$ was obtained by interpolation from Bridgman's[15] p–v–T data. Inserting these values of $v[p, S]$ in Eq. (II-1), and knowing the values of $v[0, S]=v(0, T_0)$ and $B(t_0)$ for pure water, a set of values of n was calculated for $p=5{,}000$, 15,000, 25,000 kg/cm²

[13] Private communication.
[14] Gibson and Loeffler, J. Am. Chem. Soc. **53**, 443 (1941).
[15] Bridgman, J. Chem. Phys. **3**, 597 (1935) and private communication.

and $t_0 = T_0 - 273.16 = 20°, 40°, 60°$C, the results summarized in Table IX.

Additional data (for pure water) used in Eqs. (II-1) and (II-4) were

$$B(t) = 2.996 + 7.285 \times 10^{-3}(t-25) - 1.790 \times 10^{-4}(t-25)^2 + 6.13 \times 10^{-7}(t-25)^2 \text{ kilobars},$$[13]

and

$$\frac{1}{2.303}\frac{\partial \log v(0, 273.16+t)}{\partial t} = \frac{2(t-3.98)}{244{,}860+15{,}040(t-3.98)^{0.62}} - \frac{(0.62)(15{,}040)(t-3.98)^{1.62}}{[244{,}860+15{,}040(t-3.98)^{0.62}]^2}$$

obtained from Ipatov's[16] empirical equation for v by differentiation.

The average value of n is 7.146. In the present calculations this value has been rounded off to 7.15.

The entries in Tables IV, V, and VI therefore contain more significant figures than the test justifies. On the basis of the test, the errors associated with the use of the modified Tait equation are of the order of several percent. In particular, the results obtained for low pressures will disagree with known data by several percent.

[16] I. V. Ipatov, J. Phys. Chem. (U.S.S.R.) **5**, 1230 (1934).

APPENDIX III

Symbols

$A[S]$ = parameter in modified ("adiabatic") Tait equation-of-state.
$B(t)$ = parameter in isothermal Tait equation-of-state.
c = local velocity of sound.
c_0 = velocity of sound at zero pressure.
c_p = specific heat at constant pressure.
h = dissipated enthalpy increment: $\int_{T_0}^{T} c_p(0, T')dT'$.
ΔH = enthalpy increment: $\Delta H = \omega + h$.
n = characteristic constant in Tait equation-of-state.
p_0 = initial pressure ahead of shock front, $p_0 = 0$, in these calculations.
p = pressure behind shock front.
S = entropy.
s = sea water salinity.
t = temperature in °C.
T = absolute temperature.
u = particle velocity behind shock front.
U = shock front propagation velocity.
v_0 = specific volume of medium ahead of shock front.
v = specific volume of medium behind shock front.
$\bar{\beta}_0$ = mean compressibility at zero pressure over temperature range ΔT.
ρ = density.
σ = Riemann function: $\int_{p_0}^{p} \frac{v[p', S]}{c[p', S]}dp'$.
ω = undissipated enthalpy increment: $\int_{p_0}^{p} v[p', S]dp'$.

THE JOURNAL OF CHEMICAL PHYSICS VOLUME 15, NUMBER 11 NOVEMBER, 1947

The Absorption Spectrum of Ozone in the Visible

I. Examination for Fine Structure. II. The Effect of Temperature

GEORGE L. HUMPHREY AND RICHARD M. BADGER
Gates and Crellin Laboratories of Chemistry, California Institute of Technology, Pasadena, California*
(Received July 18, 1947)

The absorption spectrum of ozone in the visible spectral region has been investigated for fine structure and for changes in absorption with temperature. No fine structure was observed in spectrograms taken in the second order of a 21-ft. grating spectrograph. The absorption coefficients remained constant within experimental error in going from room to dry-ice temperature.

INTRODUCTION

THE effect of temperature on the absorption of ozone in the visible region of the spectrum has been the subject of considerable study, the results of which have been conflicting. In 1880 Chappuis[1] discovered the visible absorption bands of ozone and two years later published observations on the change in this absorption when the ozone was cooled from room temperature to −50°C by rapid evaporation of methyl

* Contribution No. 1140 from the Gates and Crellin Laboratories of Chemistry.

[1] J. Chappuis, Comptes Rendus **91**, 985 (1880); *ibid.* **94**, 858 (1882); Ann. de l'ecole normale sup. **11**, 137 (1882).

chloride. He reported a marked increase in the intensity of absorption upon lowering the temperature. More recently, Lefebvre[2] photographed the visible spectrum of ozone at room and dry-ice temperatures, finding that the absorption did not change with temperature. Still later, E. Vassy[3] carried out investigations which confirmed Chappuis' qualitative results. Vassy also published values for the absorption coefficients of ozone in the visible at −40°C, −80°C, and −100°C.

It is important to know if there is an appreciable effect of temperature on the absorption of ozone, since this would influence photometric determinations of the amount of ozone in the atmosphere.[4] The results of such determinations are of considerable interest because of their meteorological significance.

The absorption of ozone in the visible has been studied under low dispersion by Wulf[5] and shown to consist of diffuse bands overlying a background of rather general continuous absorption. The two bands at approximately λ5730 and λ6020 are especially strong and broad. These bands fall in a region of the spectrum where glass optics may be used and where the intensity of solar radiation is high. In view of these facts the bands should be particularly adapted to a study of ozone in the atmosphere either by photographic or photoelectric methods, provided the intensity of their absorption is not too weak.

Cabannes and Dufay[6] have shown that the fractional absorption of atmospheric ozone in the orange-yellow bands is sufficiently high for photometric or bolometric measurements, and some use has been made of these bands in estimating the amount of ozone in the atmosphere.[7,8] However, the bands have not been used to their greatest advantage in the study of atmospheric ozone because the fractional absorption is small in comparison with that in the ultraviolet or infra-red bands, and also because of the uncertainty as to whether there was a temperature effect.[9] Since modern photoelectric methods are quite capable of measuring with reasonable accuracy a small fractional absorption of the order of that caused by atmospheric ozone in the visible spectral region, it has seemed profitable to undertake a reinvestigation of the temperature effect in order to resolve the existing discrepancies.

The bands in the visible region of the ozone spectrum have always been described as being diffuse, but so far as we are aware they have not been investigated under more than moderate dispersion. If these bands should contain fine structure the absorption would undoubtedly show some dependence on pressure, thereby making it necessary to take this fact into account when using the bands for determinations of ozone. It has consequently seemed desirable to settle the question of fine structure definitely by obtaining spectrograms under high dispersion and resolution.

I. Examination for Fine Structure

The possibility that fine structure is present in the broad bands at λ5730 and λ6020 was investigated by means of a 21-ft. grating spectrograph using a six-meter absorption cell containing 4 percent ozone by volume. The ozone was prepared and the concentration estimated in the manner described in Section II of this paper.

Spectrograms were taken in the second order with an average dispersion of about one angstrom per millimeter. The weak iron lines (third order) λ3878.676 and λ3878.736 near the strong line λ3878.575 were clearly resolved in the iron spectrum used as reference, but no structure was observed in the ozone bands.

An indication of the average spacing of lines which might be expected in an ozone band having structure may be obtained from observations in the infra-red. Average spacings of 1 cm^{-1} [10,11] and 5.7 cm^{-1} [12] have been reported in the infra-red bands. Even the former of these would correspond to a separation of about 0.4A in the visible region and should certainly have been resolved under the conditions described above.

[2] L. Lefebvre, Comptes Rendus **200**, 653 (1935).
[3] E. Vassy, Thesis de Doctorat, Serie **A**, No. 1695, Paris (1937).
[4] For an excellent review on atmospheric ozone, methods of measurements, etc., see: F. W. P. Götz, Ergeb. d. kosmischen Physik **I**, 180 (1931); *ibid.* **III**, 253 (1938).
[5] O. R. Wulf, Proc. Nat. Acad. Sci. **16**, 507 (1930).
[6] J. Cabannes and J. Dufay, J. de phys. et rad. **7**, 257 (1926).
[7] F. E. Fowle, Smith. Misc. Coll. **81**, 1 (1929); Trans. Am. Geophys. Union, Part I, 164 (1935); J. Gauzit, Thesis de Doctorat, Serie **A**, No. 1569, Paris (1935).
[8] G. Dejardin, A. Arnulf, and R. Falgon, Comptes Rendus **205**, 1086 (1937).
[9] See reference 4, **III**, 259.
[10] A. Adel, Astrophys. J. **94**, 451 (1941).
[11] S. L. Gerhard, Phys. Rev. **42**, 622 (1932).
[12] A. Adel and D. M. Dennison, J. Chem. Phys. **14**, 379 (1946).

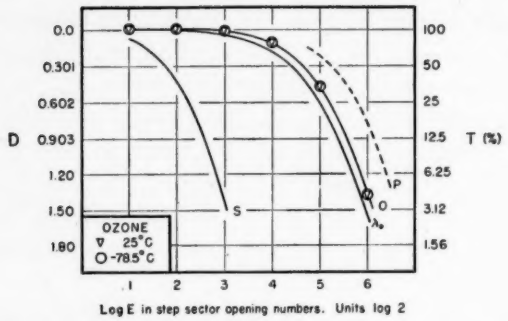

FIG. 1. Plot of density, D, against log "effective intermittent exposure," $\log E$, for the λ6020 band. Curve S: cell containing oxygen; λ_0: intensity standard, λ4300; O: cell containing the ozone-oxygen mixture at two temperatures; P: predicted for the ozone-oxygen mixture at the low temperature by use of Vassy's absorption coefficients for −80°C.

II. The Effect of Temperature

The absorption was studied under low dispersion at room (25°C) and dry-ice (−78.5°C) temperatures in the region λ3900 to λ6800 by means of a Bausch and Lomb quartz spectrograph. A dispersion of about 57A per mm was obtained in the region between λ4500 to λ6050 from which four bands were chosen for comparison of absorption at the two temperatures.

Ozone was prepared from tank oxygen by means of ice-water cooled, Siemens-type ozonizers. The rate of oxygen flow, as determined by a flow meter containing dibutyl phthalate, was 80 ml per minute. Traps containing dry-ice alcohol mixtures were provided before and after the ozonizers to dry the oxygen and to condense small amounts of oxides of nitrogen which might have been produced[13] in the ozonizers from traces of nitrogen in the tank oxygen. Oxides of nitrogen influence the decomposition of ozone and might contribute to the absorption in this region.[14] The entire apparatus was constructed from Pyrex glass, and all connections were made using ground-glass tapered joints partially lubricated with Apiezon M so as to minimize contact with ozone, although no reaction between the two was apparent.

The absorption cell, which consisted of a glass tube 3 meters in length and 1.5 centimeters in diameter with small diameter side-arm openings near each end, was filled by flowing the ozone-oxygen mixture through the tube. After about an hour, when a steady state was assumed to have been achieved, the tube was sealed by closing stopcocks near the cell in the side arms, and a series of exposures was made on the enclosed ozone alternately at room and dry-ice temperature. Cooling the gas to dry-ice temperature was accomplished by surrounding the tube by a trough filled with carbon-dioxide snow. A period of a half-hour was found sufficient to allow the tube to come to thermal equilibrium with its surroundings. Estimations of the amount of ozone in the path using absorption coefficients of Colange[15] (in the manner to be outlined later in the discussion) gave approximately 6 percent ozone by volume. The maximum decomposition observed during any series of exposures amounted to about 2 percent of the total amount of ozone present initially, and usually no appreciable decomposition was observed during a period of about five hours.

A 500-watt tungsten projection lamp was used as source. The light emerging from the absorption cell was reflected to the slit of the spectrograph where it was interrupted by means of a rotating logarithmic-stepped sector which had six steps successively increasing in angular aperture by a factor of two. Uniform illumination of the slit was obtained by means of a cylindrical lens placed before the sector.

By shifting the position of the film in the plate holder it was possible to obtain as many as four spectrograms on a single film, thus affording a comparison of spectrograms developed simultaneously under identical conditions on the same emulsion. Each set of four spectrograms always included two spectrograms at one temperature and at least one at the other temperature. In some cases the fourth spectrogram was of the blank tube containing oxygen only.

Eastman type IV-F plates or process Panchromatic film were used to photograph the spectra. The mercury-arc spectrum was used as reference. Spectrograms of the ozone spectrum obtained in our investigations were similar in appearance to those published in Wulf's paper.[5]

Density measurements of plate blackening were made from microphotometer traces of the spectrograms, and the density data so obtained were treated as though they had been obtained by the use of a neutral step weakener in front of the spectrograph slit. The validity of this pro-

[13] See, for example, J. F. Schultz and O. R. Wulf, J. Am. Chem. Soc. **62**, 2980 (1940).

[14] E. J. Jones and O. R. Wulf, J. Chem. Phys. **5**, 873 (1937).

[15] G. Colange, J. de phys. et rad. **8**, 254 (1927).

cedure has been well discussed,[16] and it has been shown that residual errors caused by failure of the intermittent exposure to compensate for reciprocity law failure are of the order of accidental errors inherent in photographic photometry.[17]

A plot of density, D, against log "effective intermittent exposure," $\log E$, of the corresponding steps of the sector produces a curve similar to the well-known density-log energy curve. If conditions of development, exposure time, etc., are identical, curves obtained at different intensity levels are parallel—at least in the middle portions of the curves—and their displacement along the axis of log "effective intermittent exposure," or opening number of the sector step to which $\log E$ is proportional, is a measure of relative intensities.

To secure ideal conditions for photographic photometry, spectrograms of blank and filled absorption tubes at the two temperatures should be photographed simultaneously, side by side, on the same film. Since this was not practical a secondary reference of intensity was chosen which was always photographed simultaneously with the absorption regions, namely, the region λ4300 at which ozone absorption is negligible. The use of this reference permitted all spectrograms taken on one and the same film to be compared directly, since it eliminated possible errors caused by fluctuations of intensity of the source, or slight inequalities of exposure times.

The use of the λ4300 region as a reference is, of course, only strictly valid for exposures made on one and the same film, and consequently developed under identical conditions. However, development conditions were sufficiently well reproduced in our work so that the $D-\log E$ curves from different films were essentially parallel, and since direct comparisons of the tube containing ozone at the two temperatures could always be made on one and the same film, we believe that serious errors could not have arisen.

The following method was used in comparing two spectrograms on the same film or on different films. The $D-\log E$ plots for the two cases were superposed so that the curves for the λ4300 region coincided. The distance parallel to the $\log E$ axis between two curves corresponding to any other spectral region of interest was taken as proportional to the difference in absorption coefficients for the two cases, as represented by the equation: $\Delta \log E=\log I_2-\log I_1=x\Delta\alpha$. The units of α are cm^{-1}, and x is the path length in cm of pure ozone at N.T.P. The amount of ozone in the path was determined from the transmission of the tube at room temperature by use of Colange's values for α_{10} at 20°C. The average transmission of the ozone mixtures used in our experiments was about 0.14. When necessary, a correction for change of ozone concentration with time was made when comparing absorption at the two temperatures. In effect, the ozone concentration during a cold exposure was taken to be the mean of the concentrations during the exposures immediately preceding and following taken at the other temperature.

Figure 1 presents the average of the data for the band at λ6020, and illustrates the method by which all data were treated.

Table I presents Colange's values for α_{10} at 20°C, the change expected from calculations based on Vassy's data, and the results from three determinations for the change in absorption coefficients obtained in the present investigation in going to the lower temperature. It should be remarked that Vassy[3] employed Colange's values for α_{10} at 20°C to obtain values for his absorption coefficient at dry-ice temperature, and that Colange[15] estimates his values of α_{10} at 20°C to be good to 5 percent.

The small variations in absorption which we observe in going from room to dry-ice temperature are not systematic, and are well within the limits of probable errors inherent in photographic photometry. We believe that our experiments show definitely that the absorption of ozone in the visible region of the spectrum is not sensibly temperature dependent.

TABLE I. Changes in absorption coefficients for ozone in going from room to dry-ice temperature.

λ	Colange α(20°C)	E. Vassy* $\Delta\alpha/\alpha\times100$	Present work $\Delta\alpha/\alpha\times100$			
			1	2	3	Average
6020A	0.050	+18.8	0.0	0.0	+1.0	+0.3
5730A	0.046	+20.7	0.0	−1.7	+1.4	−0.1
5317A	0.033	+14.6	−3.4	−6.0	0.0	−3.1
5053A	0.016	+ 7.5	—	−4.9	+4.1	−0.8

* E. Vassy's data are presented in graphical form and the wave-lengths of the maxima do not agree with those found by other investigators or by us. The disagreement appears to be due to some error in the scale of wave-lengths used on his graph. From the trend of absorption with wave-length it is possible, however, to identify the bands; the values given in column three of Table I are calculated for regions which certainly correspond to the wave-lengths given here.

[16] R. A. Sawyer and H. B. Vincent, J. Opt. Soc. Am. **33**, 247 (1943).

[17] R. Breckpot, Spectrochimica Acta **1**, 137 (1939); J. H. Webb, J. Opt. Soc. Am. **23**, 157 (1933).

It is difficult to explain the previous conflicting results from experiments on cooling the ozone because of lack of sufficient detail about the manner in which the experiments were performed and the spectrograms evaluated. It is perhaps significant that in those cases[1,3] where an increase in absorption was reported after cooling, high concentrations of ozone were used in the absorption cell. Absorption coefficients published by A. Vassy[18] for the visible bands using a 50 percent ozone-oxygen mixture in the path are approximately 30 percent higher than those of Colange, who used 4 percent ozone by volume. Colange determined the concentration of ozone in his work by chemical analyses, while A. Vassy based her determinations of concentration on the absorption in the ultraviolet bands using absorption coefficients determined by Ny and Choong,[19] who employed concentrations of ozone varying from 2–6 percent by volume (chemical analyses).

It should be remarked that the concentration of ozone in the atmosphere is greatly below that used in the experiments described here. Consequently, if there is a temperature effect which becomes apparent only at ozone concentrations considerably higher than we have employed in our work, then this effect would not render the visible bands unsuitable for determining atmospheric ozone.

[18] A. Vassy, Comptes Rendus **204**, 1413 (1937); *ibid.* **206**, 1638 (1938).
[19] Ny-Tsi-Ze and Choong-Shin-Piaw, Chinese J. Phys. **1**, 38 (1933).

CONCLUSIONS

Although the reduction of intensity of solar radiation by the ozone of the atmosphere is small in the visible region of the spectrum, modern photoelectric methods are quite capable of measuring such weak absorption. Moreover, in view of the broad and continuous character of the absorption in the visible ozone bands, the relative simplicity of photometry in the visible region compared with other regions of the spectrum, and the absence of any uncertainty from effects of temperature or pressure on the bands, it seems likely that they will find further application in the measurement of atmospheric ozone.

ACKNOWLEDGMENT

We wish to express great appreciation to Dr. Oliver R. Wulf of the U. S. Weather Bureau for bringing our attention to the investigations herein considered, and for his encouragement and very helpful discussions throughout the course of the work.

THE JOURNAL OF CHEMICAL PHYSICS VOLUME 15, NUMBER 11 NOVEMBER, 1947

Ignition of Explosive Gas Mixtures by Electric Sparks. I. Minimum Ignition Energies and Quenching Distances of Mixtures of Methane, Oxygen, and Inert Gases*

M. V. Blanc,** P. G. Guest,** Guenther von Elbe,** and Bernard Lewis**

(Received June 6, 1947)

An apparatus and experimental procedure is described for measuring capacitances and gap voltages of condensed electric spark circuits for sparks just powerful enough to ignite explosive gas mixtures. Mixtures of methane, oxygen, and inert gases are investigated. From the measured capacitances and gap voltages the minimum ignition energies are calculated. These energies are found to be independent of gap voltage. With increasing gap length they attain a minimum at critical distances which mark the farthest penetration of the flame-quenching effect of the electrode material. Above the quenching distances the energies remain constant over some range which is governed by mixture composition and pressure. Energies measured in this range may be regarded as absolute minimum energies, as defined in a subsequent paper. Data of such minimum energies and of quenching distances are presented for mixtures at room temperature and pressures ranging from 0.2 to 1 atmosphere.

CAPACITANCES and gap voltages of condensed electric spark circuits have been measured for sparks just powerful enough to ignite various explosive gas mixtures. From these data *minimum ignition energies* have been calculated. Data on the quenching of ignition

* Published by permission of the Director, Bureau of Mines, U. S. Department of the Interior.

** Scientific Aide, Electrical Engineer, Supervising Chemist of the Physical Chemistry and Physics Section, Explo-

between two plane-parallel plates are also presented. Quenching occurs below rather sharply defined plate distances, the *quenching distances*. The experiments were made with mixtures of methane, oxygen, and nitrogen. In some series, nitrogen was replaced by helium, argon, or carbon dioxide. All tests were made at room temperature (about 25°C).

APPARATUS AND EXPERIMENTAL PROCEDURE

The apparatus differed from a previously described set-up[1] by a larger capacitance range and improved circuit connections which minimize resistance and corona losses. As shown in Fig. 1, the gases were admitted to a test bomb which was made of stainless steel and had an inside diameter of 5 inches. The spark electrodes were mounted in the center of the bomb. The gap length could be adjusted accurately by means of a built-in micrometer. For the determination of quenching distances plate-shaped electrodes were required. Metal plates were not suitable because sparks tended to occur erratically at the rim even though the center was slightly raised; therefore, electrodes with precisely mounted glass flanges were used, as shown in Fig. 1. The electrode tips were rounded to minimize corona discharge, and the glass was coated with a trace of paraffin wax to eliminate surface conduction. The electrodes were connected to a system of fixed and variable air condensers and a variable-range voltmeter which was periodically calibrated against corona-shielded high precision resistors and a high precision milliammeter. The aggregate capacitance was continuously variable between 3 and 5000 micromicrofarads. Its exact value was determined for any test condition by means of a Wien bridge which was periodically checked against a Leeds and Northrup precision standard air capacitor. Measurements of very small capacitances were corroborated by other well-known methods. High voltage was supplied *via* a protective resistor to the terminal *a*, whence it was gradually transferred to the electrode-

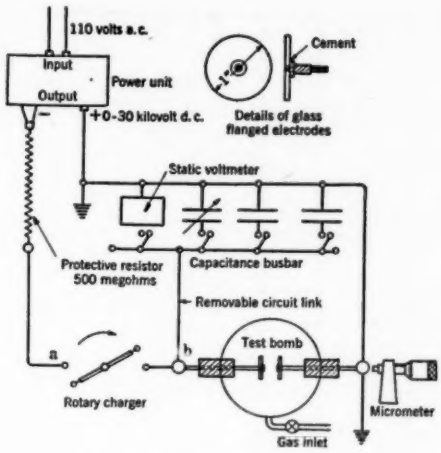

FIG. 1. Scheme of apparatus.

capacitor system by means of a rotary charger. In this device, small metal spheres mounted on hard rubber alternately touched terminals *a* and *b*, thus transferring charge at a rate governed by the speed of rotation while the spark circuit remained effectively isolated from the power source with regard to both capacitance and voltage ripple. After the bomb had been filled with an explosive mixture of accurately determined composition and pressure, the electrode and capacitor system was slowly charged, and the voltage V at which the spark occurred was observed. If the mixture did not ignite the capacitance was increased, until by trial and error the critical capacitance C for ignition was found. At capacitances below about 50 micromicrofarads it became necessary to disconnect the voltmeter from the circuit and to charge the

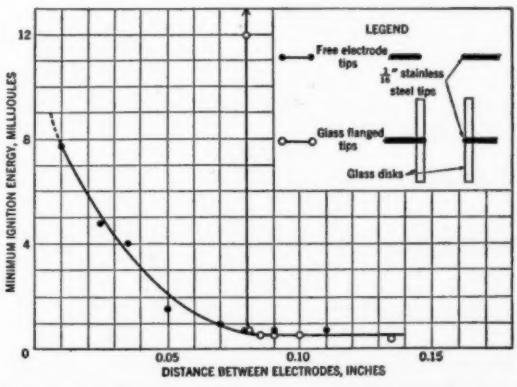

FIG. 2. Minimum ignition energies for free and glass-flanged electrode tips as function of electrode distance. Stoichiometric mixture of natural gas (about 83 percent CH_4+17 percent C_2H_6) and air at one atmosphere pressure.

ives Division, and Chief, Explosives Division, respectively, Central Experiment Station, Bureau of Mines, Pittsburgh, Pennsylvania.

[1] P. G. Guest, Apparatus for determining minimum ignition energies for electric-spark ignition. U. S. Bureau of Mines Report of Investigations 3753 (1944).

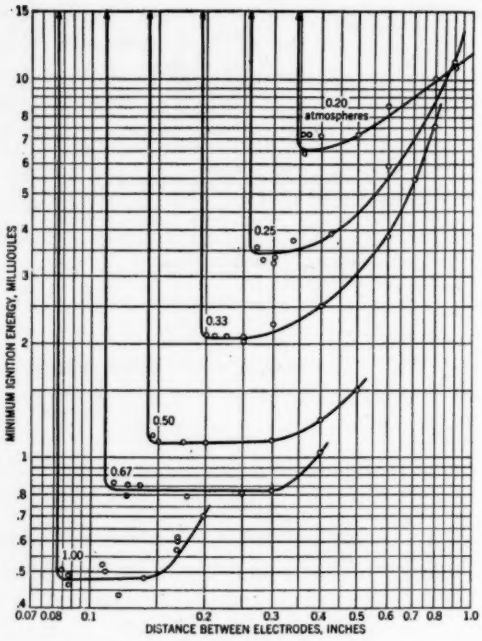

FIG. 3. Minimum ignition energies for glass-flanged electrode tips as functions of electrode distance and pressure. Stoichiometric mixture of methane and air.

electrode-capacitor system from a large capacitor which was accurately maintained at the breakdown voltage of the spark gap. The breakdown voltage was determined independently with the voltmeter in the circuit for conditions of gas mixture and electrodes identical with those of the ignition test, and the rotary charger was sometimes replaced by a Micarta rod connecting the terminal b with the terminal of the charge reservoir. This rod permitted slow leakage of electricity without increasing the effective capacitance of the spark circuit. At very low capacitances the electrode-capacitor system consisted solely of the electrode tip connected to a suitably long metal rod which below about 6 micromicrofarads was so short that it did not extend through the insulating gland to the outside of the bomb. The Micarta rod connection solved the difficulty of making contact with the outside charge source.

Sparking occurred after a statistical time lag which was often inconveniently long. Inasmuch as breakdown is initiated by extraneous ions in the gap, it was generally possible to reduce the lag substantially by placing radium capsules of various strengths into the bomb. This also caused a slow leakage of electricity from the charged electrode before breakdown, and hence the gap voltage dropped below the voltage of the charge reservoir to a value governed by the rates of charge transfer from the reservoir and leakage from the electrode. This was potentially troublesome when the voltmeter was disconnected, and hence the gap voltage was not directly observable; generally, however, it was found possible to adjust the rates of charging and ionization so that the voltage drop became inappreciable.

The product $(1/2)CV^2$ may be termed the minimum ignition energy. It represents energy expended in the spark gap where it is available for the ignition process, and also outside losses of Joule heat, Hertzian waves, and dielectric hysteresis. However, hysteresis losses have been substantially eliminated by the use of air condensers, and electromagnetic wave losses from a circuit of this type are small. Since the d.c. resistance of the metallic part of the circuit was less than 0.1 ohm it is felt that, despite a possible skin effect caused by discharge oscillations, the metallic resistance to the flow of current was much smaller than the effective resistance of the gap during the discharge, and that therefore the external heat loss was negligible. To test this point, various non-inductive resistances were introduced in the circuit in place of the removable circuit link, Fig. 1, and the minimum energy required for the ignition of near-stoichiometric methane-air mixtures was determined. No effect

TABLE I. Results showing the minimum spark ignition energy to be independent of gap voltage.

	Gap voltage,* kilovolt	Minimum ignition energy, millijoule
8.7 percent natural gas** in air at 1 atmosphere	6.1	0.5
	9.9	0.5
0.5 atmosphere	8.6	1.7
	10.2	1.7
0.33 atmosphere	5.4	2.4
	7.5	2.4
0.25 atmosphere	4.5	4.0
	6.8	4.2
8.5 percent methane in air at 0.33 atmosphere	14.2	2.6
	20.0	2.6

* The distance between the electrodes was held constant for each pair of runs.
** Approximately 83 percent CH_4, and 17 percent C_2H_6.

of the additional resistance was noted up to 30 ohms.

EFFECT OF INDUCTANCE

A number of tests in which the circuit link (Fig. 1) was replaced by a helix of heavy wire failed to show any effect of moderate changes of inductance and oscillatory frequency on the minimum ignition energy.

EFFECT OF ELECTRODE VOLTAGE

It was possible to increase the breakdown voltage between the electrodes considerably by applying an overvoltage, either taking advantage of the breakdown time lag or by charging the condensers and connecting them with the electrode circuit by a fast-acting switch in place of the removable circuit link. In the latter procedure there is a possible energy loss caused by a spark in the switch. However, while this has not been determined quantitatively it is believed to be small because of the statistical lag of the igniting spark which permits the closing of the switch before the full current flows. As shown by the data in Table I, the minimum ignition energy was found to be essentially independent of overvoltage; that is, as the gap voltage was increased the capacitance had to be correspondingly decreased.

It appears relevant to note[2] that in spark discharges only a very small fraction of the energy goes into the production of ions. By far the largest part goes into the production of atoms, free radicals, and thermal motion in general.

EFFECT OF ELECTRODE DISTANCE

Figure 2 shows a typical example of the effect of electrode distance on the minimum ignition energy. Two electrode systems are compared, one with free and the other with glass-flanged tips. Above a critical distance, which in this instance is 0.08 inch, the data with the two electrode systems practically coincide; below this distance the minimum ignition energy increases abruptly with plate electrodes and gradually with point electrodes. This distance marks the farthest penetration of the flame-quenching effect of the solid electrode material and is analogous to the critical diameter of a tube below which flame will not propagate through the tube.

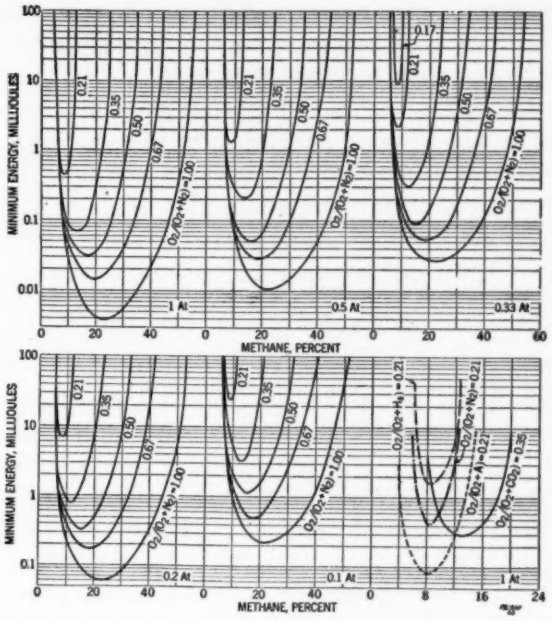

FIG. 4. Minimum spark ignition energies in millijoules of mixtures of methane, oxygen, and inert gases at one atmosphere and lower pressure. Curves correspond to constant ratios of oxygen and inert gas. $\frac{1}{16}$-in. diameter rounded electrodes cemented flush into perforated glass or quartz disks.

Above the quenching distance the minimum ignition energy is remarkably constant over a considerable range, if the pressure of the gas

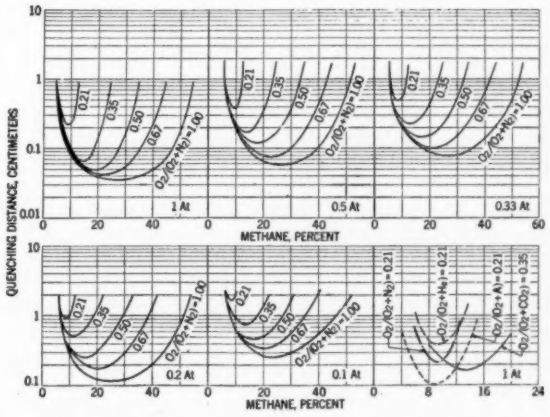

FIG. 5. Quenching distances between parallel plates for mixtures of methane, oxygen, and inert gases at one atmosphere and lower pressures. Curves correspond to constant ratios of oxygen and inert gas. $\frac{1}{16}$-in. diameter rounded electrodes cemented flush into perforated glass or quartz disks.

[2] E. L. E. Wheatcroft, *Gaseous Electrical Conductors* (Oxford University Press, New York, 1938), p. 144.

mixture is not too low. This is illustrated in Fig. 3 by a family of curves for stoichiometric mixtures of methane and air at various pressures. It appears that toward smaller distances even the data for low pressures would fall on a horizontal line if the quenching effect of the electrodes could be eliminated.

In a following paper of this series the existence of an absolute minimum ignition energy of sparks is demonstrated from theoretical considerations. This energy is the sole ignition condition if both the duration of the discharge and the volume over which the spark energy is distributed remain below some fairly well defined critical limits. If either limit is exceeded the ignition energy increases. It is easily demonstrated that in the experiments reported here the duration of the spark remains always well below the critical limit. Hence, if the horizontal part of the curves in Fig. 3 is taken to represent the absolute minimum ignition energy, the subsequent rise of the energy curves at larger electrode distances is attributable to the distribution of the spark energy over a volume exceeding a critical sphere in cubic or linear dimensions. It is obvious that as the spark electrodes are pulled apart this should become the case. It appears rather remarkable that there should be such large horizontal sections of the ignition-energy curves as have actually been found. This suggests that most of the spark energy is transferred to the gas over a fairly small fraction of the spark length. This appears to be consistent with present knowledge of the sparking mechanism.[3] At the beginning of the discharge a steep potential gradient is formed near the cathode. At the end of this gradient there exists a zone of high concentration of positive ions and high energy electrons, within which the rate of energy transfer to the gas is larger than elsewhere along the spark path.

If, as suggested by the latter considerations, the flame origin is always closer to the cathode than to the anode, then in the case of a point electrode facing a plate electrode within the quenching distance the ignition energy should be larger when the plate is the cathode than when it is the anode. This has been confirmed by experiments in which one of the electrodes was a small sphere and the other a plate.

It was found that at high gap voltage, particularly at combinations of large electrode distances and high pressures, ignition occurred statistically after a number of sparks had passed. The cause for this randomness may have been the gas motion caused by corona leakage from the electrode tips. The leakage itself was not considered to be an appreciable source of error since, as mentioned above, it was compensated by the charging rate. However, sufficiently strong gusts of "electric wind" may blow the incipient flame against the opposite electrode and thus quench it. This may be expected to occur at random with increasing probability as the variables favoring corona discharge are increased.

EFFECT OF MIXTURE COMPOSITION AND PRESSURE

The energy values corresponding to the horizontal part of the curves of minimum ignition energy *versus* electrode distance are functions only of the variables of the gas mixtures and may be regarded as absolute minimum values. Figure 4 shows families of curves of such minimum energies for various mixture compositions and pressures. Figure 5 shows corresponding families of curves for quenching distances. The limits of the U-shaped curves correspond to the limits of inflammability. A profound effect of inert gas dilution is noted. For example, near stoichiometric composition the minimum ignition energy is found to be approximately 100 times larger for air than for oxygen.

Similar families of curves are being determined for other gases, and a detailed study of the electrical characteristics of sparks and spark gaps is planned.

[3] See reference 2, p. 139.

THE JOURNAL OF CHEMICAL PHYSICS VOLUME 15, NUMBER 11 NOVEMBER, 1947

Ignition of Explosive Gas Mixtures by Electric Sparks. II. Theory of the Propagation of Flame from an Instantaneous Point Source of Ignition.[1]

BERNARD LEWIS[2] AND GUENTHER VON ELBE[3]
Central Experiment Station, Bureau of Mines, Pittsburgh, Pennsylvania

(Received August 26, 1947)

A theory of the propagation of flame from an instantaneous point source of ignition such as a capacitance spark is developed. When a mass element passes through a combustion wave, it at first gains heat by conduction from preceding hotter elements and later loses heat by conduction to succeeding cooler elements. Correspondingly, the sum h of the thermal and chemical energy per unit mass at first increases above the level h_0 for the unburned or adiabatically burned gas, and later decreases to the same level. It follows that in a unit-area segment of a plane combustion wave the excess energy $\int_{x_u}^{x_b}\rho(h-h_0)dx$ is stored, where x_u and x_b denote reference points before and behind the wave. This energy is acquired at the expense of the energy content of the burned gas as the flame grows from a small sphere to its final size. The energy that is thus lost by the burned gas is insignificant except at the flame origin. Here, the excess energy must be furnished by the ignition source. It is the function of the latter to initiate the reaction by producing a high local concentration of heat and chain carriers, and to furnish at least as much energy as is necessary to satisfy the excess energy requirement of the smallest flame that is capable of self-propagation. Such a flame may be visualized as a burning sphere of the smallest volume consistent with the condition that the rate of heat production should equal the rate of heat conduction to the surrounding unburned gas, and the minimum ignition energy is the integral $\int_0^\infty 4\pi r^2\rho(h-h_0)dr$. The calculation of this energy is made possible by assuming a simplified, partly linear temperature gradient in the combustion wave. This approximate gradient closely circumscribes the actual gradient. The resulting temperature and energy distribution can be calculated numerically from data on the flame diameter, the burning velocity, the initial and flame temperature, the heat conductivity, density and specific heat of the unburned gas. In a calculation of this kind, no issue arises concerning a "thermal" or "kinetic" theory of flame propagation. The issue arises only when, conversely, an attempt is made to calculate the burning velocity and the width of the reaction zone from speculative values of the ignition temperature and the rate of the chemical reaction.

No data are available for the diameters of the smallest self-propagating flames; however, they are smaller than the readily measurable flame quenching distances between plane parallel plates by a factor of about 2. Using energy data reported in a previous publication and the other enumerated data, flame diameters have been calculated and compared with quenching distances. A satisfactory agreement is found.

A marked difference is noted between lean and rich mixtures of methane and oxygen with and without inert gas. In the former the chemical reaction begins at a much higher temperature and the temperature gradient is much steeper, than in the latter. An explanation may possibly be found in the suggestion that in the combustion zone of rich mixtures the concentration of free radicals and particularly hydrogen atoms is much larger. If such species diffuse toward the unburned gas in considerable quantity, significant reaction occurs already at low temperature levels. The higher temperature levels are then depleted of chain carriers, and the temperature gradient correspondingly is much less steep than in lean mixtures, where rapid reaction is confined chiefly to high temperature levels.

IN a previous paper[4] the ignition of mixtures of methane, oxygen and nitrogen by capacitance sparks has been described. In this paper a theory of the process is developed assuming a very short time of electric discharge and a very small spark volume, i.e., an instantaneous point source of ignition. The theory shows the existence of an absolute minimum energy which can be correlated to the burning velocity, the width of the combustion wave, and the thermal conductivity, specific heat and density of the gas mixture.

A general picture of the distribution of temperature and energy in a combustion wave is shown in Fig. 1. For the case of a plane wave the origin of the x-coordinate is placed at a constant distance from the wave and the gas flows from left to right at the velocity of flame propagation. At any point x the sum of the rates of heat gain or loss in a unit volume of a layer dx due to thermal conduction, mass flow and chemical reaction is zero. This is expressed by the following

[1] Published by permission of the Director, Bureau of Mines, U. S. Department of the Interior.
[2] Chief, Explosives Division, Central Experiment Station, Bureau of Mines, Pittsburgh, Pa.
[3] Supervising Chemist, Physical Chemistry and Physics Section, Explosives Division, Central Experiment Station, Bureau of Mines, Pittsburgh, Pa.
[4] M. V. Blanc, P. G. Guest, G. von Elbe, and B. Lewis, J. Chem. Phys. 15, 798 (1947).

equation:

$$\mu d^2T/dx^2-\rho Sc_p dT/dx+q(x)=0 \qquad (1)$$

where T = temperature, μ = heat conductivity coefficient, ρ = density, S = velocity of the gas flow, c_p = specific heat, and $q(x)$ = rate of heat release by chemical reaction per unit volume.

The temperature rises from T_u of the unburned gas to T_b of the burned gas. The chemical term $q(x)$ is initially very small; hence, according to Eq. (1), $d^2T/dx^2 \sim dT/dx$, which means that the temperature gradient and also the temperature increase exponentially with x, until at some temperature T the chemical term becomes significantly large. d^2T/dx^2 now decreases and finally becomes negative, corresponding to the dotted temperature curve in Fig. 1. Accordingly, as shown in the lower part of the figure, a mass element entering the combustion wave first acquires some excess energy by heat conduction from preceding elements and then returns this "borrowed" energy to succeeding elements; so that, as demanded by thermodynamics, its thermal energy after passage through the combustion wave is equal to the sum of its thermal and chemical energy before it entered the combustion wave. In the aggregate, the mass elements inside a plane wave segment of unit area carry an excess energy, $\int_0^{+\infty}\rho(h-h_0)dx$, where h represents the sum of thermal and chemical energy per unit mass and the subscript zero refers to the state before and after passage through the combustion zone.

The initial small flame which is formed around a spark derives its excess energy from the spark

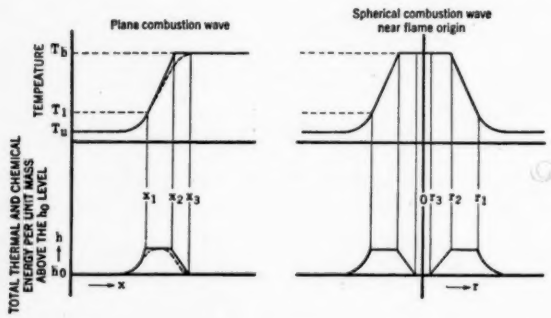

FIG. 1. Distribution of temperature and energy per unit mass in the combustion wave. h_0 = sum of thermal and chemical energy per unit mass before and after combustion.

- - - - - Actual distribution ———— Approximate distribution

itself. It is the function of the latter to initiate the reaction by producing a high local concentration of heat and chain carriers, and to furnish at least as much energy as is necessary to satisfy the excess energy requirement of the smallest flame sphere that is capable of self-propagation. Such a flame may be visualized as a burning sphere of the smallest volume consistent with the condition that the rate of heat production should equal the rate of heat conduction to the surrounding unburned gas. As the flame grows the additional energy required by the growing flame surface is taken from the burned gas; that is, the combustion temperature is slightly lower than the temperature T_b of the plane wave. However, the spark must furnish at least the energy corresponding to the integral $\int_0^{\infty}4\pi r^2\rho(h-h_0)dr$ of the smallest self-propagating flame, r being the distance from the center of the flame.

The calculation of this energy from other data, notably data on the burning velocity and the diameter of the smallest flame, is made possible by substituting for the actual temperature gradient the simple approximate gradient illustrated in Fig. 1. The term $q(x)$, Eq. (1), is taken as zero up to the temperature T_1, and thus the gradient initially rises exponentially. Between T_1 and T_b, $q(x)$ is taken as constant and d^2T/dx^2 as zero, and the gradient thus remains constant. A mass element within this part of the gradient neither loses nor gains h = thermal + chemical energy. However, heat is continually being furnished to the fresh gas at x_1; this heat is being produced at the constant temperature level T_b from residual chemical energy between x_2 and x_3, and transported down the gradient by a fictitious mechanism. Although the resulting temperature and energy distributions are not physically possible, they closely circumscribe the actual distributions. They can be calculated numerically from the data on the width of the reaction zone x_3-x_1, the burning velocity S_u, the temperatures T_u and T_b, and the heat conductivity, density and specific heat of the unburned gas.

In a calculation of this kind no issue arises concerning a "thermal" or "kinetic" theory of flame propagation. The issue arises only when, conversely, an attempt is made to calculate S_u and x_3-x_1 from speculative values of T_1 and the rate of the chemical reaction. These quanti-

ties would have to be determined from comprehensive knowledge of reaction kinetics and the diffusion of chain carriers in the reaction zone. However, if such knowledge were available, one would certainly not attempt to calculate the burning velocity and width of the reaction zone from a system of equations based on the heat balance Eq. (1) and the concept of ignition temperature. Rather, since the values of S_u and x_3-x_1 are mainly determined by chemical and diffusion processes *within the zone of active chemical reaction*, a suitable approximation may consist in the elimination of the heat balance Eq. (1) by an assumption regarding the energy content of any layer dx and giving detailed consideration to reaction and diffusion processes only. This principle was used in the calculation of burning velocity and width of the reaction zone of ozone flames by Lewis and von Elbe.[5]

For the present problem of calculating the minimum ignition energy the heat balance equation for a spherical combustion wave must be developed, using the above approximation.

For $r \geqslant r_1$ (cf. Fig. 1) the chemical term is zero; hence, the increase of heat in a unit volume of any shell $4\pi r^2 dr$ during the time dt is given by

$$\mu\left(\frac{\partial^2 T}{\partial r^2}+\frac{2}{r}\frac{\partial T}{\partial r}\right)=c_p\rho\frac{\partial T}{\partial t}. \tag{2}$$

Here $\partial T/\partial r$ is a negative quantity since the temperature decreases along the radius r, but $\partial^2 T/\partial r^2$ is positive.

As the flame spreads the radii r_1 and r_2 increase at the rate $\partial r/\partial t = S_b$, which is the velocity of the combustion wave relative to the gas at the temperature T_b. This burned gas is at rest relative to the flame center, and the sphere with radius r_2 gains the mass $\rho_b S_b$ per unit surface in unit time. In the outer colder shells a flow of gas away from the center is induced by the thermal expansion, and each shell expands relative to the moving gas at a velocity $S<S_b$. It appears consistent with the assumptions of this treatment to specify that the shells expand at such a rate that the mass crossing unit area is the same for all shells, i.e., $\rho_b S_b=\rho S=\rho_u S_u$. Thus during unit time the mass

[5] B. Lewis, and G. von Elbe, J. Chem. Phys. 2, 537 (1934).

TABLE I.

ar_1	1	2	3	4	5
$\int_{r_1}^{\infty} a^3r^2[-Ei(-ar)]dr$	0.514	0.296	0.142	0.058	0.018

$\rho_u S_u$ passes through the volume *dr times unit area* of a shell of total volume $4\pi r^2 dr$, and receives the heat $c_p\rho_u S_u dT$; hence $|c_p\rho_u S_u \partial T/\partial r|$ is the rate of increase of heat in a unit volume of the shell. Equation (2) may then be written

$$\mu\left(\frac{\partial^2 T}{\partial r^2}+\frac{2}{r}\frac{\partial T}{\partial r}\right)=-c_p\rho_u S_u\frac{\partial T}{\partial r} \tag{3}$$

or

$$\partial^2 T/\partial r^2+(a+2/r)\partial T/\partial r=0, \tag{3a}$$

where $a=c_p\rho_u S_u/\mu$. Writing $\partial T/\partial r=u$, Eq. (3a) is integrated to

$$u=u_1(r_1/r)^2 e^{-a(r-r_1)} \tag{4}$$

and further,

$$\frac{T-T_u}{|u_1|r_1}=\frac{r_1}{r}e^{-a(r-r_1)}-ar_1e^{ar_1}[-Ei(-ar)] \tag{5}$$

where

$$-Ei(-ar)=\int_r^{\infty}\frac{e^{-ar}}{r}dr.^{6}$$

The temperature T_1 and the gradient $|u_1|$ at r_1 for the spherical wave and x_1 for the plane wave, respectively (Fig. 1), are considered to be identical. For the plane wave the heat balance at x_1 is

$$\mu u_1=c_p\rho_u S_{u(r_1=\infty)}(T_1-T_u) \tag{6}$$

or

$$(T_1-T_u)/u_1=1/a_\infty \tag{7}$$

where a_∞ is the value of a for a very large flame radius, i.e., plane wave. From (5) for $r=r_1$ and $T=T_1$, and (7),

$$\frac{1}{a_\infty r_1}=1-ar_1e^{ar_1}[-Ei(-ar_1)]. \tag{8}$$

The coefficient a is thus determined from values of r_1 and the coefficient a_∞. The latter is

[6] This function is tabulated in "Tables of sine, cosine and exponential integrals," Vol. 1, Federal Works Agency, WPA, 1940; sponsored by National Bureau of Standards.

TABLE II. Average temperature T_a at radius r_a between T_1 and T_u.

ar_1	3	5	10	15	20	30	40	50
ar_a	3.90	5.82	10.77	15.74	20.73	30.72	40.69	50.68
$\frac{(T_a-T_u)}{(T_b-T_u)}$	0.263	0.166	0.0816	0.0537	0.0418	0.0254	0.0191	0.0153

larger than a corresponding to an increase of the burning velocity S_u as the flame expands from a sphere to a plane wave.

The excess energy H in the exponential part of the temperature gradient is

$$\left|H\right|_{r_1}^{\infty}=\int_{r_1}^{\infty}4\pi r^2\rho(h-h_0)dr$$
$$=\int_{r_1}^{\infty}4\pi r^2\rho c_p(T-T_u)dr. \quad (9)$$

Substituting $T-T_u$ from Eq. (5), and integrating,

$$\left|H\right|_{r_1}^{\infty}=4\pi\bar{\rho}\bar{c}_p|u_1|(r_1/a)^2$$
$$\times\left(1+ar_1-\int_{r_1}^{\infty}a^3r^2[-Ei(-ar)]dr\right) \quad (10)$$

where $\bar{\rho}$ and $\bar{c}_p$ now represent average values over the shell volume from r_1 to ∞. Values of the integral term inside the bracket have been determined and are given in Table I. Since in numerical examples the term ar_1 is generally found to be considerably larger than two, it appears that the integral term may be safely neglected.

For the linear part of the gradient between r_1 and r_2 one obtains

$$\left|H\right|_{r_2}^{r_1}=\int_{r_2}^{r_1}4\pi r^2\rho\bar{c}_p(T_1-T_u)dr$$
$$=(4/3)\pi\bar{\rho}_1\bar{c}_p(T_1-T_u)(r_1^3-r_2^3). \quad (11)$$

TABLE III. Thermal conductivities, densities and specific heats.

	μ, cal./cm sec. °C	ρ, g/cm³	c_p, cal./g °C			
T, °K	300	300	300	500	600	700
O_2	0.000062	0.00131	0.218	0.232	0.240	0.246
N_2	0.000061	0.00115	0.250	0.253	0.258	0.263
CH_4	0.000075	0.00065	0.518	0.697	0.781	0.868

The average density $\bar{\rho}_1$ is smaller than $\bar{\rho}$ because the temperature rises from T_1 to T_b between r_1 and r_2. After combining with Eq. (7), Eq. (11) may be written in a form directly comparable with Eq. (10), namely,

$$\left|H\right|_{r_2}^{r_1}=4\pi\bar{\rho}_1\bar{c}_p|u_1|(r_1^2/aa_\infty)$$
$$\times[(ar_1-ar_2^3/r_1^2)/3]. \quad (11a)$$

This shows that $\left|H\right|_{r_2}^{r_1}$ has somewhat less than one third the value of $\left|H\right|_{r_1}^{\infty}$. The term $\left|H\right|_{0}^{r_2}$ is smaller than the second term in Eq. (11a) and hence may be neglected.

The gradient $|u_1|$ is stable, i.e., the flame can propagate, when the rate of heat production in the volume $(4/3)\pi r_2^3$ equals the heat flow across the area $4\pi r_1^2$. In the smallest flame that can propagate the reaction zone is considered to extend to the center, and r_2 (Fig. 1) is zero. In unit time the heat q is liberated per unit volume. This quantity is taken as constant between $r=0$ and $r=r_1$, and zero at $r>r_1$. Thus, the flame can propagate when

$$(4/3)\pi r_2^3q=4\pi r_1^2\mu|u_1|. \quad (12)$$

Between r_1 and r_2 the heat balance equation becomes

$$q=c_p\rho_uS_u|u_1|. \quad (13)$$

Combining (12) and (13),

$$r_2^3=3r_1^2\mu/c_p\rho_uS_u=3r_1^2/a. \quad (14)$$

Since

$$|u_1|=(T_b-T_1)/(r_1-r_2), \quad (15)$$
$$|u_1|=(T_b-T_1)/r_1[1-(3/ar_1)^{\frac{1}{2}}].$$

Eliminating T_1 by Eq. (7),

$$|u_1|=a_\infty(T_b-T_u)/\{1+a_\infty r_1[1-(3/ar_1)^{\frac{1}{2}}]\}. \quad (16)$$

The final equation for the minimum ignition energy is obtained by adding Eqs. (10) and (11a) and eliminating $|u_1|$ by Eq. (16). On the basis

of previous discussions of Eqs. (10) and (11a), numerical calculations will not be significantly affected if the integral term in (10) is neglected and if the contribution of (11a) is simply expressed by changing the remaining numerical factor $1+ar_1$ in Eq. (10) to $1+1.3ar_1$. The equation may then be written

$$H=4\pi r_1^2(\bar{\rho}\bar{c}_p/a_\infty)(T_b-T_u)\times\left(\frac{a_\infty}{a}\right)^2\frac{1+1.3ar_1}{1+a_\infty r_1[1-(3/ar_1)^{\frac{1}{2}}]}. \quad (17)$$

Values of T_b may be calculated from thermodynamic data. Since the specific heat, heat conductivity and density change with temperature, values of these quantities at an average temperature T_a between T_1 and T_u are used. The following method is used to calculate T_a: A radius $r_a>r_1$ is determined so that

$$\tfrac{1}{2}\left|H\right|_{r_1}^{\infty}=\left|H\right|_{r_1}^{r_a}=\left|H\right|_{r_a}^{\infty}. \quad (18)$$

Analogous to Eq. (9) for $\left|H\right|_{r_1}^{\infty}$, and taking ρc_p as constant for the purpose of this calculation, one may write

$$\int_{r_1}^{r_a} r^2(T-T_u)dr=\int_{r_a}^{\infty} r^2(T-T_u)dr. \quad (19)$$

Substituting $T-T_u$ by Eq. (5), and integrating, one obtains

$$(ar_a+1)e^{-a(r_a-r_1)}=0.5(ar_1+1). \quad (20)$$

In this equation the terms with factors $(-Ei(-ar))$ have been neglected because, as was shown earlier in Eq. (10), they are very small for the values of ar_1 and ar_a which are of interest here.

Values of ar_a calculated from Eq. (20) are used to calculate $(T_a-T_u)/(T_b-T_u)$ from Eqs. (5) and (16). Results are shown in Table II.

Values of μ and ρ at 300°K, and c_p at 300, 500, 600, and 700°K are given in Table III. μ increases approximately proportional to the square root of the temperature and ρ is inversely proportional to the temperature.

The heat conductivity of the mixture is taken as the molar average of the heat conductivities of the component gases. Values of the burning velocity S_u for a plane wave are taken from burner-method measurements.[7] The coefficient a_∞ is thus calculated from the equation

$$a_\infty=(\bar{c}_p\rho_u S_u/\mu_u)(T_u/T_a)^{\frac{1}{2}}. \quad (21)$$

On partial substitution of Eq. (21) in Eq. (17) and since $\bar{\rho}=\rho_u T_u/T_a$, Eq. (17) may be rewritten in the form

$$H=4\pi r_1^2\frac{\mu_u}{S_u}\left(\frac{T_u}{T_a}\right)^{\frac{1}{2}}(T_b-T_u)\left(\frac{a_\infty}{a}\right)^2\times\frac{1+1.3ar_1}{1+a_\infty r_1[1-(3/ar_1)^{\frac{1}{2}}]}. \quad (22)$$

The remaining unknown quantity in this equation is the flame radius r_1. An upper limit is given by the readily measurable flame-quenching distance d between plane-parallel plates,

TABLE IV. Calculation of flame diameters $2r_1$, temperatures T_b, T_1, and T_a, and gradients $(T_b-T_1)/(r_1-r_2)$ for smallest igniting flames. Comparison of flame diameters with flame quenching distances d between parallel plates. $T_u=300$°K.

Mixture composition, percent			S_u,	T_b	T_1	T_a	Min. ignition energy H, cal. 10^3		$2r_1$,	d,		$\frac{(T_b-T_1)}{(r_1-r_2)}$,
CH_4	O_2	N_2	cm/sec.		°K		Exp.	Calc.[a]	cm	cm	$d/2r_1$	°C/cm 10^3
10	90	...	80	2200	1330	587	19	36	0.038	0.072	1.9	3.5
15	85	...	175	2650	1570	658	3.1	3.9	.017	.050	2.9	9.5
25	75	...	304	3000	822	515	1.4	...	.016	.028	1.8	8.0
40	60	...	305	3000	605	435	5.0	...	.032	.051	1.6	3.5
50	50	...	122	2650	446	379	110	...	.106	.165	1.6	0.8
52.5	47.5	...	87	2500	388	343	430	...	.192	.38	2.0	0.38
10	18.8	71.2	36	2200	1115	548	170	382	.090	.28	3.1	1.3
16.3	29.3	54.4	110	2620	1100	567	20	...	.035	.079	2.3	3.8
21.5	39.75	39.75	170	2810	791	501	9	...	.031	.053	1.7	3.9
26.4	49.1	24.5	240	2940	592	429	5.3	...	.030	.045	1.5	3.6

[a] Values obtained by minimizing Eq. (22).

[7] G. Jahn, *Der Zündvorgang in Gasgemischen* (Oldenbourg, Berlin, 1934).

which evidently must be larger than $2r_1$. It appears difficult at present to develop a quantitative theoretical relationship between d and $2r_1$; however, the two diameters cannot be very greatly different, and a factor $d/2r_1 \simeq 2$ appears reasonable. Equation (22) has therefore been used to calculate values of $2r_1$ from measured minimum ignition energies, and these values are compared with the corresponding values of d. The calculations are shown in Table IV. The examples chosen include a wide range of mixtures of methane, oxygen and nitrogen, and demonstrate that a reasonable correspondence between d and $2r_1$ indeed exists.

Equation (22) is of such a form that H, as a function of the radius r_1, passes through a minimum. This is a consequence of the approximating assumptions embodied in the treatment and cannot be considered physically significant. In some cases this calculated minimum value is larger than the experimental value of H and it becomes impossible to satisfy the experimental value by any choice of r_1. It then appears proper to solve the equation for the minimum value as this is the closest approach to the experimental value of H. It is noted in Table IV that this was done in three cases corresponding to low methane percentages. The discrepancies are not serious.

The values of T_1 and of the temperature gradient $(T_b-T_1)/(r_1-r_2)$ in Table IV indicate a marked difference between lean and rich mixtures of comparable burning velocities and combustion temperatures. In the former the chemical reaction begins at a much higher temperature and the temperature gradient is much steeper, than in the latter. An explanation may possibly be found in the suggestion that in the combustion zone of rich mixtures the concentration of free radicals and particularly hydrogen atoms is much larger. If such species diffuse toward the unburned gas in considerable quantity, significant reaction occurs already at low temperature levels. The higher temperature levels are then depleted of chain carriers, and the temperature gradient correspondingly is much less steep than in lean mixtures, where rapid reaction is confined chiefly to high temperature levels.

The treatment thus establishes a theoretical concept of the minimum ignition energy of sparks in agreement with experimental data, and also suggests further investigations of the temperature gradient in combustion waves as a means of analyzing the physical-chemical processes governing flame propagation.

In conclusion, it is noted that the treatment is applicable to sparks only when (1) the dimensions of the flame over which the spark energy is distributed during the time of discharge are smaller than the flame radius r_1, and (2) the time of discharge is small compared to the time required for a substantial growth of the flame radius r_1. The second condition is easily fulfilled. For example, in the case of a fast burning mixture of 25 percent methane and 75 percent oxygen, a 50-percent increase of flame radius requires approximately 10^{-5} seconds according to the values of S_u and r_1 in Table IV, while the time of discharge is of the order of 10^{-7} seconds. The first condition cannot remain fulfilled indefinitely when the spark electrodes are pulled apart, and thus it is understandable that at large gap lengths the minimum ignition energies increase as shown in the preceding paper. Similarly, future experiments with greatly increased duration of electric discharge should demonstrate the dependence of the minimum ignition energy on the discharge time.

THE JOURNAL OF CHEMICAL PHYSICS VOLUME 15, NUMBER 11 NOVEMBER, 1947

The Absorption Spectrum of Carbon Dioxide from 14 to 16 Microns[1-3]

LEWIS D. KAPLAN[4]
Department of Meteorology, The University of Chicago, Chicago, Illinois
(Received August 18, 1947)

Absorption of a parallel beam of radiation from 14 to 16 microns by equivalent thicknesses of 0.004, 0.05, 1, 4, and 20 centimeters of carbon dioxide is calculated on the basis of quantum mechanics considerations for stratospheric conditions. The intensity values for the vibration-rotational lines in the P and R branches of the important vibrational transitions are computed and a method is suggested for correcting the absorption values when more accurate measurements of the matrix element of the electric dipole moments of transition are made. An empirical formula suggested by Sutherland and Callendar is found to give an inaccurate representation of the dependence of absorption on path length for conditions prevailing in the lower stratosphere.

INTRODUCTION

THE accurate determination of the infra-red fine structure of most of the important gases and the recent precision in measurements of line-widths stand in ever sharper contrast to our lack of knowledge concerning absolute absorption intensities. This situation is especially deplorable since a complete theoretical treatment has been available in the literature for well over a decade.[5]

The only serious attempt that has been made to determine the absorption of terrestrial radiation by carbon dioxide is a set of empirical formulas determined by G. S. Callendar on the basis of laboratory conditions.[6] These are of the form:

$$\tau=(1+nu^x)^{-1}, \qquad (1)$$

where τ is the fractional transmission, u the equivalent gas thickness in centimeters after reduction to room temperature and a pressure of one atmosphere, and n and x empirical constants. For the carbon dioxide band interval from 14 to 16 microns Callendar obtained values of 0.9 and 0.84 for n and x, respectively. Callendar suggested modifying the formula by substituting for u the product of the equivalent path length and the square root of the pressure in fractions of an atmosphere to take into account the pressure variation with height. Since the only pressure influence on absorption is its effect on the line width, which, according to the Lorentz dispersion theory, is proportional to the collision frequency and thus to the pressure divided by the square root of the temperature, Eq. (1) becomes:

$$\tau=(1+n(u)^x(P/P_0)^{x/2}(T_0/T)^{x/4})^{-1}, \qquad (2)$$

where P_0 is one atmosphere and T_0 room temperature (about 300°K). It should be noted that other temperature effects are neglected in this formula.

In a later paper, Sutherland and Callendar were doubtful as to the validity of the empirical formulas to other than laboratory conditions under which they were made:[7]

"Although this modification may give consistent results among a set of laboratory observations, it should not be applied to atmospheric conditions without considering the possible effects of temperature and of pressure. A rise in temperature will increase the overall absorption

[1] Published with permission of the Chief, U. S. Weather Bureau, Department of Commerce.
[2] From a thesis submitted in partial fulfillment of the requirements for the degree of Master of Science in the Department of Meteorology, the University of Chicago.
[3] The basic material in this paper was presented before the annual spring meeting of the American Meteorological Society, Washington, D. C., May 1, 1947.
[4] Research Associate, Department of Physics, The University of New Mexico, Albuquerque, New Mexico.
[5] For example, D. M. Dennison, Rev. Mod. Phys. **3**, 280 (1931), and E. Teller, *Hand-und-Jahrbuch der Chemischen Physik* (Akademische Verlagsgesellschaft, Leipzig, 1934), **9**, Section II, pp. 43–160.
[6] G. S. Callendar, Quart. J. Roy. Met. Soc. **67**, 263 (1941).
[7] G. B. B. M. Sutherland and G. S. Callendar, Rep. Prog. Phys. **9**, 18 (1942–43). Note that Sutherland and Callendar do not make use of Lorentz's treatment of collision broadening. Reason (i) is of little importance for the troposphere and lower stratosphere. Since an increase in temperature under constant pressure will narrow the individual line widths, reason (ii) is not valid for atmospheric conditions.

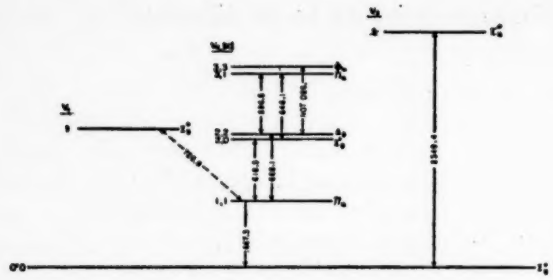

FIG. 1. Vibrational transitions for CO_2.

of a given band for the following reasons:

(i) Doppler broadening of the individual lines;
(ii) Collision broadening of the individual lines;
(iii) Additional lines and bands will appear since higher energy levels will become populated, thus permitting new transitions.

"A rise in pressure will increase absorption mainly because of collision broadening. The order of magnitude of this effect will vary with the intermolecular forces which come into play. Thus it has been found to be particularly marked for HCN where the line width alters from 0.57 cm.$^{-1}$ at 130 mm. Hg to 1.37 cm.$^{-1}$ at 650 mm. Hg (Herzberg, Spinks and Watson, 1936). An exactly similar effect will be produced by mixing a second gas with the first, so we have a third factor to take into account, *viz.*, the effect of the presence of gas A on the absorption bands of B even when these bands do not overlap. It is not possible to calculate the alterations in k_λ [absorption coefficient—L.K.] arising from these three causes, and the experimental data are too scanty to allow any empirical estimates to be made. Until further experiments have been carried out we must simply use the present data, remembering, however, that these effects must impose limitations on our conclusions in a certain direction."

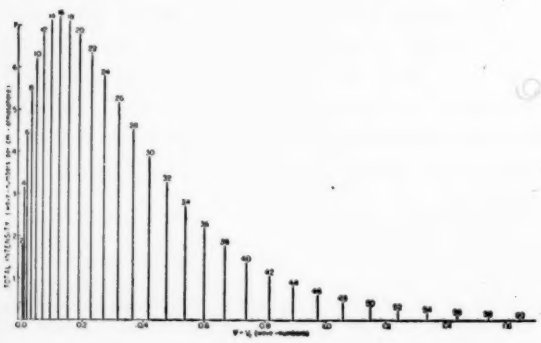

FIG. 2. Intensities of Q branch lines for $T=300°$A.

It is difficult to see how Sutherland and Callendar could have reached such a pessimistic conclusion in view of the complete treatment by Dennison of absorption by simple polyatomic molecules.

DISTRIBUTION OF ABSORPTION INTENSITY

The intensity equations for a perpendicular type band of a symmetrical top rotator are:[8]

R branch:

$$I(J, K+1\rightarrow J+1, K) = A[(J-K)(J-K+1)/2(J+1)] \times\exp(-\sigma J(J+1)-\sigma\beta K^2) \quad (3)$$

Q branch:

$$I(J, K+1\rightarrow J, K) = A[(2J+1)(J-K)(J+K+1)/2J(J+1)] \times\exp(-\sigma J(J+1)-\sigma\beta K^2) \quad (4)$$

P branch:

$$I(J+1, K+1\rightarrow J, K) = A[(J+K+1)(J+K+2)/2(J+1)] \times\exp(-\sigma(J+1)(J+2)-\sigma\beta K^2) \quad (5)$$

R branch:

$$I(J, K\rightarrow J+1, K+1) = A[(J+K+1)(J+K+2)/2(J+1)] \times\exp(-\sigma J(J+1)-\sigma\beta K^2) \quad (6)$$

Q branch:

$$I(J, K\rightarrow J, K+1) = A[(2J+1)(J-K)(J+K+1)/2J(J+1)] \times\exp(-\sigma J(J+1)-\sigma\beta K^2) \quad (7)$$

P branch:

$$I(J+1, K\rightarrow J, K+1) = A[(J-K)(J-K+1)/2(J+1)] \times\exp(-\sigma(J+1)(J+2)-\sigma\beta K^2) \quad (8)$$

where:

$$\sigma = Bhc/kT; \quad (9)$$

$$A \propto d_n \nu_{m,n} M_{m,n}{}^2 e^{-E_n/kT}(1-e^{-h\nu/kT}); \quad (10)$$

J is the rotational quantum number; K is the angular momentum quantum number; $-\beta$ is one minus the ratio of the moments of inertia of the symmetrical top; B is the rotational constant; d_n is the degeneracy of the lower vibra-

[8] D. M. Dennison, reference 5. The interactions between rotation and vibration are of course neglected, as usual.

tional state; $\nu_{m,n}$ is the transition frequency; $M_{m,n}$ is the matrix element of the electric dipole moment for the vibrational transitions; and E_n is the energy of the lower state.

For all practical purposes the factor $\exp(-\sigma\beta K^2)$ can be taken into the proportionality constant A for transitions from the "ground state" and neglected for higher vibrational transitions; $e^{-h\nu/kT}$ can be neglected in comparison with unity; and $\nu_{m,n}$ can be considered as a constant equal to the vibrational transition frequency.

For the perpendicular (15 micron) vibration of carbon dioxide, d_n is one for the lowest state and two for the first vibrational transition, B is 0.390 cm^{-1}, and E_n is given by:

$$E_n=(v_1+\tfrac{1}{2})h\nu_1+(v_2+1)h\nu_2+(v_3+\tfrac{1}{2})h\nu_3, \quad (11)$$

where ν_1, ν_2 and ν_3 are the vibrational frequencies of the symmetrical, perpendicular and antisymmetrical vibrations respectively, and v_1, v_2 and v_3 the vibrational quantum numbers.[9] The lowest vibrational levels for carbon dioxide are shown in Fig. 1, with the infra-red transition frequencies given in wave-numbers.

The shape of the individual vibration-rotational line is due to the pressure broadening effect and given by the Lorentz dispersion formula:[10]

$$k(\nu)=I\alpha/\pi((\nu-\nu_0)^2+\alpha^2), \quad (12)$$

where ν_0 is the frequency at the line center, α the half-width or spectral distance from ν_0 at which the absorption coefficient $k(\nu)$ has half the value it has at ν_0, and I the total intensity of the line, defined by:

$$I=\int_{-\infty}^{+\infty} k(\nu)d\nu. \quad (13)$$

The spacing of the lines in the P and R branches (low and high frequency, respectively) has been measured by Martin and Barker for the strong and moderate lines of the 15 micron band.[11] The spacing of the lines in the Q branch

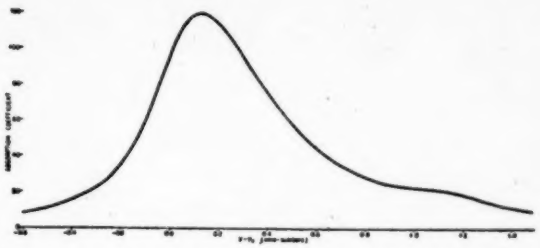

FIG. 3. Q branch absorption curve for $T=300°A$.

is given by the formula:[12]

$$Q(J)=\tilde{\nu}_2+(B'-B'')(J+J^2), \quad (14)$$

where $Q(J)$ is the position of the line J in wave-numbers, $\tilde{\nu}_2=667.3$ cm^{-1} is the vibrational frequency in wave-numbers, and B' and B'' are the rotational constants for the upper and lower states, respectively. For the first vibrational level and the "ground state" they have the values 0.38995 cm^{-1} and 0.38950 cm^{-1}.[13] Since the oxygen nuclei have zero spin, the odd vibration-rotational lines are missing. Equations (7) and (8) show that there are no zero vibration-rotational lines for the P and Q branches.

DETERMINATION OF PROPORTIONALITY CONSTANTS

Since all the absorption between 14 and 16 microns is due to transitions involving the perpendicular vibration ν_2, the above treatment enables one to calculate the absorption in this interval providing $M_{m,n}$ or A is known and α is known. The direct method for determination of

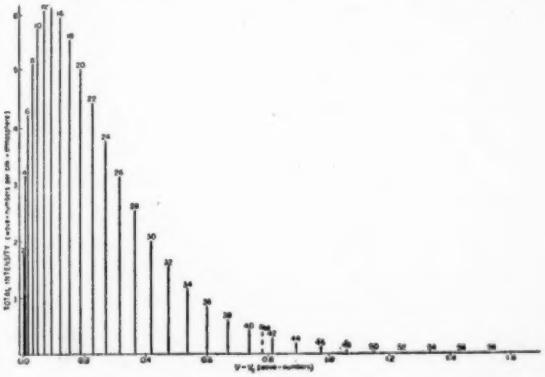

FIG. 4. Intensities of Q branch lines for $T=218°A$.

[9] For a detailed treatment, see A. Adel and D. M. Dennison, Phys. Rev. **43**, 716 (1933).

[10] H. A. Lorentz, Proc. Acad. Amsterdam **18**, 134 (1915).

[11] P. E. Martin and E. F. Barker, Phys. Rev. **41**, 291 (1932).

[12] G. Herzberg, *Infrared and Raman Spectra of Polyatomic Molecules* (D. Van Nostrand Co., New York, 1945), p. 384.

[13] *Ibid.*, p. 395.

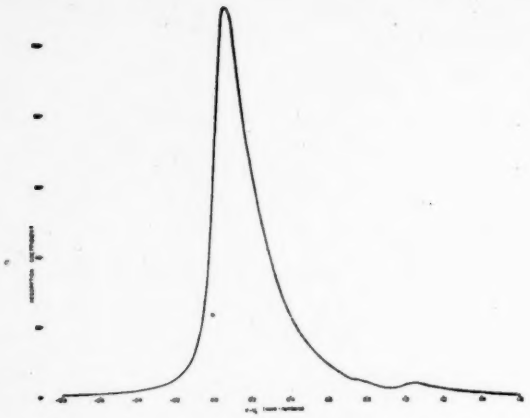

FIG. 5. Q branch absorption curve for $T=218°$A.

the proportionality constant is to measure the absorption over a small frequency interval and adjust the value of A until the calculated absorption is equal to the measured absorption.

In such a determination, several sources of error have to be eliminated or taken into account. The most important of these is the fact that a spectroscope with finite slits gives a weighted average of the transmitted radiation rather than the unweighted average of the logarithm of the transmitted radiation.[14] Another source of error is the fact that the cut-off by the edges of the slit is not sharp. These errors may be minimized by choosing a spectral interval in which most of the intensity is well within the spectral interval and, at the same time, the total intensity is so large that very small thicknesses of absorbing gas may be used, resulting in a minimum of absorption by the wings of the spectral lines.

Such a spectral interval is one including the Q branch of the ν_2 vibrational transition, for which measurements with low resolution have been made by Martin and Barker.[15] The spectral interval should be equal to the half width of the irregularities on the spectrogram, which is 2.0 cm^{-1}. For this spectral interval Martin and Barker found that an effective path length of 0.004 cm absorbed 16 percent of the incident radiation when the slit was centered on the peak of the Q branch. These values were used to determine A.

The Q branch for the first vibrational transition is due to the transition from $v_2=|K|=0$ to $v_2=|K|=1$ with $\Delta J=0$. Thus, Eq. (7) is used, becoming:

$$I(J, 0\rightarrow J, 1)=\tfrac{1}{2}A(2J+1)e^{-\sigma J(J+1)}, \quad (15)$$

where $\sigma=Bhc/kT=0.001871$ for $T=300°$K. Assigning an arbitrary value to A, the line intensities were plotted as a function of wave number, using Eqs. (14) and (15). The results are shown in Fig. 2, except that the intensity values are the final ones obtained.

Before the absorption coefficients are determined it is necessary to know the value of α. The half-width in centimeters of wave-length is equal to the distance travelled by light in the mean time between collisions; thus the half-width in wave numbers is equal to the collision frequency divided by the velocity of light. According to kinetic theory, the collision frequency for elastic collisions is given by the formula:[16]

$$F=\tfrac{1}{2}\sum_i N_i(D_1+D_i)^2 \times[2\pi kT(1/m_1+1/m_i)]^{\frac{1}{2}}, \quad (16)$$

where N_i is the number of molecules of gas "i" per unit volume, D_i is the effective diameter of a molecule of gas "i" and m_i its mass. The subscript "1" refers to the gas in the mixture whose collision frequency is to be determined. Assuming a molecular diameter of 2.9 angstrom units for O_2 and 3.3 for N_2 and CO_2,[17] and using Paneth's

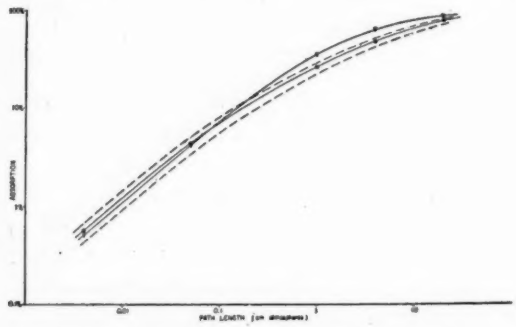

FIG. 6. Absorption from 14 to 16 μ as a function of equivalent path length, with $P=203$ mbs., $T=218°$A.
Curve through circles: $A=0.271$ cm^{-1} per cm-atmos.
Upper dashed curve: $A=0.325$ cm^{-1} per cm-atmos.
Lower dashed curve: $A=0.193$ cm^{-1} per cm-atmos.
Curve through triangles: Empirical formula of Sutherland and Callendar.

[14] E. B. Wilson and A. J. Wells, J. Chem. Phys. **14**, 578 (1946).
[15] See reference 11, Figs. 1 and 6.
[16] E. H. Kennard, *Kinetic Theory of Gases* (McGraw-Hill Book Company, New York, 1938), p. 112.
[17] The means of the values determined by molecular viscosity, van der Waal's equation, and heat conductivity

values for the composition of atmospheric air,[18] a collision frequency of 5.5×10^9 collisions per second is obtained, resulting in a half-width of 0.18 cm^{-1}. In the actual calculations the slightly lower value of 0.17 cm^{-1} was used.

A curve was drawn from Eq. (12) for each line and the absorption coefficients were added graphically by means of a light-table, each curve being placed on its corresponding line. The same procedure was followed for the transition from $v=|K|=1$ to $v=|K|=2$ with $\Delta J=0$, which has a vibrational transition frequency of 668.3 cm^{-1}. The ratio of the proportionality constants for these two transitions was determined from Eq. (10). The line $J=0$ of the R branch for the first vibrational transition, which occurs at about $\tilde{\nu}-\tilde{\nu}_2=0.78$ cm^{-1}, was taken into account using Eq. (6). The curve of absorption coefficient for the interval -0.6 $cm^{-1}\leq\tilde{\nu}-\tilde{\nu}_2\leq1.4$ cm^{-1} is shown in Fig. 3. The irregularity in the vicinity of $\tilde{\nu}-\tilde{\nu}_2=1.1$ cm^{-1} is the result of the Q branch for the transition from $v=|K|=1$ to $v=|K|=2$. The absorption coefficients given are the final ones obtained.

The 2.0 cm^{-1} spectral interval was divided into forty parts of width 0.05 cm^{-1} each, so that the mean value of the absorption coefficient k could be considered as a representative value for each of these small intervals and the fractional transmission computed from Lambert's formula:

$$\tau=\sum_i e^{-k_i u}/40. \qquad (17)$$

The values of k had to be adjusted by successive approximations until Eq. (17) gave a value of 84.0 percent for the transmission. The A value for the first vibrational transition obtained in this manner was 0.271 cm^{-1} per cm-atmosphere.[19]

EXAMPLE OF ABSORPTION CALCULATION

With the proportionality constants determined, it was possible to calculate the intensities of the individual lines, and thus the absorption. Such a calculation was made for a pressure of 203 millibars and a temperature of 218°K, corresponding to conditions in the lower stratosphere. The half-width under these conditions would be 0.040 cm^{-1}.

TABLE I. Intensity of vibration-rotational lines.*

	$00^00\rightarrow01^10$			$01^10\rightarrow02^20$		$01^10\rightarrow02^00$	$01^10\rightarrow10^00$
J	$I_Q(J)$	$I_P(J)$	$I_R(J)$	$I_P(J)$	$I_R(J)$	$I_R(J)$	$I_P(J)$
0			0.73		0.0536		0.0201
2	1.79	0.70	1.43	0.0058	0.0583	0.0036	0.0219
4	3.16	1.37	2.11	0.0201	0.0723	0.0126	0.0271
6	4.24	1.89	2.61	0.0330	0.0821	0.0206	0.0308
8	5.13	2.30	3.02	0.0438	0.0903	0.0274	0.0339
10	5.75	2.59	3.29	0.0519	0.0952	0.0324	0.0357
12	6.08	2.73	3.40	0.0565	0.0960	0.0353	0.0360
14	6.14	2.74	3.39	0.0582	0.0940	0.0364	0.0352
16	5.95	2.64	3.25	0.0570	0.0889	0.0356	0.0333
18	5.57	2.46	3.01	0.0539	0.0814	0.0337	0.0305
20	5.05	2.21	2.71	0.0489	0.0726	0.0306	0.0272
22	4.45	1.93	2.37	0.0472	0.0630	0.0295	0.0236
24	3.79	1.63	2.01	0.0367	0.0531	0.0229	0.0199
26	3.16	1.35	1.67	0.0306	0.0439	0.0191	0.0165
28	2.56	1.08	1.35	0.0246	0.0353	0.0154	0.0132
30	2.02	0.85	1.06	0.0194	0.0276	0.0121	0.0103
32	1.56	0.65	0.82	0.0149	0.0212	0.0093	0.0080
34	1.17	0.48	0.61	0.0111	0.0158	0.0069	0.0059
36	0.86	0.35	0.45	0.0081	0.0115	0.0051	0.0043
38	0.62	0.25	0.32	0.0058	0.0082	0.0036	0.0031
40	0.43	0.17	0.22	0.0040	0.0057	0.0025	0.0021
42	0.30	0.12	0.15	0.0027	0.0039	0.0017	0.0015
44	0.20	0.08	0.10	0.0018	0.0026	0.0011	0.0010
46	0.14	0.05	0.07	0.0012	0.0018	0.0008	0.0007
48	0.08	0.03	0.04	0.0008	0.0011	0.0005	0.0004
50	0.05	0.02	0.03	0.0005	0.0007	0.0003	0.0003
52	0.03	0.01	0.02	0.0003	0.0004	0.0002	0.0002
54	0.02	0.01	0.01	0.0002	0.0002	0.0001	0.0001
56	0.01	0.00	0.01	0.0001	0.0001	0.0001	0.0000
58	0.01	0.00	0.00	0.0000	0.0001	0.0000	0.0000
ΣI	70.32	30.70	40.26	0.6391	1.1809	0.3994	0.4428

* In wave numbers per cm-atmosphere, for $T=218°K$.

The intensities for the individual vibration-rotational lines were calculated by means of Eqs. (3)–(10) and the results are given in Table I. The vibrational levels for the upper and lower states are represented by the notation $v_1v_2^{|K|}v_3$. The intensities for the R branch of the $01^10\rightarrow02^00$ transition and the P branch of the $01^10\rightarrow10^00$ transition were obtained by multiplying the P and R branch intensities for the $01^10\rightarrow02^20$ transitions by 0.625 and 0.375, respectively, in accordance with the intensity distribution between the Raman resonance bands at 1286 and 1388 wave numbers.[20]

The absorption in the region of the Q branch was calculated by the method described in the preceding section. The intensities and spacing of the lines in the Q branch are shown in Fig. 4. The absorption curve was determined first for the first vibrational transition alone, then multi-

were used. *Handbook of Chemistry and Physics* (Chemical Rubber Publishing Company, Cleveland, 1945), p. 2581.

[18] F. A. Paneth, Quart. J. Roy. Meteor. Soc. **63**, 433 (1936).

[19] This results in a value of 220 cm^{-1} per cm-atmosphere for the total intensity due to all the transitions in the 15-micron band. This agrees reasonably well with values from 160 to 220 cm^{-1} per cm-atmosphere calculated by Dr. Alan M. Thorndike by methods described in reference 14, and kindly communicated to Dr. Edward Teller. If anything, the value of 220 cm^{-1} per cm-atmosphere is probably too high.

[20] See I. Hanson, Phys. Rev. **46**, 122 (1934) and A. Langseth and J. R. Nielsen, Phys. Rev. **46**, 1057 (1934).

TABLE II. Results of absorption calculations.

Equivalent path length of CO_2 (cms)	Air thickness (mbs)	Percent absorption: Sutherland and Callendar	Calculated	Intensity increased by 20%	Intensity decreased by 28.8%
0.004	0.0098	0.52	0.57	0.66	0.43
0.05	0.123	4.3	4.4	5.0	3.4
1	2.46	35.2	26.7	29.1	22.6
4	9.84	63.6	48.3	52.1	42.7
20	49.2	87.1	79.3	82	73

plied by 0.0816, corrected in the region of small J's, displaced 1.0 cm^{-1} toward higher frequencies, and added graphically. The resultant curve of absorption coefficients from $\tilde{\nu}-\tilde{\nu}_2=-0.80$ cm^{-1} to $\tilde{\nu}-\tilde{\nu}_2=1.60$ cm^{-1} is shown in Fig. 5. The Q branch for the $01^10\rightarrow02^20$ transition is clearly evident at $\tilde{\nu}-\tilde{\nu}_2=1.05$ cm^{-1} and the effect of the $J=0$ line of the R branch may be detected at $\tilde{\nu}-\tilde{\nu}_2=0.75$ cm^{-1}.

Since this procedure would have been too tedious for the P and R branches, the absorption equation derived by Ladenburg and Reiche from Eq. (12):[21]

$$A\Delta\tilde{\nu}=2\pi\alpha x e^{-x}[J_0(ix)-iJ_1(ix)], \qquad (18)$$

where $x=Iu/2\pi\alpha$, was used for the lines for which $x<3$, for which it is accurate. For the other lines, Elsasser's procedure is applicable and his equation:[22]

$$A=\varphi[(\pi\alpha u)^{\frac{1}{2}}\textstyle\sum_i I_i^{\frac{1}{2}}/d_i], \qquad (19)$$

was used, where φ is the probability function and d_i the spectral distance between two consecutive lines.

Absorption calculations were made for equivalent thicknesses of 0.004, 0.05, 1, 4, and 20 centimeters of carbon dioxide. The absorption due to the various transitions was computed separately, then combined by the following procedure.

The envelope of the absorption curve due to the $01^10\rightarrow02^20$ transition is approximately proportional to that of the first vibrational transition in relation to the intensity distribution over the band; thus if τ_1 and τ_2 represent the transmission due to these transitions for one of the spectral intervals considered,[23] the total transmission is given approximately by their product:

$$\tau_{12}=\tau_1\tau_2. \qquad (20)$$

The envelopes of the absorption curves due to the R branch of the $01^10\rightarrow02^00$ transition and the P branch of the $01^10\rightarrow10^00$ transition have, on the other hand, slopes opposite to those of the above mentioned transitions for the spectral intervals considered, so that their absorption is strongest where that due to the other transitions is weak, and *vice versa*. Thus the total absorption may be approximately determined by adding the absorptions of the asymmetrical parts:

$$A=A_{12}+A_3, \qquad (21)$$

where $A_{12}=1-\tau_{12}$ and A_3 is the absorption of the latter transitions. This procedure is necessary because the higher order transitions are so weak that the fine structure of the bands is completely masked by the lines for the first vibrational transition. But precisely because of the weakness of the higher order transitions, the error introduced by this procedure will be negligible. For simplicity it was assumed that the line spacing was the same for all transitions.

When the absorption was calculated for each of the spectral intervals chosen, the total absorption for the 14 to 16 micron interval was calculated by means of the formula:

$$A\Delta\tilde{\nu}=\textstyle\sum_i A_i\Delta\tilde{\nu}_i, \qquad (22)$$

where A_i is the absorption in the spectral interval $\Delta\tilde{\nu}_i$ and

$$\Delta\tilde{\nu}=\textstyle\sum_i\Delta\tilde{\nu}_i=89.3\ cm^{-1}.$$

The results of the calculation are given in Table II. The first column gives the path length of carbon dioxide reduced to 1013.25 millibars and 300 degrees absolute. Since the flux of radiation is diffuse in contrast to the assumption of parallel radiation in the calculations in this paper and in those of Sutherland and Callendar,

[21] R. Ladenburg and F. Reiche, Ann. der Phys. **42**, 181 (1913). J_0 and J_1 are here zero and first-order Bessel functions. A table of the function $xe^{-x}[J_0(ix)-iJ_1(ix)]$ is given by W. M. Elsasser, *Heat Transfer by Infra-red Radiation in the Atmosphere* (Harvard Meteorological Studies No. 6, Harvard University Printing Office, Cambridge, Mass., 1942), p. 30.

[22] W. M. Elsasser, Phys. Rev. **54**, 126 (1938). This equation is more applicable to the case of CO_2 absorption than to that of H_2O, for which purpose Elsasser developed it, since the CO_2 lines are evenly spaced and the intensity envelope is a smooth curve with little change in slope.

[23] The spectral intervals were that of the Q branch, those for which $x<3$ (Eq. (18)) and those for which $x>3$.

the figures in the first column must be divided by a factor of 1.66 before use in atmospheric absorption calculations.[24] Doing this, and assuming a concentration of 3.0×10^{-4} parts of carbon dioxide by volume, the corresponding thicknesses of air in millibars were computed and are given in the second column. The absorption values computed from Eq. (2), following the empirical technique of Sutherland and Callendar, are given in the third column, and those calculated by the method described in this paper are given in the fourth column.

CONCLUSIONS

It is seen from Table II that the values obtained by the empirical procedure appear to be considerably too high for moderate absorption and too low for small absorption. The question now arises as to whether a modification of the assumptions made in the theoretical calculations can give results more in conformity with those obtained with the empirical formula. Since the procedure was straightforward, the only possible source of significant error could be the values used for the half-width and the proportionality constant.

It seems unlikely that the value of 0.17 cm^{-1} used for the half-width for normal pressure and room temperature could be too low by more than 0.01 to 0.02 cm^{-1}, which would produce little effect on the absorption values.[25] The value used for the proportionality constant, on the other hand, was seen to have been very uncertain, although it also seemed to represent an upper limit.[19] For the sake of completeness, however, the absorption was determined for a proportionality constant twenty percent larger than the one originally used. This could be done very easily since the proportionality constant only enters the absorption equations as a coefficient of k and thus as a coefficient of the path length. An increase of the path length by twenty percent is therefore equivalent to an increase by twenty percent of the proportionality constant.

The original calculated values of absorption were plotted on logarithmic graph paper as a function of path length and a smooth curve was drawn for these values. This is the curve through the encircled points in Fig. 6. The absorption for a given thickness u with an increase by twenty percent in the proportionality constant is determined by following this curve to $1.2u$, then going back horizontally to u. The resultant absorption curve is the upper dashed curve of Fig. 6, from which the absorption values are taken for the fifth column of Table II. These values are still much lower than those obtained by the method of Sutherland and Callendar for moderate path lengths and the discrepancy for small path lengths has increased in the opposite direction. This is also illustrated in Fig. 6, in which the points in the triangles are those obtained by the use of Eq. (2). The absorption values with a decrease by 28.8 percent in the proportionality constant[26] are given by the lower dashed curve of Fig. 6 and the sixth column of Table II.

It seems, therefore, that the empirical formulas cannot be used for conditions different from those of the laboratory measurements, or at least for different temperatures. The reason for this is that a change in temperature changes the intensities of the lines, the shape of the absorption coefficient envelopes, and the relative total intensities for transitions of different orders.

It is probable that more accurate estimates of the total intensity of the 15-micron band will be available in the not too distant future. When such information is available, the absorption curves may be easily modified by the method described in this section. More accurate determinations of the half-width would merely change the mean pressure of the layer for which the calculated absorption is applicable.

ACKNOWLEDGMENT

The writer is greatly indebted to Dr. Edward Teller of the Department of Physics, the University of Chicago, for suggestions which resulted in the above work, as well as for his helpful interest and stimulating discussions in connection with the material and ideas presented.

[24] See Elsasser, reference 21, p. 42. For use in atmospheric calculations, the variation with wave-length of the radiation incident at the bottom of the layer must also be taken into account.

[25] There is always the possibility, of course, that it may be too high by a larger amount. This, however, would result in a larger discrepancy since little changes in absorption would be noted for small thicknesses, while the absorption for moderate thicknesses would be smaller.

[26] Corresponding to Dr. Thorndike's lower value, reference 19.

THE JOURNAL OF CHEMICAL PHYSICS VOLUME 15, NUMBER 11 NOVEMBER, 1947

The Mercury ($^3P_1$) Photo-Sensitized Hydrogenation of Ethylene

D. J. LeRoy and Allan Kahn*
Department of Chemistry, University of Toronto, Toronto.
(Received August 1, 1947)

The mercury photo-sensitized hydrogenation of ethylene has been investigated over the temperature range 42°C to 320°C. At 200°C and lower, the results are in relatively close agreement with those of Jungers and Taylor. The activation energy of the reaction, $2C_2H_5=C_2H_6+C_2H_4$, is estimated to be $\geqslant 1.2$ kcal. per mole. Above 200°C ethane formation increases rapidly, corresponding to an activation energy $\geqslant 10.5$ kcal. per mole for the reaction $C_2H_5+H_2=C_2H_6+H$. The small amount of polymerization was not affected by temperature.

THE mercury photo-sensitized reaction between hydrogen and ethylene has been investigated by a number of workers,[1] but not over a wide range of temperature. Jungers and Taylor[2] and Moore and Taylor[3] made a careful study of the reaction at room temperature and postulated the following mechanism:

$$Hg(^3P_1)+H_2=2H+Hg(^1S_0), \quad (1)$$

$$H+C_2H_4=C_2H_5, \quad (2)$$

$$2C_2H_5=C_4H_{10}, \quad (3)$$

$$2C_2H_5=C_2H_6+C_2H_4. \quad (4)$$

The only products reported by Moore and Taylor were methane, ethane and butane, in the ratio 2:14:84. Ethane formation by the reaction

$$C_2H_5+H_2=C_2H_6+H \quad (5)$$

was discounted on the basis of an estimated activation energy greater than 11 kcal. per mole. This number was assumed by analogy with the corresponding reaction with methyl radicals.[4] Reaction (5) would be expected to occur with an appreciable rate at higher temperatures, and this has been confirmed by us. Trenner, Morikawa, and Taylor[4] found considerable deuterization of ethane above 100°C in the reaction of atomic deuterium with ethane and attributed this to the reaction

$$C_2H_6+D=C_2H_5D+H.$$

Assuming a steric factor of 0.1, they estimated the activation energy of this reaction to be 11.4 kcal. per mole (110°C). It would seem likely, however, that the exchange takes place by reaction (5).

The present investigation was originally undertaken in an attempt to clarify certain points in connection with the mercury photosensitized reaction of ethylene. At room temperature the formation of the initial products, hydrogen and acetylene, is in agreement with the following mechanism:[5]

$$\left.\begin{aligned} Hg(^3P_1)+C_2H_4&=C_2H_4^*+Hg(^1S_0)\\ C_2H_4^*&=C_2H_2+H_2\\ C_2H_4^*+C_2H_4&=2C_2H_4 \end{aligned}\right\} \quad A$$

The reaction is not inhibited by nitric oxide[6] and the excited ethylene molecules can be deactivated by collisions with carbon dioxide[7] as well as with ethylene molecules. At high temperatures[6] the rapid initial pressure *decrease* is eliminated by nitric oxide, giving rise to a reaction identical with that at room temperature. The high temperature reaction is similar in many respects to the photosensitized reactions in which $Cd(^1P_1)$ and $Zn(^1P_1)$ atoms are used, and for which the alternative primary step,

$$M^*+C_2H_4=C_2H_3+H+M, \quad B$$

* Present address: Department of Chemistry, Oregon State College, Corvallis, Oregon.

[1] W. A. Noyes and P. A. Leighton, *The Photochemistry of Gases* (Reinhold Publishing Corporation, New York, 1941).

[2] J. C. Jungers and H. S. Taylor, J. Chem. Phys. **6**, 325 (1938).

[3] W. J. Moore and H. S. Taylor, J. Chem. Phys. **8**, 504 (1940).

[4] N. R. Trenner, K. Morikawa and H. S. Taylor, J. Chem. Phys. **5**, 203 (1937).

[5] D. J. LeRoy and E. W. R. Steacie, J. Chem. Phys. **9**, 829 (1941).

[6] D. J. LeRoy and E. W. R. Steacie, J. Chem. Phys. **10**, 676 (1942).

[7] Daphne Line and D. J. LeRoy, J. Chem. Phys. **13**, 307 (1945).

was assumed.[8,9] Since it is unlikely that the primary process, B, would have a large temperature coefficient, it was assumed that the marked effect of temperature was due to the free radical sensitized polymerization of ethylene. We have, accordingly, undertaken an investigation of the polymerization of ethylene initiated by hydrogen atoms and vinyl radicals; the results for atomic hydrogen are given in this report.

EXPERIMENTAL DETAILS

The reaction vessel was a fused quartz annular cell 9 inches long, having a 4-inch external diameter and a 2-inch internal diameter, and connected to the rest of the system by two quartz-to-pyrex graded seals. The gases were saturated with mercury vapor by continuous circulation over mercury dispersed throughout a trap which was maintained at room temperature. The circulating pump was of the constant pressure type referred to previously.[6] Pressures were read on a wide-bore U-tube manometer.

The three lamps used during the course of the investigation were of the low pressure, mercury-argon type and were operated by a 3000-volt, 60-ma Jefferson transformer. The central portion of the lamp was of quartz and when in use it was inserted through the hole in the annular cell, with the electrode chambers well outside the furnace. It was found that with this arrangement the light intensity is practically independent of the temperature of the furnace. At high temperatures, the natural blue color of the discharge did not appear until about ten minutes after turning on the current, but its appearance was quite sudden and coincided with the initiation of the reaction. In most experiments, the lamp was surrounded by a thin cylindrical glass tube to reduce the light intensity; this tube is referred to as the filter.

The ethylene was obtained from the Ohio Chemical and Manufacturing Company and was said to be 99.5 percent pure. It was further purified and freed from air by a series of bulb-to-bulb distillations. The middle fraction was stored in a 2-liter bulb, isolated from the rest of the system by a mercury cut-off. Hydrogen was purified as required by passing the commercial electrolytic gas through platinized asbestos at 500°C and then through two traps cooled with liquid air, the second containing silica gel. Before using the silica gel trap it was found that 0.3 percent of the gas would not diffuse through a warm palladium tube; with its use this was reduced to 0.02 percent. The ethane, propane, normal butane and acetylene used to calibrate the analytical apparatus were purified in the same manner as the ethylene.

The course of the reaction was followed both by pressure changes and by chemical analyses. At the end of an experiment, the system was opened to a trap cooled with liquid air and allowed to stand for 40 minutes. Most of the condensible gas was frozen out in this way. This trap was then opened to a second one containing silica gel and also cooled with liquid air. After 15 minutes the hydrogen was pumped off slowly until the pressure in the system had fallen to 10^{-3} mm. The traps were then isolated from each other and from the system. The first contained most of the higher hydrocarbons; the second contained methane, some residual hydrogen and a small amount of higher hydrocarbons. The gas in the first trap was transferred to a low temperature fractionating column where it was

TABLE I. Reaction products at 42°C. All measurements are in mm of mercury at 25°C.

Lamp	Time (min.)	C_2H_4	H_2	$-\Delta P$	CH_4	C_2H_6	C_3H_8	C_4H_{10}	$>C_4H_{10}$
No. 2— no filter	12	12.2	113.8	11.2	0.5_1	2.1_9	0.2_2	3.6	0.2
	12	12.4	358.8	11.1	0.3	1.7_3	0.4_3	3.9_5	0.1_6
No. 3— with filter	180	15.7	105.1	10.4	0.1	0.9_3	0.2_2	4.1_7	0.1_0
	180	15.7	309.6	9.8	0.1	1.1_3	—	4.0_2	0.0_7

TABLE II. Reaction products at higher temperatures. All measurements are in mm of mercury at 25°C. Lamp No. 3, with filter.

Temp.	C_2H_4	H_2	$-\Delta P$	CH_4	C_2H_6	C_3H_8	C_4H_{10}	$>C_4H_{10}$
200°C	14.9	99.7	5.3	0.0_3	0.6_2	0.0_3	1.3_9	0.3_2
200	14.8	278.0	5.5	0.0_4	0.6_8	0.0_3	1.3_8	0.2_5
260	14.7	96.8	7.2	0.0_6	1.5_0	0.1_2	1.7_7	0.5_0
260	14.2	182.0	7.6	0.0_7	1.5_8	0.2_3	1.7_0	0.4_3
260	14.9	274.4	8.9	0.0_8	2.4_9	0.1_9	1.8_4	0.5_0
280	15.1	92.5	6.4	0.0_9	1.1_4	0.2_0	1.7_0	0.4_8
280	15.5	176.5	8.0	0.1_0	2.5_7	0.1_6	2.0_5	0.3_2
280	15.6	280.5	10.0	0.1_1	4.1_4	0.1_2	1.9_4	0.4_1
300	15.5	92.0	7.3	0.1_7	2.1_8	0.4_4	1.5_0	0.4_5
300	14.8	176.3	9.5	0.2_0	4.5_7	0.2_2	2.0_1	0.4_8
300	15.4	289.0	12.7	0.2_4	7.1_8	0.2_9	1.9_5	0.3_4
320	18.5	89.5	7.7	0.2_2	2.5_5	0.4_1	1.8_1	0.4_2
320	21.0	279.0	15.5	0.4_0	9.5_1	0.2_9	2.5_8	0.4_1

[8] E. W. R. Steacie and D. J. LeRoy, J. Chem. Phys. **10**, 22 (1942).

[9] H. Habeeb, D. J. LeRoy, and E. W. R. Steacie, J. Chem. Phys. **10**, 261 (1942).

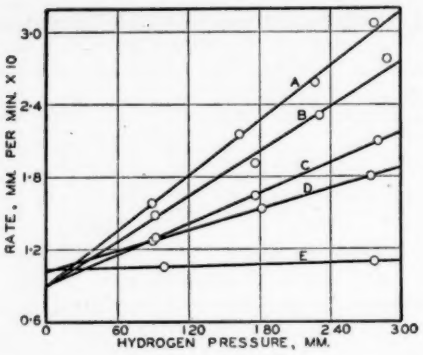

FIG. 1. Effect of hydrogen pressure on the rate of pressure decrease. *A*, 320°C; *B*, 300°C; *C*, 280°C; *D*, 260°C; *E*, 200°C.

separated according to carbon number by a method similar to that used by Ward.[10] Blank determinations with known samples showed this procedure to be satisfactory. The various fractions were collected and measured and their olefin content determined.[11] The C_2 fractions were tested for acetylene[12] but none was ever found. The hydrocarbons in the silica gel trap were analysed in the same way. The methane and residual hydrogen were collected first and the methane determined by allowing the hydrogen to diffuse through a warm palladium tube on the top of a Toepler pump. The methane analysis was confirmed by combustion, using the Blacet-Leighton apparatus.

The analytical results were expressed in terms of mm of mercury in the reaction system at 25°C. The observed pressures were also converted to the corresponding values at 25°C. This involved an empirical determination of the apparent volume of the system as a function of the furnace temperature.

EXPERIMENTAL RESULTS

Low Temperature

The data for four of the experiments at 42°C are given in Table I. The products are all saturated. Ethane and butane are the main products, and their ratio appears to depend on the light intensity. The relatively small amount of methane, propane and higher paraffins precludes any conclusion as to the effect of light intensity on their production. In both groups of experiments it is apparent that the rates are independent of hydrogen pressure. In a series of experiments of increasing duration and in which the filter was used, it was found that both ethane and butane formation are linear in time until over 80 percent of the ethylene is used up, indicating that the rates are also independent of ethylene pressure. With the exception of the effect of light intensity, these results are in essential agreement with the work of Taylor *et al.*

Higher Temperatures

The results of a series of experiments covering the range 200°C to 320°C are given in Table II. Blank experiments without illumination showed no evidence of a thermal reaction. Each experiment lasted approximately 50 minutes. As in the case of the low temperature experiments, the products are all saturated and the rate of pressure decrease remained constant throughout any one experiment. The rate of formation of methane and propane would appear to increase with temperature; a plot of one against the other points to a methane: propane ratio nearer to 2:1 than to 1:1. The rate of formation of butane and higher paraffins is relatively insensitive to hydrogen pressure and temperature; ethane production is strongly affected by both these factors.

DISCUSSION OF RESULTS

Our results can be interpreted on the basis of reactions (1) to (5). The rate equations are:

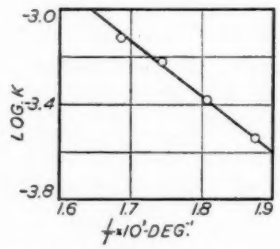

FIG. 2. Log_{10} of the slopes of curves *A*, *B*, *C* and *D* (Fig. 1) *vs.* the reciprocal of the absolute temperature. (Notation below the figure should read $\frac{1}{T}\times 10^3 - DEG.^{-1}$)

[10] E. C. Ward, Ind. Eng. Chem. Anal. Ed. **10**, 169 (1938).
[11] Rowena Pyke, Allan Kahn and D. J. LeRoy, Ind. Eng. Chem. Anal. Ed. **19**, 65 (1947).
[12] F. E. Blacet, A. L. Sellers and W. J. Blaedel, Ind. Eng. Chem. Anal. Ed. **12**, 356 (1940).

$$-d[C_2H_4]/dt=2I_a\left(1-\frac{k_4}{2(k_3+k_4)}\right)+k_5\left(\frac{I_a}{k_3+k_4}\right)^{\frac{1}{2}}[H_2],$$

$$d[C_2H_6]/dt=\frac{k_4I_a}{k_3+k_4}+k_5\left(\frac{I_a}{k_3+k_4}\right)^{\frac{1}{2}}[H_2],$$

$$d[C_4H_{10}]/dt=\frac{k_3I_a}{k_3+k_4}.$$

Since all the products are saturated, the rate of disappearance of ethylene is equal to the rate of pressure decrease. The effect of hydrogen pressure and temperature on the rate of pressure decrease is shown graphically in Fig. 1. The logarithms of the slopes of these curves are plotted against the reciprocal of the absolute temperature in Fig. 2. The corresponding "activation energy," E', is 10.5 kcal. per mole.

Under conditions where the rate is independent of the hydrogen pressure (i.e. $\leqslant$200°C) the ethane:butane ratio is equal to k_4/k_3. The experimental ratio, with the filter, at 42°C and 200°C leads to the value $E_4-E_3=1.2$ kcal. per mole. If E_3 can be assumed to be zero[13] the term (k_3+k_4) in the slopes of Fig. 1 can be written in the form $k_3[1+n\cdot\exp(-E_4/RT)]$, where n is equal to unity if the pre-exponential factors of the two rate constants are equal. By plotting the logarithms of $[1+n\cdot\exp(-E_4/RT)]$ *vs.* $1/T$ for various values of n it is seen that the "activation energy," E'', of (k_3+k_4) is $\leqslant E_4$. For example, if E_4 is 1.2 kcal. and n is equal to unity then E'' is approximately equal to 0.16 kcal. The activation energy of reaction (5) is equal to $E'+\frac{1}{2}E''$, and hence $10.5\leqslant E_5\leqslant 11.1$. Regardless of the assumptions made about E_3 and E_4, $E_5\geqslant 10.5$ kcal. per mole. It should be noted that the effect of temperature on the intercepts of Fig. 1 is in agreement with the fact that $E_4>E_3$.

The C−H bond strength in ethane[14] has been estimated to be 98 kcal. by Kistiakowski, 97.5 by Polanyi and 96.8 by Stevenson. Since the H−H bond strength is 103.7 kcal., the value of ΔH for reaction (5) is 5.7, 6.2 or 6.9 kcal. The activation energy of the reverse reaction,

$$H+C_2H_6=C_2H_5+H_2 \qquad (6)$$

would then be in the range 3.6 to 5.4 kcal. per mole, somewhat lower than previous estimates.[14] Since the formation of products other than butane and ethane is not sensitive to temperature, a more elaborate mechanism than the one given would not increase E_5 (and hence E_6) appreciably. Most estimates of E_6 have been based on collision yields, assuming a steric factor of 0.1, and consequently, the solution of the problem will be contingent on future measurements in which an unequivocal value of E_6 is obtained.

There are not sufficient data to interpret the effect of light intensity on the ethane:butane ratio at low temperatures, but it is hoped that experiments now being planned will enable some conclusions to be made regarding light intensity and surface reactions.

It is clear from our work that the polymerization of ethylene sensitized by atomic hydrogen is relatively unimportant. This is surprising in view of the low activation energies assigned to reactions of the type $C_2H_5+C_2H_4=C_4H_9$.[13]

It is a pleasure to acknowledge the financial assistance received from the National Research Council of Canada, which enabled this research to be carried on. The junior author would also like to express his appreciation of the National Research Council Studentship which he held during the year 1946–47.

[13] Annual Tables of Physical Constants, Section 602.

[14] E. W. R. Steacie, *Atomic and Free Radical Reactions* (Reinhold Publishing Corporation, New York, 1946).

THE JOURNAL OF CHEMICAL PHYSICS VOLUME 15, NUMBER 11 NOVEMBER, 1947

The Asymmetric Rotor. VI. Calculation of Higher Energy Levels by Means of the Correspondence Principle

GILBERT W. KING*
Arthur D. Little, Incorporated, and Research Laboratory of Electronics, Massachusetts Institute of Technology, Cambridge, Massachusetts

(Received August 26, 1947)

The rotational levels of the rigid asymmetric rotor can be calculated by means of the correspondence principle. It is shown that the quantum-number ratio $K/J(J+1)$ is the complete elliptic integral of the third kind tabulated by Heuman in the case of the energy levels of a hypothetical rotor with reciprocal moments of inertia -1, κ, and $+1$. The parameter of the integral is the reduced-energy ratio $E(\kappa)/J(J+1)$, and its modulus is a function of both the reduced-energy ratio and asymmetry parameter. A double inverse interpolation has been made by Heuman's table to give the energy ratio directly in terms of quantum-number ratio and asymmetry. Power series expansions have been developed around limiting cases and around each point in the table, so that formulas for interpolation and estimating errors are available.

NEED FOR HIGHER ENERGY LEVELS

PROGRESS in the analysis of infra-red spectra and the recent discovery of microwave absorption lines of polyatomic molecules have caused a demand for the higher energy levels of asymmetric rotors. At present, only in the case of rigid rotors is the theory tractable enough for numerical solutions, but these results are of value, as a basis for further elaboration.

THE CORRESPONDENCE-PRINCIPLE FORMULATION

Just before the advent of the rigorous approach of the new quantum theory, several authors[1-4] applied the old quantum theory to the problem of the higher energy levels, showing it involved the complete elliptic integrals of the third kind; but no computations were recorded. The application of the correspondence principle involves the same type of integrals, but the whole problem can be simplified by two factors appearing after these papers. Quite recently tables of the complete elliptic integral of the third kind were prepared and published by Heuman.[5] The other step was made by Ray[6] in the application of the new quantum theory to the asymmetric rotor. The energy $E(a, b, c)$ of a rigid rotor with reciprocal moments $a \geqslant b \geqslant c$ can be expressed in terms of a "reduced energy" $E(\kappa)$ by

$$2E(a, b, c) = (a-c)E(\kappa) + (a+c)J(J+1). \quad (1)$$

The quantity $E(\kappa)$ can be formally considered as the energy of a hypothetical rotor with moments $1 \geqslant \kappa \geqslant -1$, $\kappa = (2b-a-c)/a-c$ being a parameter of asymmetry. Thus the difficult part of the calculation can be reduced to a problem in one parameter, κ, rather than in the three, a, b, c, previously used. This simplification is equally applicable to the correspondence-principle approach.

The value of $E(\kappa)$ has been computed by the new (matrix) quantum mechanics for all possible degrees of asymmetry $\kappa = -1$ to $+1$ in steps of 0.1 for each quantized energy level up to $J = 12$.[7] In this article we extend the calculation of $E(\kappa)$ to high J values by application of the correspondence principle.

The energy of the hypothetical rotor is

$$E(\kappa) = P_a^2 + \kappa P_b^2 - P_c^2, \quad (2)$$

where P_a, P_b, and P_c are the components of the total angular momentum along three axes identified by subscripts a, b, c about which the "moments of inertia" are 1, κ, and -1, respectively. The total angular momentum is given by

$$P^2 = P_a^2 + P_b^2 + P_c^2. \quad (3)$$

* The calculations in this article were done under the auspices of the Office of Naval Research, contract N6-ori-228/T.O. 1, Arthur D. Little, Incorporated.

[1] F. Reiche, Physik. Zeits. **19**, 394 (1918).
[2] P. S. Epstein, Physik. Zeits. **20**, 289 (1919).
[3] F. Lütgemeier, Zeits. f. Physik **38**, 251 (1926).
[4] E. E. Witmer, Proc. Nat. Acad. Sci. **12**, 602 (1926).
[5] C. Heuman, J. Math. and Phys. **20**, 127 (1941).
[6] B. S. Ray, Zeits. f. Physik **78**, 74 (1932).
[7] G. W. King, R. M. Hainer, and P. C. Cross, J. Chem. Phys. **11**, 27 (1943). The values for $J = 11$ and 12 will be published shortly.

The phase space in which the motion of the rotor can be described is reduced to three-dimensional momentum space, since there is no potential energy. The motion of the system is constrained by Eqs. (2) and (3), which define a conoid and sphere, and is described by the vector P moving only along the intersections of these two geometrical surfaces.

The Eulerian angles,[8] θ, χ, ϕ, permit[9] separation of the Hamiltonian. The direction of the total angular momentum can be taken parallel to a fixed external axis, Z, whence $P_\theta=0$ and $P_\chi=P$, since χ measures the angle around Z. The projection of P on the c axis is $P_\phi=P\cos\theta$. Thus

$$P_c=P\cos\theta, \quad P_a=P\sin\theta\sin\phi, \quad P_b=P\sin\theta\cos\phi. \tag{3a}$$

According to the correspondence principle the areas swept out by the separated components of the vector in its constrained motion are simple multiples of Planck's constant. Since one equation is trivial there are two quantum conditions:

$$\oint P_\chi d\chi=2\pi P=(J(J+1))^{\frac{1}{2}}h, \tag{4}$$

$$\oint P_\phi d\phi=P\phi\cos\theta d\phi=Kh. \tag{5}$$

In the first equation the multiple of h was chosen as $(J(J+1))^{\frac{1}{2}}$ rather than an integer J in order to give the correct value obtained from the new quantum mechanics. There are other cases where the total energy contains a term of the type $J(J+1)$ instead of a simple square of a quantum number obtained from the correspondence principle. In the second equation the multiplier of h was chosen as the simple integer K, since this gives the correct value in the limiting case of the symmetric rotor.

According to the new quantum theory these levels are doubly degenerate, and when the rotor becomes asymmetric they are split. In the two limiting cases of prolate ($\kappa=-1$) and oblate ($\kappa=+1$) symmetric rotors, each asymmetric-rotor level has true (symmetric-rotor) quantum numbers, which we have previously labelled K_{-1}, K_1, respectively. The correspondence principle makes no distinction between the separated levels, so that they are both identified by the K of the symmetric rotor. Since K_{-1} and K_1 are, in general, not the same, the correspondence-principle labeling would lead to ambiguities were it not for the fact, investigated in detail below, that one cannot treat the asymmetric-rotor level as a perturbation of a symmetric-rotor level over the whole range of κ. There is a limit, $E(\kappa)=J(J+1)\kappa$, where the integral (5) has a singularity. The value of $E(\kappa)_{K_{-1}K_1}{}^J$ has to be calculated on one side of this boundary as the level with $K_{-1}=K$ and on the other as $K_1=K$. The relation between the levels, as calculated by the correspondence principle and new quantum mechanics, is discussed again after the properties of the integral (5) have been found.

From the form of the Hamiltonian (2) in terms of the Eulerian angles, $\cos\theta$ can be evaluated as a function of $E(\kappa)$, P, and ϕ.

$$E(\kappa)=P^2[\sin^2\theta(\sin^2\phi+\kappa\cos^2\phi)-\cos^2\theta], \tag{6.1}$$

or

$$E(\kappa)=P^2[(\sin^2\phi+\kappa\cos^2\phi)-\cos^2\theta(1+\sin^2\phi+\kappa\cos^2\phi)], \tag{6.2}$$

so that

$$\cos^2\theta=\frac{\sin^2\phi+\kappa\cos^2\phi-E(\kappa)/P^2}{(\sin^2\phi+\kappa\cos^2\phi)+1}. \tag{6.3}$$

On substitution, the second integral (5) simplifies to the quantum-number ratio

$$\lambda=\frac{K}{(J(J+1))^{\frac{1}{2}}}=\frac{1}{2\pi}\oint\left(\frac{(\sin^2\phi+\kappa\cos^2\phi)-\eta}{(\sin^2\phi+\kappa\cos^2\phi)+1}\right)^{\frac{1}{2}}d\phi, \tag{6}$$

where

$$\eta=\eta(\kappa)_{J,K}=\frac{E(\kappa)_{J,K}}{J(J+1)}$$

can be called the "reduced-energy ratio" of the level J, K for asymmetry κ. As noted above, K is either K_{-1} or K_1, depending on the singularities of the integral as will be discussed below.

The reduced-energy and quantum-number ratios are natural quantities to be considered in

[8] These are the angles relating a right-handed set of external axes x, y, and z to the right-handed internal axes a, b, and c. θ is measured from the c axis, χ from the a axis, and ϕ from the line of nodes.

[9] M. Born, *Atommechanik* (Springer, Berlin, 1925), p. 130.

the treatment of the asymmetric rotor. Reference[7] to the table of reduced-energy levels $E(\kappa)$ shows that if each block, for a given J, in that table be divided by $J(J+1)$, the energy ratios as functions of quantum-number ratios are even at low values of J, already only slightly dependent on J, and as J increases the blocks are converging to a definite function, η.

In other words, if a table were prepared giving the energy ratio η as a function of the quantum-number ratio λ and the asymmetry κ, the reduced energy $E(\kappa)$ (and hence ultimately the true energy $E(a, b, c)$) could be obtained by simple multiplication by $J(J+1)$. One of the objectives of this article is to determine how accurately the various levels can be calculated from such a table.

GEOMETRY OF THE INTERSECTION OF CONOID AND SPHERE

A discussion of the symmetry properties of η, and of the integral (6), is made clearer by examination of the geometry of the intersection of the sphere and conoid in momentum space. It is convenient to use momenta ratios, $p_c=P_c/P$, etc. The sphere is then fixed in size with the radius unity, and the conoid can be written

$$p_a^2+\kappa p_b^2-p_c^2=\eta. \tag{7}$$

Now

$$\frac{x^2}{u^2}+\frac{y^2}{v^2}-\frac{z^2}{w^2}=1$$

is a hyperboloid of one sheet around the z axis (Fig. 1a). The sections of the planes zx, zy are hyperbolas

$$\frac{x^2}{a^2}-\frac{z^2}{c^2}=1; \quad \frac{y^2}{b^2}-\frac{z^2}{c^2}=1.$$

The section of the plane xy and parallel planes is an ellipse

$$\frac{x^2}{a^2}+\frac{y^2}{b^2}=1,$$

with axes a and b. The equation

$$\frac{x^2}{u^2}+\frac{y^2}{v^2}-\frac{z^2}{w^2}=-1$$

is a hyperboloid of two sheets around the z axis (Fig. 1b). The sections of the planes zx and zy are

$$\frac{z^2}{c^2}-\frac{x^2}{a^2}=1 \quad \text{and} \quad \frac{z^2}{c^2}-\frac{y^2}{b^2}=1,$$

the section of any plane $z=\pm\gamma$, $|\eta|>c$ being the ellipse

$$\frac{x^2}{a^2}+\frac{y^2}{b^2}=\frac{\gamma^2}{c^2}-1.$$

Returning to the conoid (7) we see there are four cases:

	η	κ	
i	+	+	one sheet around c axis,
ii	−	+	two sheets around c axis,
iii	+	−	two sheets around a axis,
iv	−	−	one sheet around a axis.

That is, passing to negative values of η changes the surface from one to two sheets. Changing the sign of κ changes the surface from one to two sheets and also changes the enclosed axis from c to a. The larger η, the larger the size. The distance between apices of two sheets is $(\eta)^{\frac{1}{2}}$.

When $\eta=0$ (κ positive) the conoid reduces to an elliptical cone around the c axis (Fig. 1c). With κ negative the surface is an elliptical cone around the a axis. When $\eta=0$, $\kappa=0$ the surface is the intersection of two planes at 45° to the c and a axes. When $\kappa=1$ the cross sections are circles.

In considering the integral (6) it is important to find the limits reached by ϕ in the cyclic path. In particular, we shall be interested only in the cases where ϕ varies from 0 to 2π. Geometrically this corresponds to the requirement that the intersection of sphere (of unit radius) and the conoid forms a loop enclosing the c axis.

As the simplest case consider case ii. Clearly the intersection (if there is one) of the sphere and hyperboloid of two sheets is around the c axis (Fig. 1e). The maximum value of η will be $\eta=1$ when the sphere just touches the two sheets on the z axis (Fig. 1g). The minimum value (for this configuration) is $\eta=0$, when the hyperboloid becomes a cone. Thus in case ii ϕ varies from 0 to 2π. For values of η negative the cone expands to form a hyperboloid of one sheet around the c axis, so that the intersection still loops the c axis (Fig. 1d) provided that $\eta/\kappa<1$

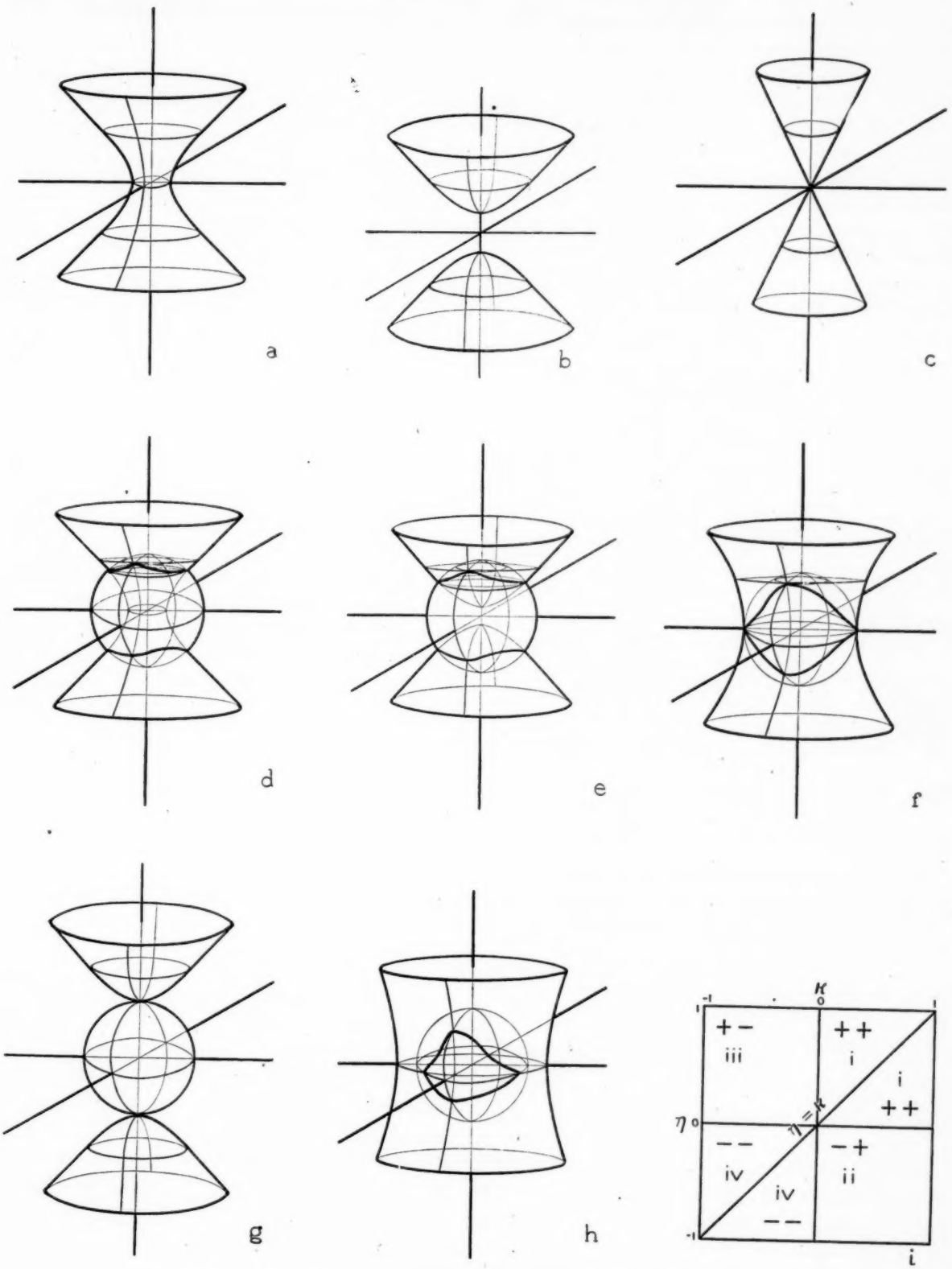

FIG. 1. Illustrations of the intersections of the conoid and sphere in phase space.

or $\eta<\kappa$. The maximum value of η occurs when the sphere just touches on the $z=0$ plane (Fig. 1f). The cross section is an ellipse with axes η and η/κ. When the sphere touches the minor axis $\eta=\kappa$. After that the loop is around the a axis. Thus in case i, ϕ varies from 0 to 2π for $\eta<\kappa$. When $\eta/\kappa>1$ or $\eta>\kappa$ the intersection loops the a axis (Fig. 1h).

Exactly the same relationships hold for cases iii and iv, although now the principal axis is the a axis. Figure 1i summarizes the results. The intersections loop the c axis for $\eta<\kappa$, the a axis for $\eta>\kappa$.

THE INTEGRAL FOR THE QUANTUM-NUMBER RATIO

Because of the symmetry of the geometrical figures we have $\eta(\kappa)=-\eta(-\kappa)$ as is known for $E(\kappa)$. It is therefore only necessary to calculate η for one-half of its possible values. In presenting[7] the results for $E(\kappa)$ we took the division at $\kappa=0$ as the symmetry axis, for convenience in printing. From an analytical point of view the division occurs at $\eta(\kappa)=\kappa$, i.e., a diagonal in Fig. 1i.

Because of the necessity of fixing the Eulerian angles relative to the Cartesian axes in formulating (6), one region of Fig. 1i is more suitable for integration, namely, $\eta<\kappa$. In this case ϕ varies from 0 to 2π and solution of the problem is

$$\lambda=\frac{1}{2\pi}\int_0^{2\pi}\frac{(\sin^2\phi+\kappa\cos^2\phi)-\eta}{(\sin^2\phi+\kappa\cos^2\phi)+1}d\phi. \tag{8}$$

In accordance with the above geometrical discussion, this integral has singularities in passing the boundary $\eta=\kappa$. In the special case of $\eta=\kappa$

$$\lambda=\frac{k}{2\pi}\int_0^{2\pi}\frac{\sin\phi}{(1+k^2\sin^2\phi)^{\frac{1}{2}}}d\phi, \tag{9}$$

where $k=[(1-\eta)/(1+\eta)]^{\frac{1}{2}}$, which is an elementary integral giving

$$\eta=\cos\lambda\pi. \tag{10}$$

There is another limiting case, of course, when $\kappa=1$. Here (8) can be integrated to give

$$\eta=1-2\lambda^2, \tag{11}$$

which is the correct form for the symmetric (oblate) rotor.

TRANSFORMATION OF INTEGRAL

Epstein showed[2] that (6) is a complete elliptic integral of the third kind by making a transformation which in the case of the hypothetical rotor would be

$$\cos^2\phi=\frac{\cos^2\psi}{1-p^2\sin^2\psi}. \tag{12}$$

This gives

$$\lambda=\frac{1}{2\pi}\frac{\kappa-\eta}{((1+\kappa)(1-\eta))^{\frac{1}{2}}}\times\int_0^{2\pi}\frac{d\psi}{(1-p\sin^2\psi)(1-\sin^2\alpha\sin^2\psi)^{\frac{1}{2}}}, \tag{13}$$

where the parameter is

$$p=(1-\kappa)/(1-\eta), \tag{14}$$

and the modulus is

$$\sin^2\alpha=(1+\eta)(1-\kappa)/(1-\eta)(1+\kappa). \tag{15}$$

More recently, tables of the complete elliptical integral of the third kind have been published by Heuman,[5] who uses a different canonical form of the integral. The integral belongs to Heuman's first class (circular), since the function $\tau(p)$ is less than zero,

$$\tau(p)=p(p-\sin^2\alpha)(p-1)=\frac{-(1-\kappa)^2(\eta-\kappa)^2}{(1-\eta)^3(1+\kappa)},\quad \eta\leqslant\kappa.$$

There is then a unique angle $0<\beta<\pi/2$, such that $\eta=\cos2\beta$. Substituting for η, the basic integral (8) becomes

$$\lambda=\frac{2}{\pi}\int_0^{\pi/2}\frac{\cos^2\alpha\sin\beta\cos\beta\Delta'\beta}{\cos^2\alpha\cos^2\beta+\sin^2\alpha\cos^2\phi}\frac{d\phi}{\Delta\psi}, \tag{16}$$

where

$$\Delta'\beta=(1-\cos^2\alpha\sin^2\beta)^{\frac{1}{2}},$$

which is exactly the integral $\Lambda_0(\alpha,\beta)$ which Heuman tabulates.

The two parametric angles are related to the energy η and asymmetry κ by the following relations:

$$\eta=\cos^2\beta, \tag{17}$$

and

$$\sin\alpha=\cot\beta\tan\gamma, \tag{18}$$

TABLE I. Values of the parameter, η, as a function of the complete elliptic integral of the third kind, λ, and its modulus κ. The parameter η is the reduced-energy ratio, $E(\kappa)_{J,K}/J(J+1)$. The integral, λ, is the quantum-number ratio $K/[J(J+1)]^{\frac{1}{2}}$. The modulus, κ, is the asymmetry $(2b-a-c)/a-c$ defined in terms of the reciprocal moments of inertia $a \geqslant b \geqslant c$. Here K is the quantum number a level has in one limiting case, either the prolate or the oblate symmetric rotor. For values of η and κ lying above the dividing line in the table ($\eta = \kappa$) the former applies, and the λ is given at the left of the table. Below the dividing line the levels are to be considered as perturbations of the oblate rotor, with λ given at the right of the table. For positive values of κ the table is inverted, and the sign of η changed.

In the table the value of η is given in the first row, the first and second derivatives lying immediately below. For interpolation use Eq. (38), in a direction toward the dividing line. The first derivative is negative above the line, positive below, and the second derivative is positive above, negative below.

λ \ κ	−1.0	−0.9	−0.8	−0.7	−0.6	−0.5	−0.4	−0.3	−0.2	−0.1	0	
1.0	1.0	1	1	1	1	1	1	1	1	1	1	
	4	3.898 718	3.794 733	3.687 818	3.577 709	3.464 102	3.346 640	3.224 903	3.098 387	2.966 479	2.828 427	
	2	1.95	1.90	1.85	1.80	1.75	1.70	1.65	1.60	1.55	1.50	
0.9	.62	.629 629	.639 530	.649 726	.660 242	.671 111	.682 367	.694 053	.706 220	.718 932	.732 259	
	3.6	3.508 693	3.414 638	3.317 599	3.217 307	3.113 454	3.005 671	2.893 532	2.776 523	2.654 006	2.525 214	
	2	1.950 248	1.901 041	1.852 392	1.804 408	1.757 119	1.710 617	1.665 053	1.620 541	1.577 251	1.535 498	
0.8	.28	.298 262	.317 084	.336 502	.356 578	.377 371	.398 958	.421 426	.444 878	.469 443	.495 277	
	3.2	3.118 603	3.034 272	2.946 741	2.855 728	2.760 895	2.661 843	2.558 101	2.449 084	2.334 091	2.212 225	
	2	1.950 690	1.902 862	1.856 624	1.812 163	1.769 710	1.729 542	1.692 064	1.657 749	1.627 339	1.601 840	
0.7	−.02	.005 913	.032 692	.060 416	.089 166	.119 047	.150 173	.182 685	.216 752	.252 588	.290 454	
	2.8	2.728 393	2.653 392	2.574 704	2.491 983	2.404 815	2.312 694	2.215 004	2.110 967	1.999 588	1.879 522	
	2	1.951 523	1.906 275	1.864 594	1.826 938	1.793 917	1.766 359	1.745 488	1.733 044	1.731 731	1.745 905	
0.6	−.28	−.247 408	−.213 566	−.178 363	−.141 679	−.103 356	−.063 216	−.021 040	.023 453	.070 624	.120 962	
	2.4	2.337 936	2.271 524	2.200 338	2.123 882	2.041 566	1.952 413	1.855 428	1.748 985	1.630 668	1.496 461	λ
	2	1.953 234	1.913 401	1.881 295	1.858 295	1.846 470	1.848 424	1.869 480	1.917 970	2.009 861	2.179 734	
0.5	−.50	−.461 658	−.421 540	−.379 480	−.335 284	−.288 701	−.239 411	−.186 978	−.130 754	−.069 616	0	0.5
	2.0	1.946 951	1.887 422	1.820 678	1.745 673	1.660 872	1.563 850	1.450 410	1.312 001	1.124 704		
	2	1.957 247	1.930 197	1.921 741	1.937 014	1.985 294	2.084 667	2.275 255	2.668 312	3.755 152		
0.4	−.68	−.636 752	−.590 862	−.542 037	−.489 871	−.433 739	−.372 482	−.301 958	−.234 464	−.175 176	−.120 962	0.6
	1.6	1.554 586	1.497 437	1.426 389	1.337 300	1.221 241	1.051 641	.728 891	1.135 891	1.338 470	1.496 461	
	2	1.968 517	1.979 149	2.047 690	2.213 094	2.590 044	3.724 087	16.473 421	3.418 067	2.520 645	2.179 734	
0.3	−.82	−.772 433	−.720 378	−.662 802	−.597 138	−.528 478	−.471 301	−.420 306	−.373 763	−.330 693	−.290 454	0.7
	1.2	1.157 639	1.086 220	0.967 908	.671 829	1.010 726	1.253 461	1.442 829	1.604 895	1.748 898	1.879 522	
	2	2.011 360	2.192 356	2.821 485	10.600 475	3.249 118	2.314 839	2.003 924	1.858 221	1.783 187	1.745 905	
0.2	−.92	−.867 563	−.802 230	−.742 531	−.694 699	−.653 345	−.616 401	−.582 729	−.551 618	−.522 581	−.495 277	0.8
	0.8	.735 464	.525 306	.965 928	1.227 668	1.441 012	1.626 211	1.791 914	1.942 947	2.082 347	2.212 225	
	2	2.262 034	9.540 869	2.226 196	1.807 343	1.661 715	1.599 770	1.575 761	1.572 735	1.582 823	1.601 840	
0.1	−.98	−.922 562	−.885 341	−.857 158	−.833 546	−.812 834	−.794 174	−.777 065	−.761 183	−.746 301	−.732 259	0.9
	0.4	.630 477	1.017 250	1.300 419	1.534 964	1.739 318	1.922 524	2.089 821	2.244 596	2.389 165	2.525 214	
	2	1.844 124	1.442 075	1.371 153	1.359 775	1.371 127	1.394 035	1.423 792	1.458 094	1.495 599	1.535 498	
0.0	−1	−1	−1	−1	−1	−1	−1	−1	−1	−1	−1	1.0
	0	.894 427	1.264 911	1.549 193	1.788 854	2	2.190 890	2.366 432	2.529 822	2.683 282	2.828 427	
	1.00	1.05	1.10	1.15	1.20	1.25	1.30	1.35	1.40	1.45	1.50	

where it is convenient to define an angle γ such that

$$\kappa = \cos 2\gamma. \tag{19}$$

The quantum-number ratio is then the complete elliptic integral of the third kind, which has been tabulated for values of two parametric angles, one of which is a function of the energy ratio and the other a function of both the energy ratio and asymmetry. Because both η and κ occur in α, the table of Heuman is not very useful as it stands. The problem from the spectroscopic point of view is: given κ and λ, what is η? This involves double inverse interpolation, and is not very practical when a large number of energy levels are required.

TABLE OF THE REDUCED-ENERGY RATIOS

To facilitate the calculation of η we have inverted Heuman's table of the complete elliptic integral to give one of η in terms of λ and κ. The labor involved is considerable, and we have so far only obtained values for $\lambda = 0.0(0.1)1.0$ and $\kappa = -1.0(0.1)1.0$ which is roughly ten times as coarse as Heuman's table.

Table I gives the value of the energy η for values of the quantum number λ and asymmetry κ. For convenience, and for comparison with our previously published tables of $E(\kappa) = \eta(\kappa)J(J+1)$, the triangular region in which η conforms to the integral (8) has been folded into the range $\kappa = -1$ to 0. The diagonal boundary in Fig. 1i (considered as λ as a function of η and κ) is indicated by the heavy lines in Table I (η as

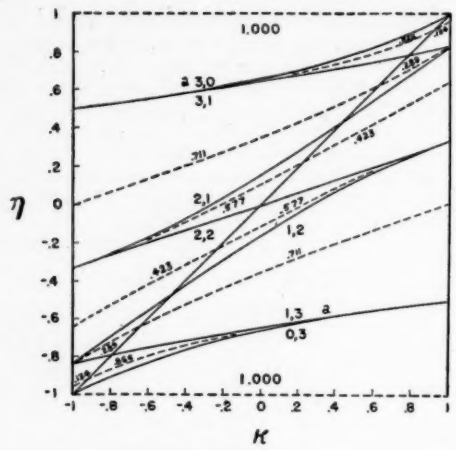

FIG. 2. Correspondence-principle and new quantum theory levels for $J=3$. The energy ratio, η, is plotted as a function of the asymmetry, κ, for each of the $2J+1$ levels. The new quantum theory levels are drawn in solid lines, and each is identified by K_{-1}, K_1, the (integral) values of the internal quantum the level has in the limiting cases of prolate ($\kappa=-1$) and oblate ($\kappa=+1$) symmetric rotor; e.g., the highest level is 3, 0. The correspondence-principle levels are drawn in dashed lines. There are $2J+2$ of them, including the top and bottom horizontal lines marked 1.000. Each of these levels is labelled with the value of λ it has on each side of the diagonal. (Their sum is unity.) On upper side of the diagonal, $J+1$ of the correspondence-principle levels converge to the symmetric rotor levels, and these have $\lambda=K_{-1}/(J(J+1))^{\frac{1}{2}}$. On the other side of the diagonal their value of λ is $\lambda'=1-\lambda$, corresponding to a K_1 of $[J(J+1)^{\frac{1}{2}}-K_{-1}]/(J(J+1))^{\frac{1}{2}}$, which is between the values of K_1 of the doubly degenerate level from which it originated on the upper side of the diagonal. We see then that the correspondence principle gives only $J+1$ levels on either side of the diagonal (of which one, for $\lambda=0.000$ is only a point at the corner of the triangles, the other part of the level marked 1.000 on the other side). The new quantum theory levels for the same K lie on each side of the correspondence-principle level for the most part. However, the points a mark the places at which the correspondence-principle level actually crosses the 3, 1 and 1, 3 levels.

function of λ and κ). Along the boundary $\eta=\cos\lambda\pi$, $\kappa=\eta$. Although the function is continuous over this boundary, interpolation across it is dangerous because there is an inflection point there.

The table was prepared by double inverse interpolation of Heuman's values of the complete elliptic integral of the third kind. Quadratic interpolation was used throughout, which according to Heuman's study of the function $\Lambda_0(\alpha, \beta)$ should give six-figure accuracy. Each entry has been studied carefully as a function of α and β, and we believe some of the values given may be in error by one part in the sixth decimal because of the number of interpolations necessary.

We have also investigated the interpolation of our table by using it to find η for an intermediate value of λ, and comparing the result with double inverse interpolation of Heuman's table for the values in question. The number of points necessary for a required accuracy can be found from the magnitude of the coefficients of the power series expansion obtained in the following section. In the upper left-hand corner of the table a sufficiently high order of interpolation will give the correct value to one part in the sixth decimal. Near the boundary $\eta\sim\kappa$, however, the derivatives of η with respect to λ or κ become very high, and ordinary interpolation is not applicable. This is just the region where the exact value of η is not particularly useful anyway, since the correspondence principle level is actually split, the two components pairing (on the other side of the boundary) with a neighboring level.

RELATION OF THE CORRESPONDENCE PRINCIPLE TO THE NEW QUANTUM THEORY LEVELS

We have seen that the reduced-energy ratio (for a given J) $\eta(\kappa, \lambda)$ is a function of the asymmetry κ and the quantum-number ratio λ, and it can be considered as a perturbation of either a prolate or oblate symmetric rotor. In the new quantum theory the quantum-number ratio λ has an exact meaning in either limiting case, but in the correspondence principle it only characterizes the level from the limiting case ($|\kappa|=1$) to the boundary $\eta=\kappa$. On the other side of the boundary η has an analytical continuation but is the level $\eta(\kappa, \lambda')$, where $\lambda'=1-\lambda$. Because the quantum-number ratio is defined as the integral quantum number K of the symmetric rotor divided by $(J(J+1))^{\frac{1}{2}}$, λ' cannot correspond to an integral value of K in the other limiting case. Thus the analytical continuation of $\eta(\kappa, \lambda)$ across the boundary does not correspond to the best approximation to the asymmetric level. On the other side of the boundary the levels are best characterized by the quantum-number ratios they will have in the other limiting case.

There are $2J+1$ levels according to the new quantum theory. The correspondence principle only admits of one level for each symmetry-rotor level and does not recognize the double degeneracy of each level with quantum number K,

($K\neq 0$), i.e., there are only $J+1$ distinct levels which are perturbations of the symmetric rotor. However, because of the boundary $\eta=\kappa$ the correspondence principle admits another complete distinct set of $J+1$ levels, perturbations of the other limiting case. Thus there are in all $2J+2$ correspondence principle levels of which two ($K_{-1}=0$ and $K_1=0$) are trivial.

The relationship between the correspondence principle and new quantum theory levels is shown in the sketch of Fig. 2, where the levels of $J=3$ are plotted. This figure also shows the correspondence-principle levels are better approximations in some regions than in others. In general, the error at the boundary $\eta=\kappa$ is of the order of the separation of the levels. It is interesting to note that this becomes highest at the corners, close to the limiting cases of the symmetric rotor. The highest and lowest levels $\eta=+1$ and $\eta=-1$ for all values of κ never apply except in the sense that the infinitesimal part to the right and left of the boundary is the level for K_1 and $K_{-1}=0$, respectively.

POWER SERIES EXPANSIONS

The complete elliptic integral of the third kind can be put in still another canonical form by the transformation

$$z=\sin^2\phi+\kappa\cos^2\phi, \tag{20}$$

namely, (for the case $\eta<\kappa$)

$$\lambda=1/\pi\int_1^\kappa[(z-\eta)/(z+1)(z-1)(\kappa-z)]^{\frac{1}{2}}dz. \tag{21}$$

Lutgemeier[3] used this form of the elliptic integral for the three distinct moments of inertia and pointed out that it could be expanded in a Taylor's series whose coefficients are integrable at $\eta=-1$.

In the case of the reduced energies the derivatives are

$$\frac{\partial^n\lambda}{\partial\eta^n}=-\frac{1}{2\pi}\frac{1}{2}\frac{3}{2}\cdots\frac{2n-3}{3}\int_1^\kappa dz/(z-\eta)^{n-1}X, \tag{22}$$

where $X^2=-(z-1)(z-\kappa)(z-\eta)(z+1)$. On expanding around $\eta=-1$ these integrals are all algebraic, and the coefficients a_n of the Taylor's expansion are on integrating, putting $\delta=\frac{1}{2}(\kappa+1)$,

$$a_0=1,$$

$$a_1=1/4\delta^{\frac{1}{2}},$$

$$a_2=2^{-6}(1+\delta)\delta^{-\frac{3}{2}},$$

$$a_3=2^{-6}\delta^{-1}[12(1+\delta)a_2-a_1],$$

$$a_4=\frac{5}{96\delta}[5(1+\delta)a_3-a_2],$$

$$a_n=\frac{2n-3}{2n(2n-2)4\delta}\left[(2n-3)2(1+\delta)a_{n-1}-\frac{(2n-5)(2n-4)}{2n-2}a_{n-2}\right]. \tag{23}$$

TABLE II. Coefficients of the power series (31) for various values of κ.

κ	d_1	$-d_2$	$-d_3$	$-d_4$	$-d_5$
1.0	4	2	0	0	0
0.9	3.8987 1772	1.95	0.0_364 12364	0.0_380 18092	0.0_396 27248
0.8	3.7947 3320	1.90	0.0026 35231	0.0032 98611	0.0039 67945
0.7	3.6878 1780	1.85	0.0061 01169	0.0076 51654	0.0092 35028
0.6	3.5777 0876	1.80	0.0111 80340	0.0140 62500	0.0170 58753
0.5	3.4641 0160	1.75	0.0180 42196	0.0227 86458	0.0278 38544
0.4	3.3466 4012	1.70	0.0268 92644	0.0341 51786	0.0421 21804
0.3	3.2249 0308	1.65	0.0379 85638	0.0485 87740	0.0606 69729
0.2	3.0983 8668	1.60	0.0516 39778	0.0666 66667	0.0845 60136
0.1	2.9664 7940	1.55	0.0682 62736	0.0891 69034	0.1153 53358
0	2.8284 2712	1.50	0.0883 88348	0.1171 87500	0.1553 70142
−0.1	2.6832 8156	1.45	0.1127 35094	0.1523 00347	0.2081 78269
−0.2	2.5298 2212	1.40	0.1423 02495	0.1968 75000	0.2794 90993
−0.3	2.3664 3192	1.35	0.1785 38836	0.2546 31696	0.3789 36724
−0.4	2.1908 9024	1.30	0.2236 53377	0.3317 70833	0.5238 38145
−0.5	2	1.25	0.2812 50000	0.4394 53125	0.7481 68945
−0.6	1.7888 5440	1.20	0.3577 70873	0.6	1.1269 78260
−0.7	1.5491 9332	1.15	0.4663 71750	0.8654 94792	1.8578 35567
−0.8	1.2649 1108	1.10	0.6403 61218	1.3921 87500	3.6350 50516
−0.9	0.8944 2720	1.05	1.0090 25665	2.9613 28125	10.9045 72004
−1.0	0	1.00	∞	∞	∞

It is convenient to rewrite the Taylor expansion with

$$x=(\eta+1)/\delta, \tag{24}$$

$$z=4(1-\lambda)\delta^{-\frac{1}{2}}, \tag{25}$$

so that

$$z=x+b_2x^2+b_3x^3+\cdots b_nx^n\cdots, \tag{26}$$

with

$$b_1=1,$$

$$b_2=2^{-4}(1+\delta),$$

$$b_3=2^{-6}[12(1+\delta)b_2-\delta],$$

$$b_4=\frac{5}{96}[5(1+\delta)b_3-\delta b_2],$$

$$b_5=\frac{7}{2^8.5}[56(1+\delta)b_4-15\delta b_3],$$

$$b_n=\frac{2n-3}{4.2n(2n-2)^2}[2(2n-2)(2n-3)(1+\delta)b_{n-1}-(2n-4)(2n-5)\delta b_{n-2}]. \tag{27}$$

It is now convenient to reverse the power series to get

$$x=z+c_2z^2+c_3z^3\cdots c_nz^n, \tag{28}$$

where the coefficients c_n are known functions of the b_n's.[10] If we put $1-\lambda=\lambda'$ for convenience, the result is

$$\eta=-1+d_1\lambda'+d_2\lambda'^2+d_3\lambda'^3\cdots+d_n\lambda'^n\cdots, \tag{29}$$

where

$$d_n=2^{2n}\delta^{(2-n)/2}c_n. \tag{30}$$

Explicitly,

$$\eta=-1+\lambda'\{4\delta^{\frac{1}{2}}-(1+\delta)\lambda'-2^{-2}(1-\delta)^2\delta^{-\frac{1}{2}}\lambda'^2-5.2^{-5}(1+\delta)(1-\delta)^2\delta^{-1}\lambda'^3\cdots\}. \tag{31}$$

Unfortunately the c's do not have a linear recursion formula, so that it becomes cumbersome to carry out this expansion any further algebraically.

Nevertheless, this expansion is not at all unwieldy to evaluate numerically to several higher terms than are expressed in (31). It is very simple to calculate the b_n's, say up to $n=10$, by their recursion formula (27). The c_n's are little more troublesome. Formulae are indeed given[11] for them up to $n=12$. The coefficients, d_n, in (29) are then easily computed.

We have calculated the coefficients d_n up to $n=5$ for all values of κ in Table I. They are given in Table II. From them η has been calculated from the expansion (29) for each value of λ in Table I. The differences between these values and the exact values given in Table I are plotted on a logarithmic scale in Fig. 3. These plots have a number of uses. First we see that the errors get

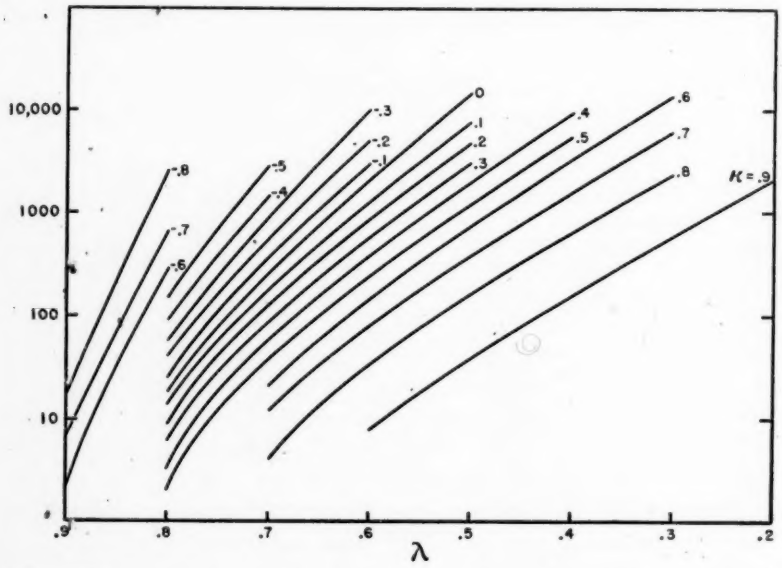

FIG. 3. Differences between exact value of η and that calculated by power series, plotted as a function of λ for various values of κ. For $\eta<\kappa$ the exact value is the lesser; and for $\eta>\kappa$ the exact value is the greater $\times 10^6$.

[10] E. P. Adams, *Smithsonian Mathematical Formulae and Tables of Elliptic Functions* (Smithsonian Institution, Washington, 1922), p. 116.

[11] C. E. VanOrstrand, Phil. Mag. **19**, 366 (1910).

TABLE III. Maximum errors in interpolating Table I. The entries at λ are Eq. (38) for $\lambda_0-\lambda=0.1$, minus $\eta(\lambda_0-0.1)$ where $\lambda<\lambda_0$. They are negative above the diagonal, positive below, with the usual symmetry around $\kappa=0\times10^6$.

κ / λ	−1.0	−0.9	−0.8	−0.7	−0.6	−0.5	−0.4	−0.3	−0.2	−0.1	0
0.9	0	0	3	8	13	21	31	43	59	79	102
0.8	0	0	7	12	22	34	52	76	105	140	184
0.7	0	5	7	22	39	68	104	148	205	281	381
0.6	0	4	19	46	84	139	217	321	467	677	1001
0.5	0	11	44	104	200	346	562	910	1512	2728	6887
0.4	0	29	118	294	610	1197	2467	5896	2609	1541	1001
0.3	0	93	436	1307	4333	2617	1524	1010	712	518	381
0.2	0	520	4194	1703	1051	732	539	408	314	240	184
0.1	0	1505	832	578	432	334	263	209	165	130	102

extremely large as η approaches κ. (We shall see below that at $\eta=\kappa$ the coefficients are infinite.) We therefore can see that each higher d_n which is computed will permit better approximations in the main part of the range, but will always leave a region near $\eta=\kappa$ where the error is very large. The error curves in Fig. 3 can be used to get a good approximation to η over most of the range. First one calculates η, using the first five d_n's, and then adds the error from Fig. 3. The resulting accuracy depends, of course, on the cycle of the error corresponding to the values of κ and λ in question. It should also be pointed out that at $\eta=\kappa$ the exact trigonometric formula (10) can be used. Precise values of η as η approaches κ, however, would have to be computed in some other way. However, since the exact value of η calculated by the correspondence principle differs, in the neighborhood of $\eta=\kappa$, from the true value for the level by an amount of the order of magnitude of the separation of the levels, there is no need to pursue these investigations further here.

EXPANSIONS AROUND EACH POINT IN TABLE I

As a matter of fact, a Taylor's expansion can be made around each point in Table I, in the sense that the integrals in (22) can be calculated in terms of complete elliptic integrals of the first and second kinds. This is accomplished by transforming to Legendre's normal forms. The range of integration relative to the poles is such that the appropriate[12] transformation,

$$z=\frac{\kappa(1-\eta)-\eta(1-\kappa)\sin^2\varphi}{(1-\eta)-(1-\kappa)\sin^2\varphi}, \tag{32}$$

reduces these integrals to

$$\frac{\partial^n\lambda}{\partial\eta^n}=-\frac{1}{2\pi}\frac{1}{2}\frac{3}{2}\cdots\frac{2n-3}{2}\left(\frac{2}{(1-\eta)(1+\kappa)}\right)^{\frac{1}{2}}\times\frac{1}{(\kappa-\eta)^{n-1}}\int_0^{2\pi}\frac{(1-p\sin^2\varphi)^{n-1}}{\Delta\varphi}d\varphi. \tag{33}$$

For $n=1$ the integral is the complete elliptic integral of the first kind

$$\frac{\partial\lambda}{\partial\eta}=\left(\frac{2}{(1-\eta)(1+\kappa)}\right)^{\frac{1}{2}}F_0(\alpha), \tag{34}$$

where $F_0(\alpha)$ is the function tabulated by Heuman, and $\sin^2\alpha$ is the modulus given in (15).

For $n=2$ the integral involves the complete elliptic integral of the second kind,

$$\frac{\partial^2\lambda}{\partial\eta^2}=-\frac{1}{4}\left(\frac{2}{(1-\eta)(1+\kappa)}\right)^{\frac{1}{2}}\frac{1}{(1+\eta)}\times\left[\frac{(1+\kappa)}{\kappa-\eta}E_0(\alpha)-F_0\right]. \tag{35}$$

For higher values of n there is a recursion formula which we can derive by the method

[12] A. Enneper, *Elliptische Functionen* (Nebert Halle, 1890), p. 21, case *Bb*.

originally outlined by Legendre. The most explicit formulation of it is given by Durège.[13] In our case we differentiate and integrate the expression $(1-p\sin^2\varphi)^n\Delta^2\varphi$ and after rearrangement get the recursion formula

$$\frac{\partial^n\lambda}{\partial\eta^n}=\frac{1}{(\eta-\kappa)(1-\eta^2)}\left[\frac{2n-4}{2}(3\eta^2-2\kappa\eta-1)\frac{\partial^{n-1}\lambda}{\partial\eta^{n-1}}+\frac{2n-5}{2}(3\eta-\kappa)\frac{\partial^{n-2}\lambda}{\partial\eta^{n-2}}+\left(\frac{2n-5}{2}\right)\times\left(\frac{2n-6}{2}\right)\left(\frac{2n-7}{2}\right)\frac{\partial^{n-3}\lambda}{\partial\eta^{n-3}}\right]. \quad (36)$$

This gives, for example, when $n=3$,

$$\frac{\partial^3\lambda}{\partial\eta^3}=\frac{1}{(\eta-\kappa)(1-\eta^2)}\left[(3\eta^2-2\kappa\eta-1)\frac{\partial^2\lambda}{\partial\eta^2}+\frac{1}{4}(3\eta-\kappa)\frac{\partial\lambda}{\partial\eta}\right]. \quad (37)$$

Thus it is possible to calculate all the coefficients in the Taylor's expansion of λ in terms of $(\eta-\eta_0)$, η_0 being the entry in Table I for λ_0. By the same procedure described above in the special case of $\eta_0=-1$, the series expansion can be reversed and $\eta-\eta_0$ found as a power series in $\lambda-\lambda_0$. The coefficients are rather involved algebraic expressions involving η, κ, $F_0(\alpha)$, and $E_0(\alpha)$:

$$\eta=\eta_0+d_1'(\lambda_0-\lambda)+d_2'(\lambda_0-\lambda)^2\cdots, \quad (38)$$

$$d_1'=[2(1-\eta)^{\frac{1}{2}}(1+\kappa)^{\frac{1}{2}}]/F_0(\alpha), \quad (39)$$

$$d_2'=\frac{1}{4(1+\eta)}\left(\frac{1+\kappa}{\kappa-\eta}\frac{E_0(\alpha)}{F_0(\alpha)}-1\right)d_1^2. \quad (40)$$

[13] H. Durège, *Theorie der Elliptischen Functionen* (B. G. Teubner, Leipzig, 1887), p. 65 *et. seq.*

The first two coefficients have been computed for every point in Table I, so that interpolation by (38) is possible. Further accuracy can be obtained by taking differences in d_2'.

These coefficients converge to those of (29) when $\lambda_0\to1$, and to those of (11) when written as

$$\eta=\eta_0+4\lambda_0(\lambda_0-\lambda)-2(\lambda_0-\lambda)^2, \quad (11a)$$

when $\kappa\to1$, $(\delta\to1)$, except at the upper right-hand entry (appearing with changed sign in the lower left-hand entry in Table I), where (29) and (11a) differ. This is, of course, a point on the diagonal (Fig. 2i), and really is the limit of the upper horizontal line, an extreme perturbation of the prolate ($\kappa=-1$) symmetric rotor, rather than a value for the oblate rotor. This, as pointed out above, is the region of maximum deviation.

The maximum error possible in interpolating by (38) is when $\lambda_0-\lambda$ is nearly 0.1, that is, extrapolating from one entry of the table, say λ_0, to the next in the direction of the diagonal, $\lambda_1=\lambda_0-0.1$. The maximum error is then $\eta(\lambda_1)-\eta(\lambda_0-0.1)$ and, if (38) is used,

$$\eta(\lambda_0-0.1)=\eta_0+0.1d_1+0.01d_2. \quad (41)$$

These maximum errors are summarized in Table III, which gives η calculated by (38), λ_1 being nearer the diagonal than λ_0, minus the tabular value of $\eta(\lambda_1)$. The error is always positive below the diagonal, and is always negative above.

ACKNOWLEDGMENT

The author is indebted to the Office of Naval Research for making these investigations possible, to Dr. H. Goheen of the Boston Office, O.N.R. for helpful discussions, and to Miss Joanne Edson for carrying out the calculations presented here.

THE JOURNAL OF CHEMICAL PHYSICS VOLUME 15, NUMBER 11 NOVEMBER, 1947

On Simple Binary Solid Solutions*

A. W. LAWSON
Institute for the Study of Metals, University of Chicago, Chicago, Illinois

(Received Spetember 17, 1947)

The effect of difference in atomic volume between two components of a simple binary solid solution on the phase equilibrium curves is investigated by calculating the energy of deformation required to replace a smaller atom by a larger atom, and *vice versa*. The strain energy is introduced to the free-energy function derived by the quasi-chemical technique of Guggenheim and leads to expressions similar to those of Hildebrand for unsymmetrical segregation. In addition, the Mie-Gruneisen equation is used to estimate the effect of vibrational entropy changes. It is found that the effect of such changes has a smaller effect on phase equilibria in general than the energy changes. Finally, the results are used to justify certain empirical thermodynamic expressions.

INTRODUCTION

VARIOUS authors, notably van Laar,[1] Hildebrand,[2] and Guggenheim,[3] have studied the problem of segregation in simple binary solutions. Van Laar's approach is through the application of van der Waal's equation of state. Although empirically successful to a limited extent, its interpretation when applied to solids is dubious. Hildebrand, directing his attention mainly to liquid solutions, has treated the problem from a thermodynamic point of view, assuming a deviation from perfect heat of mixing but a random entropy of mixing, and, by using smeared potentials, has also estimated the effect of difference in molal volumes. To a first approximation, this theory yields reasonable agreement with experiment when the solutions satisfy the assumptions required by the theory. The principal attack on the problem of segregation in solid solutions is that of Guggenheim[3] and Rushbrooke,[4] who use the so-called quasi-chemical method. This theory is a generalization of techniques previously developed by Bragg and Williams[5] and Bethe[6] for the treatment of ordered structures. In essence, the quasi-chemical theory describes the segregation process for a given lattice structure in terms of a single parameter w_{AB}, the energy required to interchange an A atom on an A lattice with a B atom on a B lattice. Unfortunately, this theory predicts the invariable occurrence of symmetrical segregation. The object of this paper is to consider the effect of differences in atomic volume between the two components on the results predicted by the quasi-chemical theory. As we shall see, this consideration is tantamount to assuming an assymmetrical dependence of w_{AB} on composition and hence leads to asymmetrical solubility gaps. Finally, we shall discuss the small corrections to the theory required by changes in vibrational entropy with composition and use this discussion as a justification for the use of the Margules type of empirical thermodynamic expansion.

THE QUASI-CHEMICAL THEORY

If we take w_{AB} to be the change in potential energy caused by creating two moles of AB pairs from one mole of AA pairs and one mole of BB pairs, then according to Rushbrooke (assuming w_{AB} to be independent of composition) the free energy of a binary mixture is given by

$$F=-N_1\chi_{AA}-N_2\chi_{BB}+q_{AB}w_{AB}+kT(N_1\ln x+N_2\ln y), \quad (1)$$

where x_{AA} and x_{BB} are the energies of an A atom in an A lattice and a B atom in a B lattice, respectively, at the zero temperature; N_1 and N_2, are the mole numbers of the two components, and x and y are the corresponding mole fractions. The first two terms represent the energy of a perfect solution, and the last term is the random mixing

* This work was supported in part by the Office of Naval Research under contract No. N-6ori-20-IV with the University of Chicago.

[1] J. van Laar, Zeits. f. physik. Chemie **63**, 216 (1908).
[2] J. Hildebrand, J. Am. Chem. Soc. **51**, 69 (1929); *ibid.*, *Solubility of Non Electrolytes* (Reinhold Publishing Corporation, New York, 1936).
[3] E. A. Guggenheim, Proc. Roy. Soc. **A169**, 134 (1938).
[4] G. Rushbrooke, Proc. Roy. Soc. **A166**, 296 (1938).
[5] Bragg and Williams, Proc. Roy. Soc. **A145**, 699 (1934).
[6] H. Bethe, Proc. Roy. Soc. **A150**, 552 (1935).

entropy of such a solution. The term $q_{AB}w_{AB}$ describes the deviation from perfect mixing and contributes both a heat of mixing and an additional entropy of mixing. The function q_{AB} has been calculated by Rushbrooke and to a sufficiently good approximation at high temperatures may be written as

$$q_{AB}=xy\left\{1-xy\left[\frac{zRT}{2w_{AB}}e^{2w_{AB}/zRT}-\frac{zRT}{2w_{AB}}-1\right]\right\}, \quad (2)$$

where Z is the number of nearest neighbors on any particular lattice under investigation.

The assumption involved in the derivation of Eq. (1) and Eq. (2) are (a) the molal volumes and free volumes of A and B differ by less than 30 percent, (b) w_{AB} is independent of composition, (c) vibrational entropy changes are negligible, and (d), the lattices of A and B are identical so that z is the same for both, and it is possible (in principle) to change the composition from pure A to pure B without a phase change.

Assumption A was introduced by Rushbrooke in order to facilitate the approximate evaluation of a grand partition function, and assumption B was made not only in the interests of simplicity but also to obtain a one-parameter theory. Actually, if the A and B atoms differ in size, then an interchange of an A and a B atom will in general introduce strains, and hence contribute to w_{AB}. As we shall see, the amount of strain energy introduced by such an interchange is in general a function of composition, and hence assumption B is only valid if the sizes of A and B are identical (i.e., no strain energy is introduced by an $A-B$ interchange).

In the following section we shall alter assumptions A and B, but retain for the time being assumptions C and D. Later, we shall discuss the effect of removing the restrictions implied by C and D.

THE EFFECT OF ATOMIC SIZE ON SEGREGATION

The influence of atomic size on solubility has long been recognized by metallurgists. In fact, Hume-Rothery[7] has pointed out that if the atomic radii of two atoms differ by more than 15 percent it is highly unlikely that any binary solution will be formed. Furthermore, it is also known that the solubility of a large atom in a small lattice is in general much smaller than the solubility of a small atom in a large lattice. The object of this section is to frame these deliberations in a somewhat more quantitative fashion. As a starting point, we shall assume that we may write the free energy of a binary mixture as the free energy of a perfect solution plus the strain energy involved in substituting an A atom for a B atom and *vice versa*. In this simple approximation the whole blame for segregation is placed upon size mismatches, and according to this point of view no segregation will take place if the A atom and B atom are the same size. Thus, we disregard the type of segregation which arises from difference in energy between an A atom surrounded by A atoms and an A atom surrounded by B atoms, even when A and B are the same size. Later, we shall amalgamate our calculations with Eqs. (1) and (2) of the quasi-chemical theory to obtain an equation of state applicable when both effects are operative.

Our primary problem, then, is to calculate the strain energy associated with the replacement of an A atom in an A lattice by a B atom. A rigorous solution to this problem for all compositions appears extremely difficult. However, we may make an approximate calculation which appears reasonable.

In the first place, we shall assume that the molal volume of the A lattice is V_A and the molal volume of the B lattice is V_B. Further, we shall make the assumption that the molal volume of an alloy consisting of x moles of A and y moles of B is given by

$$V=xV_A+yV_B. \quad (3)$$

The preceding equation would be rigorous, of course, if V_A and V_B designated partial molal volumes. However, in light of known experimental data, replacing partial molal volumes by V_A and V_B does not appear to be a serious approximation.

If now we consider an atom B of volume V_B/N to replace an A atom of volume V_A/N in an A lattice, we may immediately calculate the strain energy associated with the exchange. The B atom will be compressed, and the surrounding A lattice will be sheared until mechanical equi-

[7] W. Hume-Rothery, *Atomic Theory for Students of Metallurgy* (Institute of Metals, London, 1946).

librium is achieved. Obviously the distortion in the A lattice will drop off rapidly with distance from the B atom. Thus, for all practical purposes, we may compute the strain energy as if we have a hollow thick sphere in which the spherical cavity has been enlarged. The problem is simplified if we assume that the B atom is incompressible and the A lattice is isotropic. The first assumption appears reasonable when one remembers that interatomic repulsive forces are much more rapid functions of interatomic distance than the attractive forces. In any case, both assumptions are unnecessary and are made primarily in the interests of brevity and because the errors so introduced are smaller than other uncertainties introduced later in the development.

Now the distortion of a thick isotropic spherical shell by an internal pressure p is a classic problem of elasticity theory, whose solution may be found in detail in almost any standard text.[8]

If P and Q denote the radial and circumferential tensions in such a shell, then for sufficiently thick shell

$$P=-a^3p/r^3, \tag{4}$$

$$Q=a^3p/2r^3, \tag{5}$$

where a is the radius of the spherical cavity retaining a pressure p. Equations (4) and (5) are special solutions of the differential equations of equilibrium,

$$\frac{d}{dr}(r^2P)=2rQ, \tag{6}$$

$$E\frac{du}{dr}=P-2\sigma Q, \tag{7}$$

$$E\frac{u}{r}=(1-\sigma)Q-\sigma P, \tag{8}$$

where E is Young's modulus, σ is Poisson's ratio, and u is the displacement along r, a radius. Inserting Eqs. (4) and (5) in Eq. (8), we obtain

$$u=\frac{1+\sigma}{2E}\frac{a^3}{r^2}p, \tag{9}$$

which, in view of our assumption of isotropy, may be rewritten as

$$u=\frac{1}{4G}\frac{a^3}{r^2}p, \tag{10}$$

where G is the shear modulus.

Correspondingly, for the strain energy ΔE_B, we have

$$\Delta E_B=\int pdv=\int_0^p \frac{\pi}{G}a^3pdp=\frac{\pi}{2G}a^3p^2, \tag{11}$$

where we have utilized the fact that

$$dv=4\pi r^2du. \tag{12}$$

Hence for the final expression in terms of V_A and V_B, one finds

$$\Delta E_B=\frac{4}{3}G_A\frac{(V_B-V_A)^2}{V_AN}. \tag{13}$$

The preceding expression should be rigorous for the strain energy generated by the introduction of the first B atom into an A lattice. For a sufficiently small number of B atoms (small y) we then find for the strain energy per mole

$$\Delta E_B\cong\frac{4}{3}G_A\frac{(V_B-V_A)^2}{V_A}y. \tag{14}$$

It is clear that Eq. (14) cannot hold accurately for all values of y. Thus when $y=1$, E must be zero, since the addition of a B atom to a B lattice cannot entail strain energy. Therefore, at this juncture we must introduce an important assumption, namely, that the effective increase in volume demanded by a B atom when introduced into a lattice containing a fraction x of A atoms and y of B atoms is $(V_B-V_A)x$.

With this assumption, one has

$$\Delta E_B\cong\frac{4}{3}\frac{G_A}{V_A}(V_B-V_A)yx^2, \tag{15}$$

where we are justified in retaining V_A in the denominator provided (V_B-V_A) is not too large. Now even Eq. (15) does not provide us with an adequate expression for the strain energy, for we might expect that if we started with a pure B lattice and substituted A atoms that distortions in the B lattice would be produced and consequently an associated strain energy per mole

[8] J. Prescott, *Applied Elasticity* (Dover Publications, New York, 1946).

which would be proportional to x, the fraction of small atoms substituted for large atoms. Using similar assumptions, we would find

$$\Delta E_A = -\frac{4}{3}\frac{G_B}{V_B}(V_B - V_A)^2 xy^2. \tag{16}$$

It would appear that Eq. (15) is a good approximation for $x=1$ and Eq. (16) is a good approximation for $y=1$. How then shall we combine them to obtain an adequate expression for the strain energy for all compositions? It is clear that for $x=y=\frac{1}{2}$ our model is rather unsatisfactory, yet no simple method of estimating the strain energy for intermediate composition suggests itself. Consequently, we are forced to seize the bull by the horns, make an arbitrary assumption that the quantities ΔE_A and ΔE_B are additive, and examine the validity of our rashness in retrospect. Accordingly, consistent with this philosophy we write

$$F/N = -x\chi_{AA} - y\chi_{BB} + \frac{4}{3}\frac{G_A}{V_A}(V_B - V_A)^2 yx^2 + \frac{4}{3}\frac{G_B}{V_B}(V_B - V_A)^2 xy^2 + RT(x \ln x + y \ln y) \tag{17}$$

as the equation of state of our binary mixture. Despite the *ad hoc* nature of our assumptions, our hope is bolstered by noticing that the contribution of ΔE_B goes rapidly to zero where ΔE_A is important and *vice versa*.

In the usual straightforward manner we may differentiate the free energy with respect to $N_1 = xN$ and $N_2 = yN$ to obtain expressions for the chemical potentials:

$$\mu_1 = -\chi_{AA} + \frac{4}{3}(V_B - V_A)^2\frac{G_A}{V_A}(2xy^2) + \frac{4}{3}\frac{G_B}{V_B}(V_B - V_A)^2(y^3 - y^2 x) + RT \ln x, \tag{18}$$

$$\mu_2 = -\chi_{BB} + \frac{4}{3}(V_B - V_A)^2\frac{G_A}{V_A}(x^3 - x^2 y) + \frac{4}{3}\frac{G_B}{V_B}(V_B - V_A)^2(2x^2 y) + RT \ln y. \tag{19}$$

The phase equilibrium curve may then be found by satisfying the requirements that

$$\mu_1(x_1) = \mu_1(x_2), \tag{20}$$

$$\mu_2(1 - x_1) = \mu_2(1 - x_2). \tag{21}$$

The simultaneous solution of Eqs. (20) and (21) for a given value of T yields the compositions x_1 and x_2 of the phases in equilibrium at that temperature. Unfortunately, because of the occurrence of transcendental functions the solution of these equations must be carried out graphically. However, one may locate the position of the critical point x_c, T_c (assuming it exists) by satisfying the critical conditions.

$$\partial\mu_1/\partial x = 0, \quad x = x_c, \tag{22}$$

$$\partial^2\mu_1/\partial x^2 = 0, \quad x = x_c. \tag{23}$$

These conditions yield

$$2y_c x_c\left[(2x_c - y_c)\frac{4}{3}\frac{G_A}{V_A}(V_B - V_A)^2 + (2y_c - x_c)\frac{4}{3}\frac{G_B}{V_B}(V_B - V_A)^2\right] = RT_c, \tag{24}$$

$$y_c - x_c = \frac{8x_c^2 y_c^2}{RT_c}(V_B - V_A)^2\left[\frac{G_B}{V_B} - \frac{G_A}{V_A}\right]. \tag{25}$$

The preceding equations estimate effects arising from volume differences alone. However, as we know, segregation is possible even when no volume difference exists. We may lump the extra energy in the term w_{AB} appearing in Eq. (1). Then, retaining only the first term of q_{AB} in Eq. (2), we have approximately for the free energy

$$F/N \cong -\chi_{AA}x - \chi_{BB}y + RT(x \ln x + y \ln y) + xy\left[w_{AB} + \frac{4}{3}x\frac{G_A}{V_A}(V_B - V_A)^2 + \frac{4}{3}y\frac{G_B}{V_B}(V_B - V_A)^2\right], \tag{26}$$

in which w_{AB} is the energy required to form two AB pairs from an AA pair and BB pair assuming no volume effects. In this case, we have as before

$$\mu_1 = w_{AB}y^2 + RT \ln x + \frac{4}{3}\frac{G_A}{V_B}(V_B - V_A)^2(2xy^2) + \frac{4}{3}\frac{G_B}{V_B}(V_B - V_A)^2(y^3 - y^2 x) - x_{AA}, \tag{27}$$

$$\mu_2 = w_{AB}x^2 + RT \ln y + \text{etc.} \tag{28}$$

From Eqs. (22) and (23) we ther find

$$w_{AB}+(2x_c-y_c)\frac{4}{3}\frac{G_A}{V_A}(V_B-V_A)^2 + (2y_c-x_c)\frac{4}{3}\frac{G_B}{V_B}(V_B-V_A)^2=\frac{RT_c}{2x_cy_c}, \quad (29)$$

and

$$(y_c-x_c)=\frac{8x_c^2y_c^2}{RT_c}(V_B-V_A)^2\left[\frac{G_B}{V_B}-\frac{G_A}{V_A}\right]. \quad (30)$$

It is interesting to compare Eqs. (29) and (30) with the results of Hildebrand, namely,

$$RT_c=\frac{2x_cy_cV_A^2V_B^2}{(x_cV_A+y_cV_B)^3}\left[\frac{a_1^{\frac{1}{2}}}{V_A}-\frac{a_2^{\frac{1}{2}}}{V_B}\right], \quad (31)$$

$$x_c=\frac{(V_A^2+V_B^2-V_AV_B)^{\frac{1}{2}}-V_A}{V_B-V_A}, \quad (32)$$

in which a and V refer to the heat of vaporization and molal volume, respectively.

We may test Eq. (29) by considering the well-known case of segregation in Au-Pt alloys. In this case, $T_c=1150°C$ and the factors G/V are tabulated in Table I. Thus from Eq. (30), assuming (y_c-x_c) is small so that $x_c^2y_c^2\cong\frac{1}{16}$, we find $x_c=0.63$, in fair agreement with the observed value of 0.67 ± 0.02. Then from Eq. (30) we find w_{AB} to be 3.8 kcal. For the strain-energy contribution to the quantity $RT_c/2x_cy_c$ we find 2.3 kcal. Thus, the interchange energy involving quantities other than strain energy is of the same order of magnitude as the strain energy. This state of affairs seems to be the general rule in simple binary solids as one can see by glancing at the values of G/V in the last column of Table I. It is apparent from the order of magnitude of this quantity that values of T_c to be expected if strain energy were the sole cause of segregation would be on the average considerably lower than those observed.

TABLE I. Ratio of effective modulus to molal volume for various metals.

Metal	Shear modulus kg/mm²	Molal volume cm³	4/3 G/V kilocalories
Al	2700	9.99	0.86
Cu	4400	7.09	1.96
Au	2800	10.2	0.87
Ag	2700	10.3	0.83
Mg	1800	14.0	0.41
Zn	3700	14.0	0.84
Cd	2200	13.0	0.54
Pt	7200	9.1	2.50
αFe	8400	7.10	3.74
Ni	7370	6.6	3.53

THE EFFECT OF LOCAL ORDER AND VIBRATIONAL ENTROPY

In our foregoing discussion we have neglected the effect of thermal vibration and the contribution to entropy terms arising from local order; we need merely carry one more term in the expansion of q_{AB}. Accordingly, we write

$$q_{AB}=xy-x^2y^2(w_{AB}/ZRT), \quad (33)$$

which may be easily obtained by expanding the exponential in Eq. (2). The additional term in Eq. (33) introduces a small correction of the order of 10 percent on the value of w_{AB} and tends to broaden the segregation loop slightly in a manner illustrated near the end of this section.

The effect of vibrational entropy may be estimated by use of the Mie-Gruneisen equation of state, according to which a simple solid at high temperatures has a free energy given by

$$F/N=-\chi+3kT\ln(h\nu_0/kT), \quad (34)$$

where x is the average energy of an atom in the solid and ν_0 is the geometrical mean frequency of vibration which may be approximately taken equal to the Einstein frequency.

Our problem then is to introduce the vibrational term appearing in Eq. (34) into the free-energy expression for a binary mixture in a consistent manner. For simplicity we shall assume that $V_A=V_B$, so that the segregation is symmetrical about $x_c=\frac{1}{2}$. Thus we suppose, in analogy to Eq. (34), that

$$F/N=-x\chi_{AA}-y\chi_{BB}+q_{AB}w_{AB} -3kT\ln\frac{h\nu_0}{kT}+kT(x\ln x+y\ln y), \quad (35)$$

where now we must regard $\nu_0(x)$, the geometrical mean frequency of vibration, to be a function of composition. In order to simplify the problem we shall assume that

$$\ln\frac{kT}{h\nu_0(x)}=\ln\frac{kT}{\nu_A^x(x)\nu_B^y(y)}. \quad (36)$$

In this approximation we assume, in general, that the mean frequencies of the A and B atoms are different (e.g., because of mass differences), and our problem is to find the dependence of ν_A (or ν_B) on composition. Clearly, the average frequency of vibration of an A atom surrounded by A atoms will be different from the average frequency of A atoms surrounded by B atoms, if the energy of the A atom depends on the fractional concentration of the A atoms among the Z nearest neighbors.

A precise estimation of the dependence of ν_A on composition is an extremely intricate problem. Nevertheless, it is possible to make a rough estimate. For instance, suppose that we assume a law of force between A atoms of the type such that the free energy at absolute zero of temperature is

$$F_0(V) = -A/V^{m/3} + B/V^{n/3}. \tag{37}$$

Since to insure equilibrium at zero pressure $F'(V_0) = 0$, we are led to conclude from the definition of compressibility κ_0 that

$$F_0(V_0) = -9V_0/nm\kappa_0. \tag{38}$$

The preceding equation establishes a definite connection between lattice energy and compressibility for given values of n, m, and V_0. As a first approximation we suggest that it is reasonable to assume that the same relation holds for the alloy, assuming that n and m have approximately the same values for $B-B$ and $A-B$ interactions.

Further, for a given mass and atomic volume we have, according to the Einstein theory,

$$\nu \propto \kappa^{-\frac{1}{2}} \propto F_0^{\frac{1}{2}}(V_0). \tag{39}$$

Rewriting Eq. (36) in a more convenient form, we have

$$\ln\frac{kT}{h\nu_0(x)} = x\ln\frac{kT}{h\nu_A(1)} + x\ln\frac{\nu_A(1)}{\nu_A(x)} + y\ln\frac{kT}{h\nu_B(1)} + y\ln\frac{\nu_B(1)}{\nu_B(y)}. \tag{40}$$

Then, according to our point of view, we may write

$$\ln\frac{\nu_A(1)}{\nu_A(x)} = -\ln\left(\frac{x\chi_{AA}+y\chi_{BB}}{\chi_{AA}}\right)^{\frac{1}{2}} \cong \tfrac{1}{2}y\frac{(\chi_{AA}-\chi_{AB})}{\chi_{AA}}, \tag{41}$$

and, similarly,

$$\ln\frac{\nu_B(1)}{\nu_B(y)} \cong \tfrac{1}{2}x\frac{(\chi_{AB}-\chi_{AB})}{\chi_{AB}}. \tag{42}$$

Thus for the free energy per mole of our mixture we have

$$F = xF_A + yF_B + RT(x\ln x + y\ln y) + q_{AB}w_{AB} - \tfrac{3}{2}RTxy\left[\frac{\chi_{AA}-\chi_{AB}}{\chi_{AA}} + \frac{\chi_{BB}-\chi_{AB}}{\chi_{BB}}\right], \tag{43}$$

or, if χ_{AA} and χ_{BB} are not too different,

$$F = xF_A + yF_B + RT(x\ln x + y\ln y) + q_{AB}w_{AB} - 3RTxy\frac{w_{AB}}{\chi_{AA}+\chi_{BB}}. \tag{44}$$

Furthermore, at high temperatures, where the preceding equation is applicable, we may use the expanded form of q_{AB} given by Eq. (34). Thus, finally, for our approximate equation of state we obtain

$$F = xF_A + yF_B + RT(x\ln x + y\ln y) - 3RTxy\frac{w_{AB}}{\chi_{AA}+\chi_{BB}} + w_{AB}\left(xy - x^2y^2\frac{w_{AB}}{zRT}\right), \tag{45}$$

when volume effects are negligible.

Recalling our restriction to symmetrical segregation, we need use only one critical condition, say $\partial\mu_A/\partial x = 0$, to relate w_{AB} to T_c.

Accordingly, in the usual straightforward manner we find

$$\mu_A = F_A - 3RTy^2\frac{w_{AB}}{\chi_{AA}+\chi_{BB}} + w_{AB}y^2 + RT\ln x + (x^2y^2 - 2xy^3)\frac{{w_{AB}}^2}{zRT}, \tag{46}$$

and, correspondingly,

$$\frac{\partial\mu_A}{\partial x} = -\left(w_{AB} - 3RT\frac{w_{AB}}{\chi_{AA}+\chi_{BB}}\right)2y + \frac{RT}{x} + [2(y-x)xy - 2y^3 + 6xy^2]\frac{{w_{AB}}^2}{zRT}. \tag{47}$$

Thus the critical condition expressed by Eq. (15)

becomes

$$\frac{1}{2Z}\left(\frac{w_{AB}}{RT_c}\right)^2-\left(1-\frac{3RT_c}{\chi_{AA}+\chi_{BB}}\right)\frac{w_{AB}}{RT_c}+2=0, \quad (48)$$

or

$$\frac{w_{AB}}{RT_c}=4\left[1-\frac{3RT_c}{\chi_{AA}+\chi_{BB}} \pm\left(1-\frac{3RT_c}{\chi_{AA}+\chi_{BB}}-\frac{4}{z}\right)^{\frac{1}{2}}\right]^{-1}. \quad (49)$$

To a satisfactory degree of approximation we have then

$$w_{AB}\cong 2RT_c\left(1+\frac{3RT_c}{\chi_{AA}+\chi_{BB}}+\frac{1}{z}\right). \quad (50)$$

It appears that the ratio of the interchange energy to the critical temperature is affected by both the local order and the vibrational entropy changes. To make some quantitative estimates, $\chi_{AA}+\chi_{BB}$ may be of the order of 100–200 kilocalories/mole when w_{AB} is of the order of 9 kilocalories. Thus, it seems unlikely that the first term will introduce a correction of more than about 10 percent. The correction caused by local order is of the order of $1/z$, i.e., about 8 percent to 12 percent.

If we assume $3R_T/(\chi_{AA}+\chi_{BB})=0.1$, and $z=8$ (body-centered cubic lattice), then

$$w_{AB}=2RT_c, \text{ (Hildebrand)}$$
$$w_{AB}=2.25RT_c, \text{ (quasi-chemical)}$$

to be compared with the value obtained from the foregoing theory of

$$w_{AB}=2.45RT_c.$$

It follows that the primary effect of changes in vibrational entropy with composition is to increase the heat of solution proportionally. For the values assumed above, the increase in heat of solution is about 10 percent over that calculated by the quasi-chemical method neglecting vibrational entropy. It should be kept in mind, however, that we have used rather extreme values in making our estimate.

The equilibrium values x_1 and x_2 at any temperature may now be determined. From Eq. (46) and the equality of the chemical potentials in the two segregating phases, one obtains

$$RT\ln x_2+w_{AB}\left[1-\frac{3RT}{\chi_{AA}+\chi_{BB}}\right]y_2^2 - 2x_2y_2^3\frac{w_{AB}^2}{zRT}=h(x_2)=h(x_1). \quad (51)$$

In view of the symmetry we may set $x_2=y_1$, and $y_2=x_1$. Thus the preceding equation reduces to

$$w_{AB}(1-2y_1)\left\{\left(1-\frac{3RT}{\chi_{AA}+\chi_{BB}}\right)-\frac{2w_{AB}}{zRT}x_1y_1\right\} =RT\ln\frac{1-y_1}{y_1}, \quad (52)$$

from which one may calculate the equilibrium curve. This equation should be compared with that derived by Hildebrand for the same situation, namely,

$$w_{AB}(1-2y_1)=RT\ln\frac{1-y_1}{y_1}. \quad (53)$$

In fact, it is convenient to use the last equation as a reference for computing the corrections required by the Mie-Gruneisen version of the quasi-chemical method. Let r_0 be the ratio T/T_c corresponding to a given value of y_1 in Eq. (53). Similarly, let r_1 be the ratio of T/T_c corresponding to the same value y_1 in Eq. (52). Then, to the same degree of approximation, by substituting the appropriate values of w_{AB}, etc., into Eq. (52) and Eq. (53) and taking the ratio

$$\frac{r_1}{r_0}=1+0.1(1-r_0)+\frac{4.4}{z}\left[0.25-\frac{x_1y_1}{r_0}\right]. \quad (54)$$

In this equation, r_0 has been substituted for r_1 on the right-hand side of the equation, and the coefficient of the last bracket has been chosen somewhat arbitrarily (to remove discrepancies arising from previous approximations) so that $r_1/r_0=1$ when $T/T_c=1$. The value of Eq. (54) is the simplicity which it introduces to the numerical calculations.

Thus, from Eq. (53) by assigning values to y_1, we may calculate the appropriate value r_0 of T/T_c corresponding to the chosen value of y_1 on the equilibrium curve resulting from Hilde-

brand's theory. Then Eq. (54) permits us to calculate the corrected value r_1 of T/T_c corresponding to y_1 according to the Mie-Gruneisen approach. The curves obtained by such calculations are shown in Fig. 1. Curve A is that calculated from Hildebrand's theory according to Eq. (53). Curve B is that obtained from the quasi-chemical method without taking into account changes of vibrational entropy with composition. Curve C is the final corrected curve to the approximation involved in the Mie-Gruneisen method. Thus it appears that, at least for the case of symmetrical segregation, the energy effects predominate over the entropy effects. It is reasonable to inquire, however, how the situation will be altered if the molal volumes of the two components differ appreciably, since the Einstein frequency depends directly on volume. Clearly, we must consider changes in F_A and F_B with the volume changes induced by varying the composition, and we may draw some rough conclusions by differentiating Eq. (45) with respect to volume. At zero pressure, F', F_A', and F_B must be zero to insure equilibrium. The quantities F_A'' and F_B'', however, are not in general zero if $V_A \neq V_B$ but contribute terms to the free energy which we have estimated above as strain energy. Since w_{AB} is very small in general compared to F_A and F_B, we may assume that w_{AB}' and w_{AB}'' are negligibly small compared to either F_A'' or F_B''. To this approximation then, no additional contributions are made to the entropy because of differences in volume. As the volume changes the changes in vibrational frequency are just compensated by changes in potential energy. This conclusion cannot, of course, be rigorously true since the strain-energy terms are bound to affect the local order. However, since the strain-energy terms cannot exceed $RT_c/(2x_cy_c)$, and the local order for the case $x_c=0.5$ is very small, we may conclude that the local order will have only a minor effect on the phase equilibrium curves for quite a range of x_c.

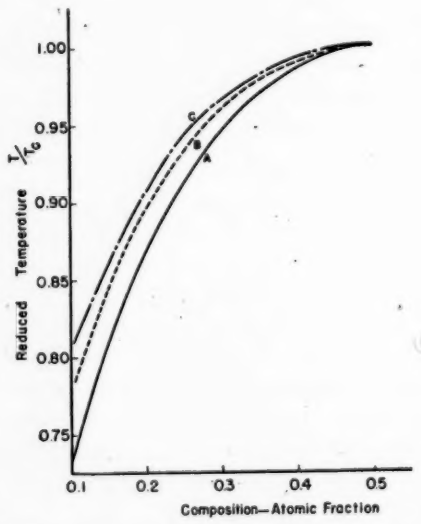

FIG. 1. The effect of local order and vibrational entropy on the solubility limit. Curve A is the calculated limit using Hildebrand's theory. Curve B takes into account the effect of local order. Curve C takes into account both local order and vibrational entropy.

In summary, we conclude that the assumption of perfect mixing entropy used by many investigators is a justifiable first approximation, particularly when volume effects are small. When we recall that solid solutions do not form if very large volume differences exist between the component atoms, this restriction would not appear to be very severe.

EXPIRICAL EXPANSIONS ABOUT THE CRITICAL POINT

Because of the nature of the assumptions required in the foregoing treatment, we must not expect widespread quantitative agreement of computed phase diagrams with observed phase diagrams. The usefulness of the statistical approach is the guidance we receive in setting up empirical equations of state which in conjunction with known phase diagrams yield analytic expressions for certain thermodynamic quantities (e.g., heat of solution) which are otherwise difficult to ascertain (even experimentally) in solid solutions. For this reason we diverge temporarily to consider a variety of possible empirical approaches. We shall center our attention on the critical point which the critical conditions suggest would be a suitable origin for some type of Taylor expansion in terms of composition. In making such an expansion, however, we must be careful to satisfy the Duhem equation

$$x(\partial\mu_1/\partial x)+y(\partial\mu_2/\partial y)=0. \tag{55}$$

This equation may be used to define a useful quantity μ_{12} as follows,

$$\mu_{12}\equiv x(\partial\mu_1/\partial x)=-y(\partial\mu_2/\partial x)=y(\partial\mu_2/\partial y). \tag{56}$$

In terms of μ_{12} we have for $\mu_1(x)$ and $\mu_2(y)$ the symmetrical expressions:

$$\mu_1(x)=\int\frac{\mu_{12}(x)}{x}dx, \tag{57}$$

$$\mu_2(y)=\int\frac{\mu_{12}(y)}{y}dy. \tag{58}$$

Thus if we expand $\mu_{12}(x)$ in a series about the critical point we may immediately calculate μ_1 and μ_2, and they will automatically satisfy Eq. (55). Furthermore, from the critical condition

$$\frac{\partial\mu_1}{\partial x}=0$$

we have

$$\mu_{12}(x_cT_c)=0, \tag{59}$$

and from the second critical condition

$$\partial^2\mu_1/\partial x^2=0,$$

$$\left.\frac{\partial\mu_{12}}{\partial x}\right|_{x=x_c,\ T=T_c}=0. \tag{60}$$

Equations (59) and (60) suggest that we write

$$\mu_{12}=a(x-x_c)^2+b(T-T_c). \tag{61}$$

Referring to either Eqs. (57) or (58), we see that this equation will not correspond to complete segregation at absolute zero as required by the third law of thermodynamics (assuming simple systems with no dissociation or internal entropy changes) unless $ax_c^2=ay_c^2=bT_c$. Hence Eq. (61) leads automatically to symmetrical segregation. Furthermore, the laws of dilute solution require that the coefficient of T be R, the universal gas constant.

Thus, we have

$$\mu_1(x)=RT_c(2x^2-4x+T/T_c\ln x), \tag{62}$$

$$\mu_2(x)=RT_c(2y^2-4y+T/T_c\ln y). \tag{63}$$

The preceding equations are, of course, exactly those obtained by Hildebrand using the first terms of a power series expansion in the Margules equation. From this point of view one would expect Eq. (62) to be a good approximation for small values of x, and Eq. (63) to be a good approximation for small values of y. No estimates of the validity of the Margules expansion for intermediate compositions are possible, since the region of good behavior of Eq. (62) is just where Eq. (63) is uncertain and *vice versa*. The advantage of starting from Eq. (61) is now evident, for this equation indicates clearly that Eqs. (62) and (63) will lead to small errors near the critical point.

Comparing Eqs. (62) and (63) with the symmetrical case discussed in the previous section, we see that they lead immediately to Eq. (53) and hence are equivalent to the zero-order approximation in the quasi-chemical theory. Indeed, it is not difficult to show that if we think of a pure A lattice and a pure B lattice as perfectly ordered structures, and an alloy of intermediate composition as disordered, that we may define an order parameter in terms of composition after the manner of Bragg and Williams, and that the phase equilibrium curve A of Fig. 1 is just that which would be computed using Bragg and William's theory with a negative interchange energy.

The success of Eq. (61) in treating symmetrical segregation invites us to examine the possibility of extending the expansion to handle unsymmetrical cases also. Obviously, we must add higher terms in the series which are unsymmetrical in x. We consider two possibilities:

$$\mu_{12}=a(x-x_c)^2+b(x-x_c)(T-T_c)+c(T-T_c), \tag{64}$$

and

$$\mu_{12}=a'(x-x_c)^3+b'(x-x_c)^2+c(T-T_c). \tag{65}$$

We consider first Eq. (64). Integrating, we obtain

$$\mu_1=a/2x^2-2ax_cx+(c-bx_c)T\ln x+bTx+(ax_c^2-cT_c+bx_cT_c)\ln x+\text{const}. \tag{66}$$

For complete segregation at $T=0$

$$ax_c^2-cT_c+bx_cT_c=0. \tag{67}$$

A similar integration for μ_2 yields the condition

$$ay_c^2-cT_c-by_cT_c=0. \tag{68}$$

Solving Eqs. (67) and (68) simultaneously we find

$$b/a=\frac{y_c-x_c}{T_c}, \tag{69}$$

$$c/a=\frac{x_cy_c}{T_c}. \tag{70}$$

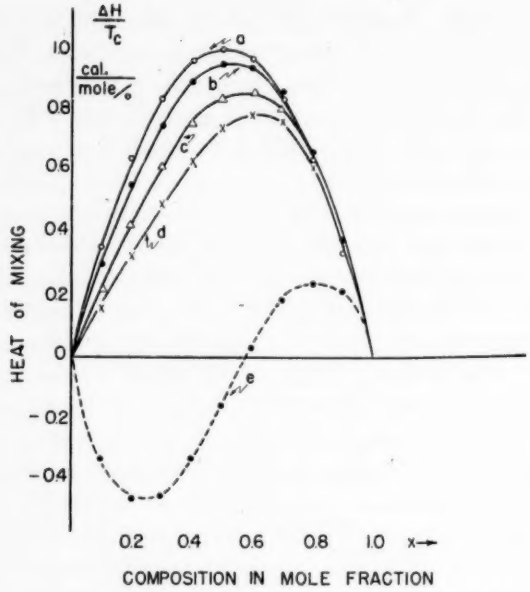

FIG. 2. Calculated heat of solution curves using Eq. 75. Curve a corresponds to $x_c=0.5$; b to $x_c=0.6$; c to $x_c=0.67$; d to $x_c=0.7$; e to $x_c=0.8$. Curve e is dotted to emphasize the break-down of this model for large x_c.

Introducing Eqs. (69) and (70) into Eq. (66) we find

$$\mu_1=a\left\{\frac{x^2}{2}-[2x_c+(1-2x_c)(1-T/T_c)]x+x_c^2T/T_c\ln x\right\}+\text{const.} \quad (71)$$

Similarly,

$$\mu_2=a\left\{\frac{y^2}{2}-[2y_c+(1-2y_c)(1-T/T_c)]y+y_c^2\frac{T}{T_c}\ln y\right\}+\text{const.} \quad (72)$$

It is apparent from Eqs. (71) and (72) that the type of expansion used in Eq. (65) throws the brunt of the burden for unsymmetrical segregation on extra entropy terms. Furthermore, Eqs. (71) and (72) can only obey the law of dilute solutions for the symmetrical case $x_c=y_c$, since only then can $x_c^2T/T_c=y_c^2T/T_c=R$ as required. In view of these difficulties, we are encouraged to investigate the alternative expansion of μ_{12} expressed by Eq. (65). Proceeding exactly as above, one finds in this case

$$\mu_1=\frac{RT_c}{x_c^2y_c^2}\left[\frac{x^3}{3}(2x_c-1)-\frac{x^2}{2}(3x_c^2-1)+(3x_c^2-2x_c)+x_c^2y_c^2T/T_c\ln x\right]+\text{const.}, \quad (73)$$

$$\mu_2=\frac{RT_c}{x_c^2y_c^2}\left[\frac{y^3}{3}(2y_c-1)-\frac{y^2}{2}(3y_c^2-1)+y(3y_c^2-2y_c)+x_c^2y_c^2\frac{T}{T_c}\ln y\right]+\text{const.} \quad (74)$$

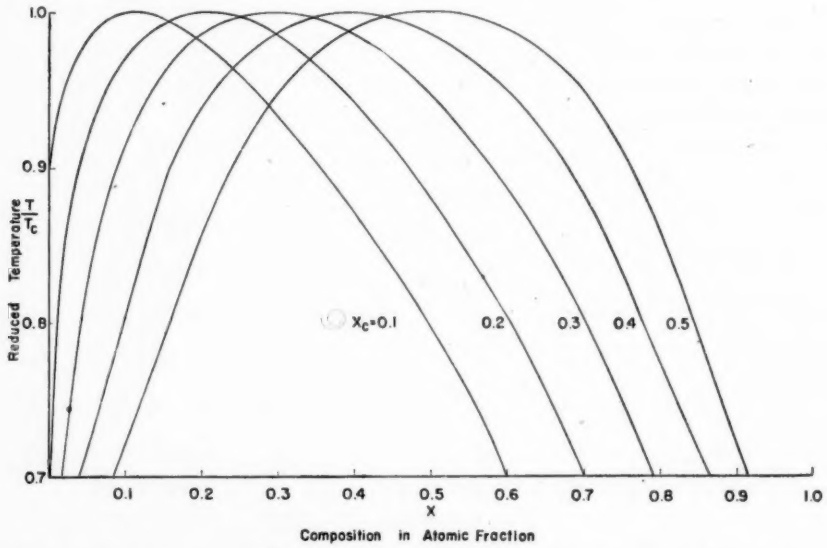

FIG. 3. Calculated equilibrium curves using Eqs. 71 and 72. These curves do not satisfy the law of delute solutions (see text) but illustrate the behavior to be expected near the critical point.

These equations are just those which are obtained by carrying the second approximation in Margules expansion, and their use in treating unsymmetrical segregation has been discussed by Hildebrand. These equations involve the assumption of regular mixing entropy and require an asymmetrical heat of solution in general. The terms in the heat of solution are very similar to those obtained in the first section of this paper. It is interesting to compare the two results in detail, and for convenience we repeat them below. From the thermodynamic approach, we have for the heat of solution

$$\Delta H = xH_x + yH_y - xH_x(1) - yH_y(1)$$

$$= \frac{RT_c}{x_c^2 y_c^2}\left[\left(\frac{x^4}{3} - \frac{x^3}{2}\right)(2x_c - 1)\right.$$

$$(x^3/2 - x^2)(3x_c^2 - 2x_c)$$

$$+ (y^4/3 - y^3/2)(2y_c - 1)$$

$$- (y^3/2 - y^2)(3y_c^2 - 2y_c)$$

$$+ (4/3x_c - \tfrac{1}{6} - 3/2x_c^2)x$$

$$\left. + (4/3y_c - \tfrac{1}{6} - 3/2y_c^2)y\right], \quad (75)$$

while for the statistical approach we have

$$\Delta H = Mx^2y + Ny^2x + w_{AB}xy, \quad (76)$$

where M and N are used as abbreviations for $4/3(G_A/V_A)(V_B - V_A)^2$ and $4/3(G_B/V_B)(V_B - V_A)^2$, respectively. Equation (75) suggests that Eq. (76) may also be written in a normalized form. This may be done as follows. Rewrite Eq. (76) as

$$\Delta H = [(M - N)x + N + w_{AB}]xy. \quad (77)$$

Then substitute for $(M - N)$ its value from Eq. (30), and for $N + w_{AB}$ the corresponding value from Eq. (29). After minor manipulations one finds

$$\Delta H = xy\left\{\frac{RT_c}{2x_c y_c} + \frac{RT_c(x_c - y_c)}{12x_c^2 y_c^2}\right.$$

$$\left. \times (x - y - 3x_c + 3y_c)\right\}. \quad (78)$$

Equation (78) now represents the heat of mixing predicted by the statistical analysis in a form directly comparable with Eq. (75) developed by

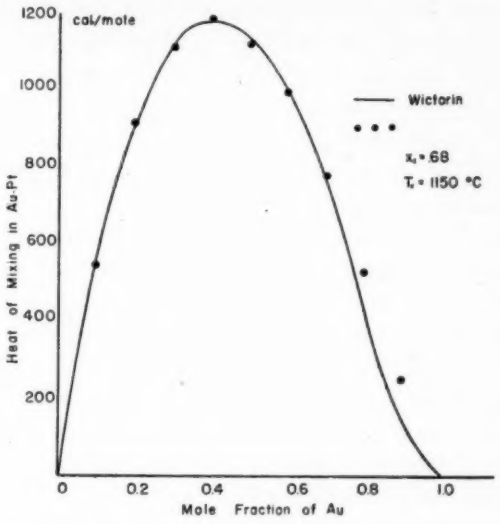

FIG. 4. Comparison of the heat of mixing calculated from Eq. 75 represented by dots with the calculated results of Wictorin for the special case of Au-Pt alloys.

empirical expansion about the critical point. It is interesting to observe that one need not know M, N, and w_{AB} in order to compute the various thermodynamic quantities, which are determined to this approximation solely by the reduced parameters T/T_c and x_c.

A further study of Eqs. (75) and (78) reveals that the computed heats of mixing are in satisfactory agreement for small values of $(x_c - y_c)$. As the latter parameter becomes larger, the deviations become more appreciable. However, for larger values of $(x_c - y_c)$ a much more serious phenomena occurs, namely, ΔH assumes negative values in contradiction to our physical assumptions. The curves of Fig. 2 illustrate this situation. These curves were computed using Eq. (78). However, it is easy to show that a similar situation results from Eq. (75). This situation may be understood as follows. To obtain large deviations of x_c from 0.5, $(M - N)$ must be large. In this case, in order to satisfy the critical conditions w_{AB} becomes so negative that it outweighs the positive contributions from the strain energy and negative values of ΔH result. In this case, of course, we no longer have a simple segregation loop; the phase diagram is much more complicated than that assumed here, and the whole model is invalidated.

It is interesting to note that the expansion expressed in Eq. (64) does not lead to such

difficulties. In fact, one may obtain segregation loops for any x_c. See Fig. 3. However, the difficulties discussed above with dilute solutions remain as an unsurmountable hurdle.

We are forced to conclude then that, at least in *simple* binary solids, the range of permissible segregation loops is very limited. This is in accordance with observation. In more complicated structures, where orientation and other entropy factors play a role, this conclusion is invalidated. In this case, however, we must use a more complete expansion involving a combination of Eqs. (64) and (65). The evaluation of the resulting equations then requires additional physical data. Nevertheless, it is not difficult to estimate from a known phase diagram the relative magnitudes of the extra entropy and the heat of mixing, using a combined expansion.

Borelius[9] and Wictorin[10] have used an empirical expansion of the type

$$F=ax_1^4x_2+bx_1^3x_2^2+cx_1^2x_2^3+dx_1x_2^4 +RT(x\ln x+y\ln y) \quad (79)$$

to analyze the case of Pt-Au. The coefficients a to d were force-fitted from the known phase diagram, and then used to evaluate a heat of mixing which is plotted in Fig. 4. Borelius, although assuming random mixing entropy, does not appear to have utilized the Duhem equation to provide additional relations between the coefficients. It is, therefore, of some interest to compare our two-constant theory with the four-constant expression used by Borelius. This comparison made in Fig. 4 appears to be quite satisfactory. Since Borelius' equation has been made to fit the phase diagram, we may expect our theory to do likewise to a reasonable approximation. In view of the labor involved, this computation has not been made.

[9] G. Borelius, Am. J. Phys. **28**, 507 (1937).
[10] C. G. Wictorin, Am. J. Phys. **33**, 509 (1938.)

CONCLUSION

A great deal of the somewhat lengthy discussion above does not contribute anything essentially new. However, the author feels that the arguments present some justification for the judicious use of empirical expressions. In the case of binary alloys, the use of such empirical attacks may enjoy rather limited use. However, as a guidance in the study of ternary systems, where the situation is vastly more complicated, their use may have more appeal. The application of such expressions to the analyses of ternary systems is now under investigation, and the preliminary results appear to be most promising.

In conclusion, several criticisms should be made of this type of approach. In the first place w_{AB}, N, and M have all been assumed independent of temperature and composition. Both of these assumptions are only approximately true and must invariably lead to errors. Secondly, for larger values of (x_c-y_c) the local order will play a more and more important role. No estimate of such correlations terms has been made. Nevertheless, with a realization of the limitations and pit-falls, the quasi-empirical approach appears to yield reasonable first approximations to thermodynamic data otherwise unavailable.

The author takes this occasion to express appreciation to Messrs. Zener and Meyer, of the Institute of Metals, for many valuable comments and criticisms.

Letters to the Editor

THIS section will accept reports of new work, provided these are terse and contain few figures, and especially few halftone cuts. The Editorial Board will not hold itself responsible for opinions expressed by the correspondents. Contributions to this section should not exceed 600 words in length and must reach the office of the Managing Editor not later than the 15th of the month preceding that of the issue in which the letter is to appear. No proof will be sent to the authors. The usual publication charge ($4.00 per page) will not be made and no reprints will be furnished free.

Restricted Bond Rotation and Shape of Unbranched Saturated Hydrocarbon Chain Molecules

HANS KUHN
Department of Physical Chemistry, University of Basel, Basel, Switzerland
October 14, 1947

LET us consider an unbranched, saturated, long-chain hydrocarbon molecule with a number ν of C atoms joined to the chain. As commonly accepted, there is restricted rotation around the C−C bonds as axis. The restriction potential for rotations about a given bond, for instance, about the bond between the kth and the $k+1$st C atom in the chain, can be described approximately by the expression:

$$E_{\text{pot},k} = -a\cos 3\varphi_k - b\cos\varphi_k, \tag{1}$$

where a and b are constants and φ_k represents the angle of rotation, i.e., the angle between the two planes containing the centers of C atoms number $k-1$, k, $k+1$, and k, $k+1$, $k+2$, respectively. It is defined so that $\varphi_k=0$ for the planar transposition of the atoms number $k-1$ and $k+2$. From a paper by K. S. Pitzer,[1] giving the values of the maxima and minima of the restriction potential as determined from infra-red spectra of hydrocarbon vapors, it follows that $a=1700$ cal./mole, $b=500$ cal./mole.

It can easily be seen that the average dimensions of our chain molecule, for instance, the average $\bar{h}^2$ of the square of the distance h between the chain ends, are highly influenced by the angular dependence of the restriction potential E_{pot}, especially by the value of constant b in (1).

The average square distance $\bar{h}^2$ of the chain ends of a molecule, consisting of a number $\nu-1$ of chain bonds of length l (C−C bond distance [$1.54\cdot10^{-8}$ cm] in the case of a hydrocarbon), joined under a constant valence angle $180°-\beta$(C−C−C bond angle [109° 28′] in the case of a hydrocarbon) can be expressed by the following equation given by the author[2]

$$\bar{h}^2 = \nu l^2 \operatorname{cotg}^2\frac{\beta}{2}\left[1+2\,\frac{\overline{\cos\varphi_k}}{1-\overline{\cos\varphi_k}}\right] (\text{for } \nu\gg 1), \tag{2}$$

where

$$\overline{\cos\varphi_k} = \int_0^{2\pi} W(\varphi_k)\cos\varphi_k d\varphi_k. \tag{2a}$$

φ_k is the angle of rotation as defined above, and $W(\varphi_k)d\varphi_k$ represents the probability that the angle of rotation around a given chain bond lies between φ_k and $\varphi_k+d\varphi_k$. Equation (2) is valid only for large values of ν and for arbitrary but even functions $W(\varphi_k)$. According to Boltzmann's principle $W(\varphi_k)$ can be expressed in terms of the rotational restriction potential $E_{\text{pot},k}$ as follows:

$$W(\varphi_k) = A\exp\{-E_{\text{pot},k}/RT\}, \tag{3}$$

where

$$1/A = \int_0^{2\pi}\exp\{-E_{\text{pot},k}/RT\}d\varphi_k. \tag{3a}$$

By introducing expression (1) for $E_{\text{pot},k}$ into (3), (3a), inserting the result into (2), (2a), and using the numerical values given above ($a=1700$ cal./mole, $b=500$ cal./mole, $l=1.54\cdot10^{-8}$ cm, $180°-\beta=109°\,28'$), one finds for $T=300°$ (room temperature) the average square distance $\bar{h}^2$ of the ends of a hydrocarbon chain to be equal to:

$$\bar{h}^2 = 13\times10^{-16}\nu \text{ cm}^2 \quad (\nu\gg1\text{; steric influence neglected}). \tag{4}$$

Equation (2) (and thus Eq. (4)) is valid under neglection of the steric influence of accidentally coinciding chain parts. This phenomenon, first considered by W. Kuhn,[3] causes an increase in $\bar{h}^2$.

In the case of an unbranched hydrocarbon there is to be expected only a moderate enlargement of $\bar{h}^2$ caused by steric reasons. This follows from a treatment[4] that has been carried out under the assumption that the positions of the chain atoms are restricted to the three positions of minimum potential energy ($\varphi_k=0$; $\varphi_k=2\pi/3$; $\varphi_k=4\pi/3$), and that these three positions are, when sterically possible, equally probable. Under these assumptions it follows for $\nu\gg1$, that $\bar{h}^2$ is 1.61 times as large with consideration as with neglect of the steric coincidence phenomenon. Considering, furthermore, that the three positions of minimum potential energy are, in fact, not equally probable, but that the transposition ($\varphi_k=0$) is (according to the b value given above) about three times as probable as the other two positions, one can estimate that there is to be expected an increase in $\bar{h}^2$ by steric reasons by a factor 1.3. Thus we have instead of (4):

$$\bar{h}^2 = 1.3\times13\times10^{-16}\nu = 17\times10^{-16}\nu \text{ cm}^2 \quad (\nu\gg1^6 \text{ steric influence considered}). \tag{5}$$

This value is 3.5 times as large as it would be with the assumption of free bond rotation and with neglect of the steric influence.

It has been shown by W. Kuhn and H. Kuhn[5] that the actual value of $\bar{h}^2$ can be obtained, on the other hand, from viscosity and double refraction of flow of dilute solutions. The $\bar{h}^2$ values thus obtained in the 1943 paper for a large number of chain molecules were found to be throughout distinctly (in the case of polystyrene by a factor 8 and in the case of polyvinylacetate by a factor 13) greater than the values calculated with the assumption of free bond rotation and with neglect of the steric influence. The actual value of $\bar{h}^2$ of an unbranched hydrocarbon, in which we are interested here, can be obtained from intrinsic viscosity measurements by W. O. Baker, C. S. Fuller, and J. H. Heiss[6] in chloroform solution at 25°C. Using a recently

reported equation[7] for the intrinsic viscosity of chain molecules, it is thus found:

$$\bar{h}^2 = 16\times10^{-16}\nu \text{ cm}^2 \text{ (chloroform solution, } \nu\gg1\text{;}$$
$$\text{from viscosity measurements).} \quad (6)$$

The close agreement of the calculated value (5) and of the actual value (6) is much better than might be expected. Probably this is to some extent accidental; in general, it will have to be assumed that the values of constants a and b and thus the $\bar{h}^2$ values will be somewhat dependent upon the solvent used.

[1] K. S. Pitzer, J. Chem. Phys. **8**, 711 (1940).
[2] H. Kuhn, Habilitationsschrift, Basel (June 1946). The same Eq. (2) has been obtained recently also by W. J. Taylor, J. Chem. Phys. **15**, 412 (1947). An equation that represents the special case of (2) for free rotation has been given by H. Eyring, Phys. Rev. **39**, 746 (1932), and an equation valid for nearly free rotation has been reported by C. Sadron, J. Chem. Phys. **43**, 12 (1946). P. Debye got in an unpublished work recently an equation, representing another special case of (2), namely, the case that only part of the rotational angle φ_k is allowed and that there is a constant probability distribution in the allowed range. (Reported after H. Benoît, Report of a lecture at the High Polymer Conference, Strasbourg, November, 1946.)
[3] W. Kuhn, Koll. Zeits. **68**, 2 (1934), see also reference 5.
[4] H. Kuhn and O. Künzle, to be published.
[5] W. Kuhn and H. Kuhn, Helv. Phys. Acta **26**, 1293 (1943); *ibid.* **28**, 1533 (1945); *ibid.* **29**, 71 (1946).
[6] W. O. Baker, C. S. Fuller, and J. H. Heiss, J. Am. Chem. Soc. **63**, 2142, 3316 (1941). In that paper are reported viscosity measurements of ω-hydroxy-undecanoic acid polymers. We assume that there is no considerable difference in $\bar{h}^2$ of that polymer and of a hydrocarbon with the same number of chain members, i.e., it is assumed that the disturbing influence of the few 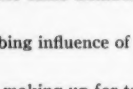 groups in the chain, each of which making up for two CH_2 members, can be neglected.
[7] H. Kuhn and W. Kuhn, in preparation; previously reported by W. Kuhn and H. Kuhn, Helv. Phys. Acta **30**, 1233 (1947).

Determination of Molecular Weights from the Activation Energy for Viscous Flow of Liquids

M. S. Telang
Laxminarayan Institute of Technology, Nagpur University, Nagpur, India
October 3, 1947

THE following equation has been recently proposed by the writer:[1]

$$\eta = Ze^{\gamma(M/D-d)^{\frac{2}{3}}}\cdot N^{\frac{1}{3}}/RT, \quad (1)$$

where η = the viscosity, γ = the surface tension, M = the molecular weight, D and d are the orthobaric densities of the liquid and vapor, respectively, N = the Avogadro number, Z = the "frequency factor," R = the gas constant, and T = the absolute temperature. However, for theoretical reasons which will be incorporated in a forthcoming paper, Eq. (1) has now been slightly modified as

$$\eta = Ze^{\gamma(M/D-d)^{\frac{2}{3}}}\cdot N^{\frac{1}{3}}/(\cos30°)^{\frac{1}{3}}/RT, \quad (2)$$

or,

$$\ln\eta = \ln Z + \gamma\left(\frac{M}{D-d}\right)^{\frac{2}{3}}\cdot\frac{N^{\frac{1}{3}}}{(\cos30°)^{\frac{1}{3}}}/RT, \quad (3)$$

or,

$$\log_{10}\eta = \log_{10}Z + \frac{0.4343\cdot N^{\frac{1}{3}}}{(\cos30°)^{\frac{1}{3}}\cdot R}\cdot M^{\frac{2}{3}}\cdot\frac{\gamma/(D-d)^{\frac{2}{3}}}{T}. \quad (4)$$

One of the ways in which (4) can be tested is to utilize it for the determination of molecular weights as shown below.

If T_1 and T_2 are sufficiently close to each other, Z may be assumed to be a constant, and below the boiling point d becomes negligible in comparison with D. On the basis of these assumptions, and writing the subscripts 1 and 2 for the respective values at T_1 and T_2, it follows from (4) that

$$\log_{10}\eta_1 - \log_{10}\eta_2 = \frac{0.4343N^{\frac{1}{3}}}{(\cos30°)^{\frac{1}{3}}\cdot R}\cdot M^{\frac{2}{3}}\left\{\frac{\gamma_1/D_1^{\frac{2}{3}}}{T_1} - \frac{\gamma_2/D_2^{\frac{2}{3}}}{T_2}\right\}. \quad (5)$$

Rearrangement of (5) gives

$$M = 3.176\left\{\frac{\log_{10}\eta_1/\eta_2}{(\gamma_1/D_1^{\frac{2}{3}}\cdot T_1) - (\gamma_2/D_2^{\frac{2}{3}}\cdot T_2)}\right\}^{\frac{3}{2}} \quad (6)$$

expressing R and γ in the same units. Hence, we can see that the molecular weight can be determined from the experimental values of η, γ, and D at two temperatures.

TABLE I.

Substance	Melting point °C	Temperature °C	Viscosity $10^3\eta$	Surface tension γ vap.	Density D	Mole. wt. M calc. from (6)	% Deviation
Benzene	5.5	0.0	9.00	31.70	0.9000	80.54	+3.1
		20.0	6.47	29.02	0.8790		
Ethylene dibromide	10.01	10.0	(2.034)†	40.05	(2.2014)	179.8	−4.3
		20.0	(1.718)†	38.75	2.1805		

† $10^2\eta$.

The necessary data given in Table I for purposes of illustration have been taken from the *International Critical Tables*, and the values given in parentheses have been calculated from the formulae given in the *I.C.T.*

Considering the possibility that some uncertain factors might have been incorporated in the utilization of (6), the agreement between the theoretical and the observed value of the molecular weight may be deemed to be satisfactory. The uncertainties involved may be the unknown reliability of viscosity data; moreover, a temperature difference of 10° or 20° may be too much for assuming the value of Z to be a constant. It has been found that the molecular weight calculated from (6) at higher temperatures decreases gradually with increasing temperature, and it is observed to be a characteristic of other liquids also, such as chloroform, ether, etc. It is to be concluded, therefore, that the method is reliable only near the melting point of a substance. This behavior is not surprising in view of the derivation of (2), which is based on the assumption that a liquid has a structure resembling that of a solid, and this would be true in the neighborhood of the melting point only.[2] At higher temperatures, thermal agitations may cause a considerable amount of disturbance of this structure.

The main purpose of this paper has been to point out that we have here a new method by which we can determine the molecular weight of a substance in its pure state. Most of the hitherto existing methods of molecular weight determination are applicable to solutions or vapors which may not give the correct picture of the pure liquid state. For instance, vaporization may decompose a substance or

alter the molecular complexity, and in the dissolved state, combination between the solute and the solvent may take place. The method proposed in the present paper is being extensively tested by the writer.

[1] M. S. Telang, J. Chem. Phys. 15, 525 (1947).
[2] The theoretical basis of this derivation will be the subject of a future paper by the writer.

A Possible Contributing Mechanism of Catalysis

U. Fano
X-Ray Section, National Bureau of Standards, Washington, D. C.
October 15, 1947

IT seems remarkable that organic catalysts, and most inorganic ones, have a large mass, often much larger than that of their substrate. For example, catalase is about 10,000 times heavier than H_2O_2. It may, therefore, be worth while to consider types of mechanism in which the mass of the catalyst could play a role.

It is generally assumed that the effect of a catalyst is to establish some course for the reaction to follow which does not involve as high an energy of activation as the uncatalyzed reaction. A catalytic effect would also be afforded, however, by establishing a course in which the reaction is accompanied by a large increase in the entropy of the catalyst.

Calling S the substrate and S' the product of the reaction catalyzed by C, the reaction might involve the following steps:

(1) $S+C\rightarrow SC$ accompanied by a moderate release of energy and a large loss of entropy.

(2) $SC\rightarrow S'C$ requiring a large activation energy E but accompanied by a regain of the entropy lost in (1).

(3) $S'C\rightarrow S'+C$ accompanied by a moderate uptake of energy.

If, for example, the loss of entropy Δs in (1) were equal to $E/2T$, the rates of reaction of (1) and (2) would be both moderately slow, being proportional, respectively, to $\exp(-\Delta s/R)=\exp(-E/2RT)$ and to $\exp[(\Delta s/R)-(E/RT)]=\exp(-E/2RT)$, but far higher than the rate of the uncatalyzed reaction.

Consider now the possible influence of the mass of a catalyst on this type of reaction, for example, in a case where $S=A-A'$, $S'=A+A'$. Step (1) of the reaction might be further resolved into:

(1a) $A-A'+C\rightarrow CA-A'$ accompanied by a moderate release of energy and no loss of entropy.

(1b) $CA-A'\rightarrow CA-A'$ accompanied by a further moderate release of energy and a large loss of entropy. As a concrete model, S might be a particle suspended in water and consisting of two blocks hinged together carrying specific receptor spots B and B' (for A and A') at the positions indicated on the sketch. Step (1a) may then occur according to the usual picture, step (1b) when the blocks happen to come in the right configuration; the absorption of A' onto B' then locks the blocks together, preventing their free rotation. This entails a loss of entropy of the

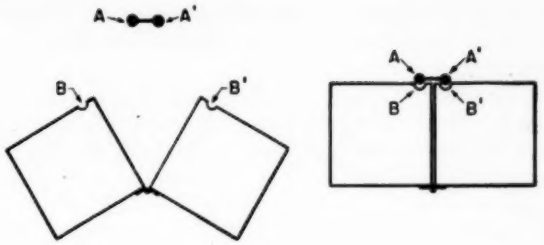

FIG. 1.

order of $R\log(IkT/\hbar^2)^{\frac{1}{2}}$, where I is the rotational moment of inertia of the hinged blocks and R, k, T, and $\hbar$ have their usual meaning. The quantity in parentheses is of the order of magnitude of 100 for diatomic molecules and may be taken as 10^7 for an enzyme of molecular weight between 10^4 and 10^5. The resulting entropy change affects the free energy by about 5000 calories, an amount which is not large but yet is significant. From an atomistic standpoint it may be said that Brownian fluctuations of the pressure of water molecules on the large faces of the blocks tend to tear the bond between A and A'.

In general, a catalyst of this type might be described as a particle so constructed that: (a) a very low zero-point energy corresponds to some of its internal degrees of freedom (this can happen only if the mass of the particle is large), and (b) those degrees of freedom can be nearly frozen in a particular configuration by specific absorption of a substrate molecule, so that their zero-point energy is thereby raised very much. For comparison it is recalled that the entropy increase in the reversible denaturation of proteins is equivalent to more than 50,000 calories.

Dr. J. E. Mayer, to whom I am also indebted for other suggestions, pointed out that step (2) in the reaction above would have a high temperature coefficient corresponding to the full activation energy E while its rate is determined by the lower free energy change $E-T\Delta s$. In fact, the temperature coefficient of enzymatic reactions is rather low.

This discrepancy and the result of the numerical calculation above make it unlikely that the mechanism suggested here is the main factor of catalysis. It may, however, be one among several concurrent factors of comparable importance.

The Dependence of Quenching Efficiency on Temperature

W. M. Smith and F. W. Southam
Department of Chemistry, Queens University, Kingston, Ontario
October 13, 1947

A SMALL cross section for the process in which electronically excited atoms are quenched by other molecules may be theoretically associated with a small temperature coefficient if the non-adiabatic step or entropy of activation is the principal factor restricting the occurrence

of quenching, or with an appreciable temperature coefficient if an energy of activation is the principal restrictive factor.

In continuation of work instigated by Professor R. G. W. Norrish on the factors influencing degradation of electronic excitation energy to thermal energy, we have investigated a quenching process of small cross section; the quenching of excited sodium by methane. Norrish and Smith[1] found that the cross section for the quenching of sodium atoms in the 3^2P state by methane is approximately 0.11×10^{-16} cm^2 at 130°C. We have carried out measurements at 585°C and at 615°C, using the method developed by Terenin[2] and by Winans[3] in which sodium atoms excited to the 3^2P state are produced by photo-dissociation of sodium iodide, the energy absorbed in excess of that required to produce dissociation going into kinetic energy of the sodium and iodine atoms. Nickel and cadmium condensed sparks have been used as sources of the radiation producing photolysis. The details of our experimental method resembled those of Winans.

Methane proved to be weakly quenching under our experimental conditions and in consequence cross sections have been calculated on the assumption that, before suffering quenching, sodium atoms attain velocities characteristic of the temperature of the quenching gas. The values for the cross sections evaluated in this manner are 0.19×10^{-16} cm^2 for 585°C and 0.16×10^{-16} cm^2 for 615°C. (There was no significant dependence of quenching ratio on the nature of the spark.) Because of the difficulties in photometry associated with the presence of a perceptible background of radiation and the low intensities of the radiation from the sodium, and because of the small extent of the quenching, these values are probably not significantly different and cannot be considered alone to indicate the magnitude of the temperature coefficient. However, taken in conjunction with the value 0.11×10^{-16} cm^2 obtained by Norrish and Smith by the resonance method at 130°C, they do indicate that the temperature coefficient for quenching by methane is very small.

If the only restrictions on the occurrence of quenching are the approach of the centers of the sodium atom and methane molecule to within about 4×10^{-8} cm and an activation energy (localized in two square terms), then a change in temperature of the system from 130°C to 585°C should be accompanied by a change in cross section from 0.11×10^{-16} cm^2 to approximately 4.5×10^{-16} cm^2. Our results consequently indicate that an activation energy is not the important restrictive factor.[4] They do not, however, allow separate evaluation of the factors which lead to the small cross section.

The methane was prepared by the action of a zinc copper couple on a solution of methyl iodide, and was purified by passage through fuming sulfuric acid, over heated copper oxide, and by several distillations in vacuum. A portion of the gas subjected to a second purification showed no significant change in quenching properties.

[1] Norrish and Smith, Proc. Roy. Soc. London **A176**, 295 (1940).
[2] Terenin, Zeits. f. Physik **37**, 98 (1926).
[3] Winans, Zeits. f. Physik **60**, 631 (1930).
[4] K. J. Laidler, J. Chem. Phys. **10**, 34 (1942).

On the Structure of Ozone

D. M. Simpson
Laboratory of Physical Chemistry, Cambridge, England
July 8, 1947

THE shape of the ozone molecule is still a subject for controversy. Adel and Dennison,[1] from investigations of the rotational fine structure of the infra-red bands, considered that they had obtained conclusive evidence for an acute-angled structure, and this seemed supported by the bond-energy calculations of Glockler and Matlack.[2] More recently Eberhardt[3] has shown that the bond energies can equally well be interpreted on the basis of a wide-angled model with dimensions given by the electron-diffraction investigations.[4] It is the purpose of the present note to indicate that the interpretation of the infra-red bands given by Adel and Dennison is not unique, and that their experimental data are not incompatible with a wide-angled structure.

Adel and Dennison suggest: (a) that the strong band at 705 cm^{-1} is near perpendicular in type, with a coarse rotational spacing ~5.7 cm^{-1} and subsidiary fine structure, so that the change in electric moment for this vibration must be along the middle axis of inertia; (b) that since both the strong bands at 1043 and 2108 cm^{-1} have Q branches and a rotational spacing of ~1 cm^{-1}, and since their appearance is very different from that of the 705-cm^{-1} band, they must both be near parallel bands with change in electric moment along the least axis of inertia.

Taken together, these arguments indicate that if the three strongest regions of absorption correspond to the three fundamental frequencies, that since 1043 and 2108 cm^{-1} are near parallel bands and 705 cm^{-1} is near perpendicular, the assignment to ν_1, ν_2, and ν_3, respectively, follows; moreover, the molecule must be acute-angled, the least axis of inertia coinciding with the symmetry axis. The moments of inertia may then be calculated from the observed rotational spacings, and the apical angle so derived (34°) is in good agreement with that obtained from the fundamental frequencies (39°) using a central force field.[5]

From the published curves for the bands at 1043 cm^{-1} and 2108 cm^{-1},[6,7] it is seen that the latter has a pronounced Q branch, while the former, at least under low dispersion, has none. The dissimilarity of the contours is striking. It should also be noted that the published curves were not obtained under ideal conditions, the band at 1043 cm^{-1} is overlaid with carbon dioxide absorption, that at 2108 cm^{-1} was observed using a specimen admittedly contaminated with nitrogen pentoxide, a substance which absorbs in the same region.[8] The fine structure observed, therefore, cannot be due entirely to ozone. There is thus some justification in criticizing Adel and Dennison's conclusion that both 1043 and 2108 cm^{-1} are near parallel bands. Further, unless *both* are near parallel bands, the molecule is not necessarily acute-angled and their interpretation of the rotational fine structure is not unique.

For the wide-angled model, the middle axis of inertia coincides with the symmetry axis. A_1 bands (eg., ν_1, ν_2) have a doublet structure, B_1 bands (e.g., ν_3) a Q branch. For this

model the observed spacing of the rotational fine structure is the true spacing for both A_1 and B_1 bands, in spite of the identity of the oxygen nuclei with their zero nuclear spin. It is clear that the 705-cm^{-1} absorption corresponds to an A_1 band; the change in electric moment for the 2108-cm^{-1} frequency is probably along the least axis of inertia (on account of its pronounced Q branch), making it a B_1 band. The moments of inertia may be calculated from the observed spacings 5.7 and 1 cm^{-1}, using the method of Adel and Dennison. The second column of Table I shows the results of these calculations for the wide-angled model. The third column gives the observed electron-diffraction data for the bond length and apical angle, together with the moments of inertia derived from them. Adel and Dennison's results for the acute-angled model are included for comparison in the fourth column.

The agreement between the electron-diffraction data and the present calculations is moderately good. Exact agreement would not be expected. It should be emphasized that these calculations are not very accurate; the formulae used to obtain the moments of inertia from the line spacings are rough approximations—modifications of those for a symmetrical top; further, the observed line spacings are not known precisely (particularly that for the near parallel band at 2108 cm^{-1}), and the moments of inertia are rather sensitive to small changes in these spacings.

The electron-diffraction data may be used to calculate corresponding line spacings, which are found to be 0.8 and 9.0 cm^{-1}, respectively, for near parallel and near perpendicular bands. Reduction in apical angle or increase in bond length both lead to a decrease in the line spacing of near perpendicular bands without seriously affecting that of near parallel bands. Small changes of both angle and bond length would be sufficient to give much closer agreement between the calculated and observed line spacings, though such changes would be larger than the published limits of error.

It is clear from the above considerations that the fine structure observed in the infra-red absorption of ozone may be interpreted on the basis of a wide-angled model. A detailed comparison of the molecular dimensions derived from electron diffraction and the fine structure of the infra-red bands must be reserved until the complete analysis of this fine structure has been carried out. It will then be possible to consider whether in fact the electron-diffraction data require modification.

For the wide-angled model, if any permutation of the three strongest bands (705, 1043, and 2108 cm^{-1}) is chosen for the fundamental frequencies, it is impossible to obtain sensible values of the force constants from a valency force field. The only other suitable frequency is at 1740 cm^{-1}, a weak band of uncertain contour observed to date only under low dispersion.[5] If a plausible value of the O—O force constant is to be derived, consistent with the observed bond length of 1.26A, it may readily be shown that 1740 cm^{-1} must be assigned to ν_3. Since 2108 cm^{-1} cannot be an A_1 band because of its pronounced Q branch, it follows that 1043 and 705 cm^{-1} must correspond to ν_1 and ν_2, respectively. This interpretation, first proposed by Penney and Sutherland[9] has its difficulties, in particular, unreal values of the deformation force constants are obtained for most types of force field.[10] Calculations using a valency force field with $\nu_2=705$ cm^{-1} $2\alpha=127°$ and a bond force constant of 9.53×10^5 dyne/cm (derived from Badger's relationship, the O—O distance being 1.26A) indicate that a small change in the frequency of either ν_1 or ν_3 would be sufficient to make the deformation force constant real. The unreality of the force constants as calculated directly from the observed frequencies, therefore, cannot be considered as a serious objection to this interpretation, which has the merit that it is in agreement both with the dipole moment[11] and the electron-diffraction data.

TABLE I.

	Present work error ±20%	Electron diffraction	Adel and Dennison error ±20%
I_A	60.5×10^{-40} g cm^2	73.16×10^{-40} g cm^2	64×10^{-40} g cm^2
I_B	52.0×10^{-40} g cm^2	67.56×10^{-40} g cm^2	50×10^{-40} g cm^2
I_C	8.5×10^{-40} g cm^2	5.60×10^{-40} g cm^2	14×10^{-40} g cm^2
O—O side	1.2A	1.26±0.02A	1.8A
O—O basal	2.0A	2.24±0.06A	1.0A
2α	110°	127±3°	34°

[1] A. Adel and D. M. Dennison, J. Chem. Phys. **14**, 379 (1946).
[2] G. Glockler and G. Matlack, J. Chem. Phys. **14**, 505 (1946).
[3] W. H. Eberhardt, J. Chem. Phys. **14**, 641 (1946).
[4] W. Shand and R. A. Spurr, J. Am. Chem. Soc. **65**, 179 (1943).
[5] G. Hettner, R. Pohlman, and H. J. Schumacher, Zeits. f. Physik **91**, 372 (1934).
[6] A. Adel, Astrophys. J. **94**, 451 (1941).
[7] S. L. Gerhard, Phys. Rev. **42**, 622 (1932).
[8] E. Warburg and G. Leithäuser, Ann. Phys. **28**, 313 (1909); F. Daniels, J. Am. Chem. Soc. **47**, 2856 (1925).
[9] W. G. Penney and G. B. B. M. Sutherland, Proc. Roy. Soc. **A156**, 654, 678 (1936).
[10] D. M. Simpson, Trans. Faraday Soc. **41**, 209 (1945).
[11] G. L. Lewis and C. P. Smyth, J. Am. Chem. Soc. **61**, 3063 (1939).

Acta Crystallographica

A NEW journal of crystallography, Acta Crystallographica, sponsored by the recently formed International Union of Crystallography, will start publication in January, 1948. The journal is intended to take the place of the former Zeitschrift für Kristallographie, but in recognition of the rapid development of structural studies in recent years it is intended that it shall be somewhat broader in its scope and that it shall concern itself with all those physical and chemical properties of matter intimately connected with atomic arrangement. The journal will thus be one touching the interests of the chemist, the physicist, the metallurgist, the mineralogist, and even the biologist.

The journal will be published by the Cambridge University Press under the editorship of Professor P. P. Ewald, a former editor of the Zeitschrift für Kristallographie, and a panel of regional co-editors. It will appear in six issues a year. The annual subscription will be $10.00 or £2. 10.0., and by courtesy of the American Institute of Physics arrangements have been made for subscribers in

the U.S.A., its possessions, and Canada to subscribe through that body. Subscribers in other countries should subscribe directly through the Cambridge University Press, Bentley House, Euston Road, London, N.W. 1., England. Both of these organizations are now ready to receive subscriptions for the first volume.

Articles for publication will be accepted in English, French, German, or Russian, and authors are now invited to submit manuscripts for consideration by the co-editors as follows.

In English to Professor I. Fankuchen
Polytechnic Institute of Brooklyn
85 Livingston Street
Brooklyn 2, New York, U.S.A.

or

Dr. R. C. Evans
Crystallographic Laboratory
Cavendish Laboratory
Cambridge, England

In French to Professor J. Wyart
Laboratoire de Mineralogie
La Sorbonne
1 rue Victor-Cousin
Paris V, France

In German to Professor P. P. Ewald
Queen's University
Belfast, Northern Ireland

In Russian to Professor A. V. Shubnikov
c/o Academy of Sciences
Moscow, U.S.S.R.